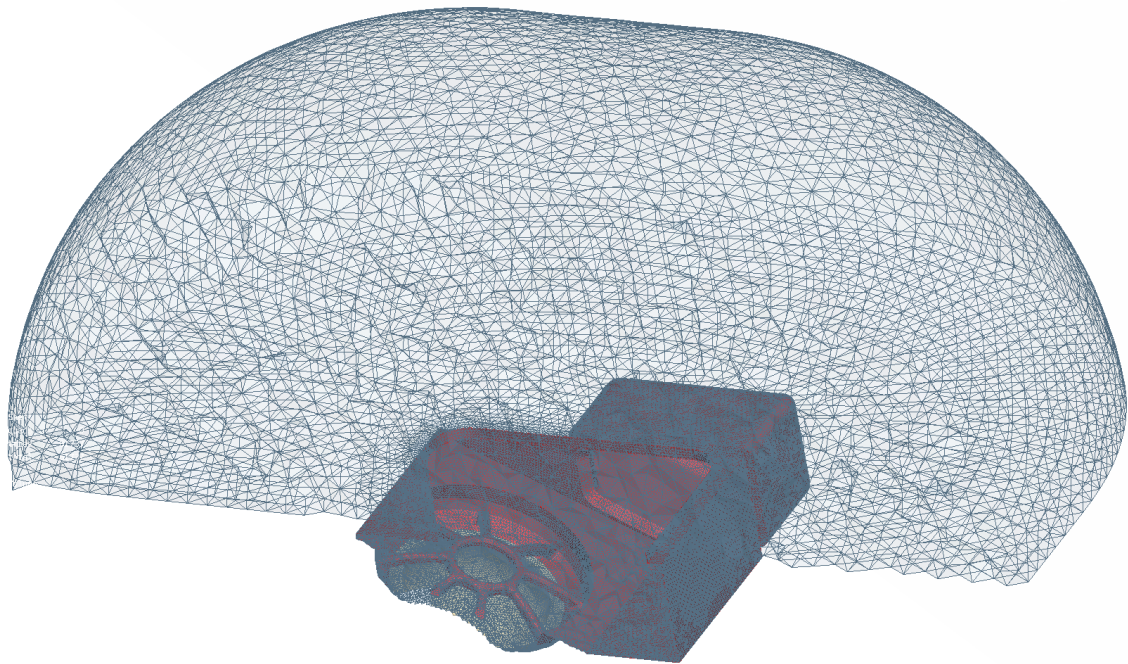




CHALMERS
UNIVERSITY OF TECHNOLOGY



Application of CAE techniques in solving tweeter installation issues

High frequency study focused on the effect of grilles, cavities and nearby reflecting surfaces on tweeter performance in cars.

Master's thesis in Sound and Vibration

RALPH HADDAD

MASTER'S THESIS 2018:ACEX30-18-32

Application of CAE techniques in solving tweeter installation issues

High frequency study focused on the effect of grilles, cavities and nearby reflecting surfaces on tweeter performance in cars.

RALPH HADDAD



CHALMERS
UNIVERSITY OF TECHNOLOGY

Department of Architecture and Civil Engineering
Division of Applied Acoustics
CHALMERS UNIVERSITY OF TECHNOLOGY
Gothenburg, Sweden 2018

Application of CAE techniques in solving tweeter installation issues.
High frequency study focused on the effect of grilles, cavities and nearby reflecting surfaces on tweeter performance in cars.
HADDAD RALPH

© RALPH HADDAD, 2018.

Supervisor: Andrzej Pietrzyk, Volvo Cars
Jens Ahren, Division of Applied Acoustics
Examiner: Jens Ahrens, Division of Applied Acoustics

Master's Thesis 2018:ACEX30-18-32
Department of Architecture and Civil Engineering
Division of Applied Acoustics
Chalmers University of Technology
SE-412 96 Gothenburg
Telephone +46 31 772 1000

Cover: Mesh of the tweeter mounted in one of the interfaces studied in the thesis and the air surrounding it

Typeset in L^AT_EX
Printed by the Department of Architecture and Civil Engineering
Gothenburg, Sweden 2018

Application of CAE techniques in solving tweeter installation issues.

High frequency study focused on the effect of grilles, cavities and nearby reflecting surfaces on tweeter performance in cars.

RALPH HADDAD

Department of Architecture and Civil Engineering

Division of Applied Acoustics

Chalmers University of Technology

Abstract

Nowadays the automotive industry is faced with new features that customers demand, which were not a priority a few years ago. Audio performance is one of them and it is quite challenging. To be able to detect, before any physical prototyping if the speaker mounting or installation is acceptable will allow the teams to perform faster design iterations to achieve better audio performance.

This paper tackles how different installation details of a tweeter will affect its directivity radiation. Installation details within the automotive industry are usually interfaces, grilles or nearby reflecting surfaces. The investigation is made through numerical modeling, specifically Finite Element Method in this thesis and it is then validated with experimental measurements. As this study is done at high frequencies, some of the issues faced during modeling and measurement will also be discussed.

Keywords: Tweeter, Thiele and Small Parameters, Finite Element Method, Loudspeaker Directivity, Acoustic impedance, Resonance, Frequency response function

Acknowledgements

I am very grateful for this Master thesis opportunity made possible by the NVH department at Volvo Cars Corporation.

Special thanks to Andrzej Pietrzyk my supervisor for his insights, support and guidance in CAE. To Jonatan Ewald my co-supervisor for all the 3D printed baffles, CAD drawings and emphasizing on what is useful for the audio team. To Kristofer Weiner for taking care of all the managerial details. To Jens Ahrens my supervisor at Chalmers for always being available to answer my questions.

I also want to thank Mikaela Zetterberg for her tips in Ansa, FFT support for their fast replies in Actran related issues and Börje Wijk for his help in the measurement done at the Applied Acoustics Division.

Finally a big thanks to my family, which without their moral and financial support would have made the completion of this Master thesis much harder.

Ralph Haddad, Gothenburg, June 2018

Contents

List of Figures	xii
List of Figures	xii
List of Tables	xv
List of Tables	xv
1 Introduction	1
2 Theory	2
2.1 Finite Element Method	2
2.2 Exterior Acoustic domains	2
2.3 Electroacoustic	4
3 Methods	7
3.1 Measurement setup	7
3.2 Simulation	13
4 Results & Discussions	18
4.1 Preliminary testing	18
4.2 Interfaces	23
4.3 Grilles	34
4.4 Frequency Equalization	54
5 Conclusion	57
References	I
A Appendix	II
A.1 Background noise	II
A.2 More results	III

List of Figures

2.1	Topology of triangle-based infinite elements showing the finite nodes (black) and the infinite nodes (white) [2].	3
2.2	Simplified diagram of the simulation model using Infinite Element Domain.	3
2.3	Simplified diagram of the simulation model using Perfectly Matched Layer.	4
2.4	Different speaker names [3].	5
2.5	Common speaker configuration.	5
2.6	Electrodynamic model of a loudspeaker considering lumped elements [2].	6
3.1	Sketch of the measurement setup.	7
3.2	Picture of the Tweeter.	8
3.3	Pictures of the four different interfaces.	9
3.4	Baffle 4 detail.	9
3.5	Picture of the 3 mm thickness and 2 mm hole grille.	10
3.6	Picture of the 0.5 mm thickness and 2 mm hole grille.	10
3.7	Picture of the 3 mm thickness and 4 mm hole grille.	11
3.8	Picture of the measurement setup without edge absorption.	11
3.9	Picture of the measurement setup with edge absorption.	12
3.10	First method (on the right) and second method (on the left) to model a loudspeaker [7].	13
3.11	Meshes of the different interfaces.	14
3.12	Meshes of the different grilles on baffle 1	15
3.13	Adaptive mesh generation for different frequency bands [2].	16
3.14	Automatic mesh generation by Actran for Baffle 2 at the frequency bands 5 kHz-6.3 kHz and 8 kHz-10 kHz.	16
3.15	Automatic mesh generation by Actran for Baffle 2 with the 3 mm thickness 2 mm holes grille at the frequency band 5 kHz-6.3 kHz. . .	17
4.1	Sound pressure level comparison of the tweeter with and without edge absorbers.	18
4.2	Sound pressure level comparison level of the tweeter with and without capacitor.	19
4.3	On-axis sound pressure level comparison between different mesh parameters.	19
4.4	Meshes of the different "test" diaphragm shapes.	20
4.5	On-axis sound pressure level comparison between the three different simplified membrane shapes.	20
4.6	Directivity comparison between 2 kHz and 20 kHz of the dome and flat piston.	21

4.7	Directivity comparison between a flat and dome piston.	21
4.8	On-axis sound pressure level comparison between different heights of the baffle.	22
4.9	On-axis sound pressure level comparison between simulation and measurement of baffle 1.	23
4.10	On-axis sound pressure level comparison between simulation and measurement of baffle 2.	24
4.11	25 degrees off axis sound pressure level comparison between simulation and measurement of baffle 3.	24
4.12	25 degrees off axis sound pressure level comparison between the measurement of baffle 4's three different configurations.	25
4.13	25 degrees off axis sound pressure level comparison between simulation and measurement of baffle 4's open and closed configuration.	25
4.14	Sound pressure level comparison between the measurement of all the baffles.	26
4.15	Sound pressure level comparison between the simulation of all the baffles.	27
4.16	Directivity comparison of baffle 1 between measurement and simulation.	27
4.17	Directivity comparison of baffle 2 between measurement and simulation.	28
4.18	dB difference between baffle 2 and baffle 1.	28
4.19	Mechanical representation of a piston with and without cavity.	29
4.20	Electroacoustic representation of a piston without cavity in mechanical impedance circuit.	29
4.21	Electroacoustic representation of a piston with and without cavity in acoustical impedance circuit.	30
4.22	Directivity comparison of baffle 3 between measurement and simulation.	31
4.23	Directivity comparison of open/closed baffle 4 between measurement and simulation.	31
4.24	Comparison of the standing waves patterns between the open and closed configurations of baffle 4.	32
4.25	On-axis sound pressure level comparison between simulation and measurement of baffle 1 with 3 mm thick 2 mm hole grille.	34
4.26	On-axis sound pressure level comparison between the measurement of baffle 1 with the different grilles.	35
4.27	On-axis sound pressure level comparison between the simulation of baffle 1 with the different grilles.	35
4.28	Directivity comparison between measurement and simulation of baffle 1 with 3 mm thick and 2 mm hole grille.	36
4.29	dB difference between baffle 1 with 3 mm thick and 2 mm hole grille and baffle 1 without grille.	36
4.30	Directivity comparison between measurement and simulation of baffle 1 with 3 mm thick and 4 mm hole grille.	37
4.31	dB difference between baffle 1 with 3 mm thick and 4 mm hole grille and baffle 1 without grille.	37
4.32	Directivity comparison between measurement and simulation of baffle 1 with 0.5 mm thick and 2 mm hole grille.	38

4.33	dB difference between baffle 1 with 0.5 mm thick and 2 mm hole grille and baffle 1 without grille.	38
4.34	Comparison of the resonances occurring inside the interface between all the grille configuration for baffle 1 at 9.5 kHz.	39
4.35	Comparison of the resonances occurring inside the interface between all the grille configuration for baffle 1 at 11.5 kHz.	40
4.36	Comparison of the resonances occurring inside the interface between all the grille configuration for baffle 1 at 13.2 kHz.	40
4.37	Comparison of the extended pressure maps between the 3 mm thick 2 mm hole grille and without grille for baffle 1 at 13.2 kHz.	41
4.38	On-axis sound pressure level comparison between simulation and measurement of baffle 2 with 3mm thick 2mm hole grille.	42
4.39	On-axis sound pressure level comparison between the measurement of baffle 2 with the different grilles.	42
4.40	On-axis sound pressure level comparison between the simulation of baffle 2 with the different grilles.	43
4.41	Directivity comparison between measurement and simulation of baffle 2 with 3 mm thick and 2 mm hole grille.	43
4.42	dB difference between baffle 2 with 3 mm thick and 2 mm hole grille and baffle 2 without grille.	44
4.43	Directivity comparison between measurement and simulation of baffle 2 with 3 mm thick and 4 mm hole grille.	44
4.44	dB difference between baffle 2 with 3 mm thick and 4 mm hole grille and baffle 2 without grille.	45
4.45	Directivity comparison between measurement and simulation of baffle 2 with 0.5 mm thick and 2 mm hole grille.	45
4.46	dB difference between baffle 2 with 0.5 mm thick and 2 mm hole grille and baffle 2 without grille.	46
4.47	Comparison of the resonances occurring inside the interface between all the grille configuration for baffle 2 at 6.1 kHz.	46
4.48	Comparison of the resonances occurring inside the interface between all the grille configuration for baffle 2 at 9 kHz.	47
4.49	Comparison of the resonances occurring inside the interface between all the grille configuration for baffle 2 at 11 kHz.	47
4.50	Comparison of the resonances occurring inside the interface between all the grille configuration for baffle 2 at 14 kHz.	48
4.51	25 degrees off axis sound pressure level comparison between simulation and measurement of baffle 3 with 3 mm thick 2 mm hole grille.	48
4.52	25 degrees off axis sound pressure level comparison between the measurement of baffle 3 with the different grilles.	49
4.53	25 degrees off axis sound pressure level comparison between the simulation of baffle 3 with the different grilles.	49
4.54	Directivity comparison between measurement and simulation of baffle 3 with 3 mm thick and 2 mm hole grille.	50
4.55	dB difference between baffle 3 with 3 mm thick and 2 mm hole grille and baffle 3 without grille.	50

4.56	Directivity comparison between measurement and simulation of baffle 3 with 3 mm thick and 4 mm hole grille.	51
4.57	dB difference between baffle 3 with 3 mm thick and 4 mm hole grille and baffle 3 without grille.	51
4.58	Directivity comparison between measurement and simulation of baffle 3 with 0.5 mm thick and 2 mm hole grille.	52
4.59	dB difference between baffle 3 with 0.5 mm thick and 2 mm hole grille and baffle 3 without grille.	52
4.60	Comparison of the resonances occurring inside the interface between all the grilles configuration for baffle 3 at 6 kHz.	53
4.61	Comparison of the resonances occurring inside the interface between all the grilles configuration for baffle 3 at 10.5 kHz.	53
4.62	Directivity comparison before and after on-axis frequency equalization for baffle 2.	54
4.63	Directivity comparison before and after on-axis frequency equalization for baffle 2 with 3 mm thick 2 mm hole grille.	54
4.64	Directivity comparison before and after 25 degrees off axis frequency equalization for baffle 3.	55
4.65	Directivity comparison before and after 25 degrees off axis frequency equalization for baffle 2 with 3 mm thick 2 mm hole grille.	55
4.66	Directivity comparison before and after 25 degrees off axis frequency equalization for baffle 4 open.	56
A.1	Measurement of the background noise in the anechoic chamber.	II
A.2	25 degrees off axis sound pressure level comparison between the simulation of baffle 4's three different configurations.	III
A.3	Directivity comparison between measurement and simulation of baffle 1 with 3 mm thick and 4 mm hole.	IV
A.4	Directivity comparison between measurement and simulation of baffle 1 with 0.5 mm thick and 2 mm hole.	IV
A.5	Directivity comparison between measurement and simulation of baffle 2 with 3 mm thick and 4 mm hole.	V
A.6	Directivity comparison between measurement and simulation of baffle 2 with 0.5 mm thick and 2 mm hole.	V
A.7	25 degrees off axis sound pressure level comparison between simulation and measurement of baffle 3 with 3 mm thick 4 mm hole grille.	VI
A.8	25 degrees off axis sound pressure level comparison between simulation and measurement of baffle 3 with 0.5 mm thick 2 mm hole grille.	VII
A.9	Comparison of the extended pressure maps between the 3 mm thick 2 mm hole grille and without grille for baffle 2 at 13.5 kHz.	VII

List of Tables

3.1	Thiele and Small parameters of tweeter	13
4.1	RMS error for the different interfaces in dB.	33
4.2	RMS error for the different grilles on baffle 1 in dB.	34
A.1	RMS error for the different grilles on baffle 2 in dB.	VI
A.2	RMS error for the different grilles on baffle 3 in dB.	VII

1 Introduction

Nowadays audio performance is crucial within the premium automotive industry and it is not acceptable to have a bad sounding set up. Traditionally the audio system was measured and tuned based on physical prototypes and finally fine-tuned by subjective evaluation.

As physical prototyping of cars is time consuming, costly and has limited availability within the whole company, a different procedure can be implemented to overcome these problems. Computer Aided Engineering softwares and computer hardware are becoming more efficient and versatile, allowing engineers to design and iterate virtually before any physical prototypes.

The ultimate goal is the Auralization of the car's acoustic performance based on the CAD design drawings. However there are a lot of different problems to tackle, like the estimation of the surface impedance of the different materials, loudspeaker description, body flexibility, simulation methods and finally verifying with physical measurements.

This Master thesis will focus mainly on the modeling of tweeters and how their installation details, grilles, cavities and nearby reflecting surfaces will affect their radiation and directivity performance. The investigation is made through the development of CAE models corresponding to the physical experiment. Then it will be validated with experimental measurement. Some of the issues faced during modeling and measurement will also be discussed as the study is done at high frequencies.

Some previous work was done on this subject. First a paper titled "Numerical Methods for Loudspeaker Installation Effects Prediction: Detailed Evaluation on a Car Door Model" presented at the Hong-Kong Inter Noise conference in 2017. This paper is more focused on the lower frequencies with larger loudspeakers and how they interact with a car door. Another paper closely related to this thesis is titled "On acoustical modeling and validation of automotive loudspeaker grilles" presented at the San Francisco Audio Engineering Society conference in 2017. This paper focuses on tweeters, however it takes into account only one grille and one interface.

The report is organized the following way. First, theory will be shortly summarized into key-points that are crucial to understanding the physics behind the CAE software. Second, the methods used for the measurement procedures and the simulation parameters. Third the results will be shown and discussed, they are organized in three parts, the preliminary testing of the software/measurement setup, the different interfaces and the different grilles. Finally the conclusion and future work will be proposed.

2 Theory

2.1 Finite Element Method

Actran is a finite element acoustic simulation commercial software used at Volvo cars. The non-homogeneous Helmholtz equation (2.1) is solved in a discretized space with suitable boundary conditions between the nodes to compute the sound pressure at specific points in space. The Helmholtz equation comes after computing the Fourier transform of the time domain wave equation [1]. The nodes are the discretized points where the equation is exactly solved, interpolation is used between the nodes to approximate the results.

$$\nabla^2 p(x, y, z, w) + k^2 p(x, y, z, w) = Q(x, y, z, w) \quad (2.1)$$

where p being the pressure, $\nabla^2 = \frac{\partial^2}{\partial x^2} + \frac{\partial^2}{\partial y^2} + \frac{\partial^2}{\partial z^2}$, k is the acoustical wave number and Q the exiting source term inside the domain [1]. Note that the equation 2.1 is valid only for a stationary fluid.

Mapping all over the discretized nodes and arranging the equations for each node with the proper boundary conditions will result in the matrix equation (2.2)

$$(\mathbf{K} + iw\mathbf{C} - w^2\mathbf{M})\mathbf{x}(w) = \mathbf{F}(w) \quad (2.2)$$

where \mathbf{K} , \mathbf{C} and \mathbf{M} are the stiffness, damping and mass matrices respectively and \mathbf{F} the force excitation vector and \mathbf{x} the nodal unknown vector, in this case it will be the pressure [2].

The limiting factor of FEM is how many discretized nodes can be solved at the same time. Increasing discretized nodes will make the matrices \mathbf{K} , \mathbf{C} , \mathbf{M} and \mathbf{F} larger and require more memory and run time to solve. FEM is usually not run at high frequencies as the domain needs to be discretized in smaller steps so that the results at higher frequencies are accurate.

2.2 Exterior Acoustic domains

To simulate free field condition, Actran has two built-in functions to build a domain mesh around the radiating structure, Infinite Element Domain and Perfectly Matched Layer. These special functions are used because putting a pressure release boundary conditions at the end of the finite element domain is not correct to simulate an anechoic chamber. There should be a gradual absorption of the sound pressure to have a relatively correct impedance change compared to free field condition.

2.2.1 Infinite Element Domain

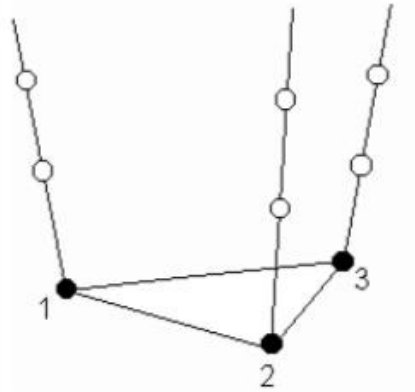


Figure 2.1: Topology of triangle-based infinite elements showing the finite nodes (black) and the infinite nodes (white) [2].

Infinite Element Domain creates a finite element domain around the radiating structure. Then the infinite elements are created in the radial direction of the convex shell of the finite element (Figures 2.1, 2.2). The number of infinite nodes depends on the radial interpolation order set by the user. The infinite nodes will have a special shape function to discretize the growth to infinite.

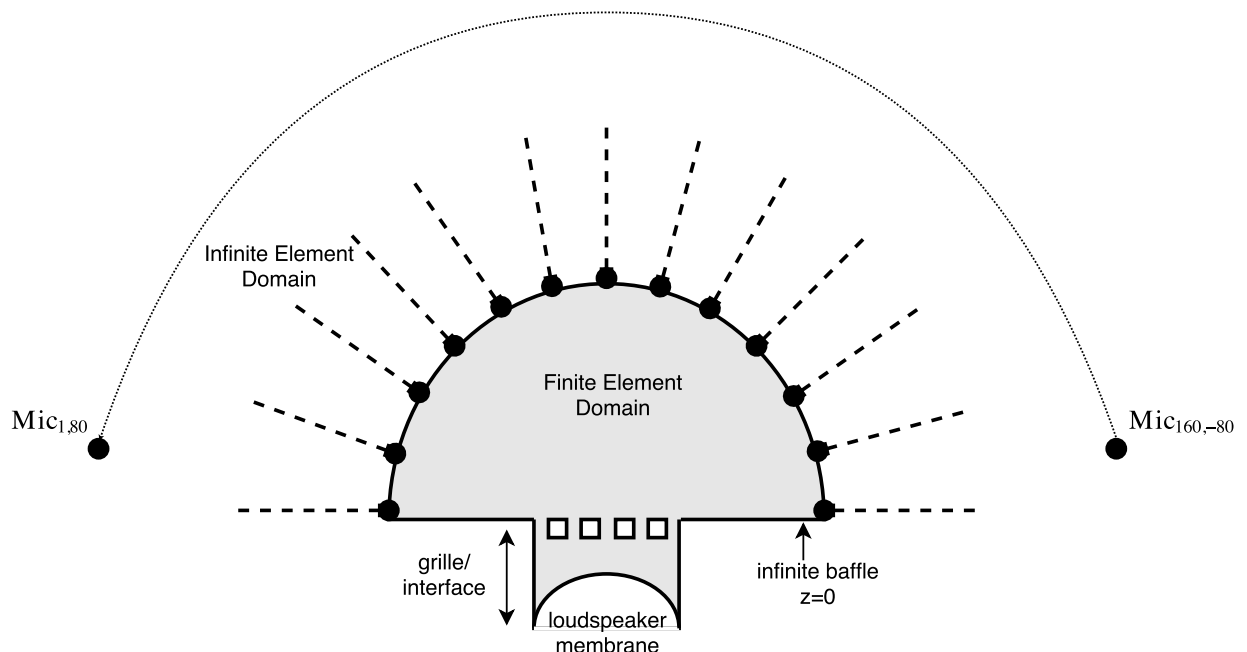


Figure 2.2: Simplified diagram of the simulation model using Infinite Element Domain.

2.2.2 Perfectly Matched Layer

PML is a different approach to the non-reflection boundary condition problem. The interior acoustics domain is the same as the finite element domain. An external PML domain is added with an extreme absorbing property, so that when the incident sound wave reaches the PML domain boundary condition the amplitude of the reflected wave in the Interior Acoustics Domain has relatively low amplitude. The far field sound pressure is then calculated using a Ffowcs-Williams and Hawking integral formulation [2].

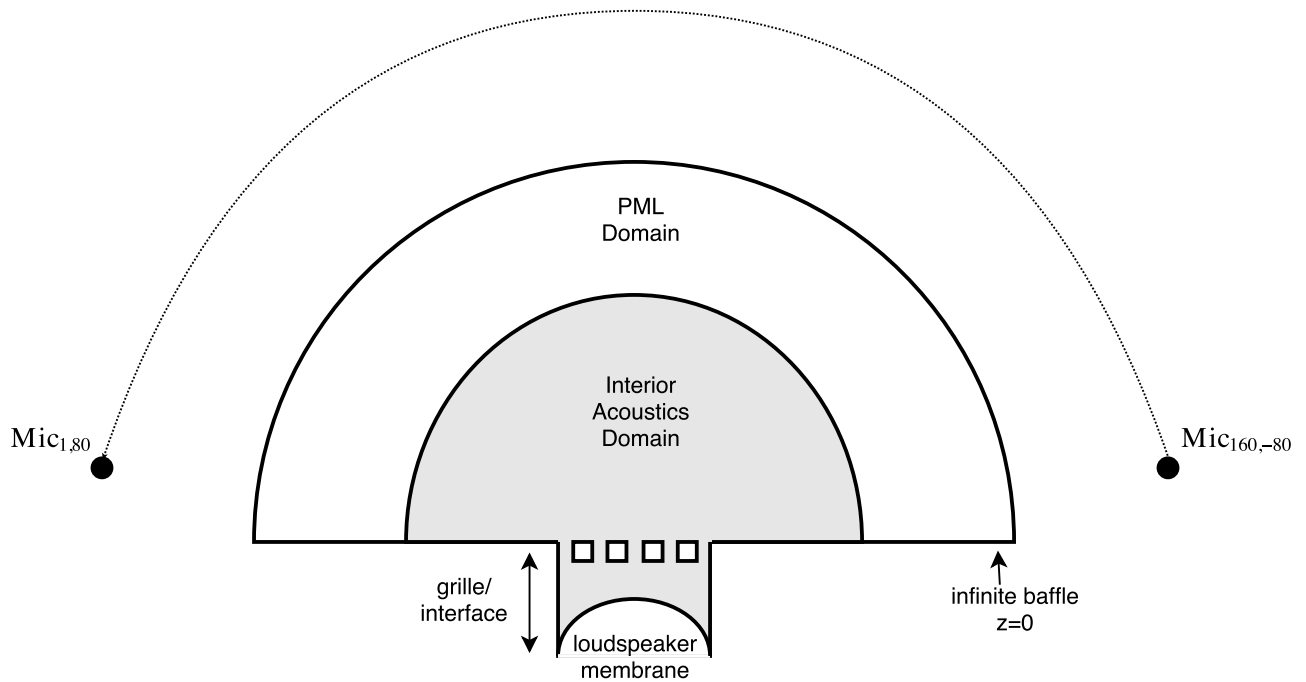


Figure 2.3: Simplified diagram of the simulation model using Perfectly Matched Layer.

2.3 Electroacoustic

This section presents a brief summary of electroacoustics theory. In this paper the focus is mainly applied to tweeter speakers. As it is seen in Figure 2.4 different diaphragm sizes handle different frequencies more efficiently. Large diaphragm speakers called Woofers radiate low frequencies while small diaphragm speakers called Tweeters radiate high frequencies. Electrical filters take care of the crossover frequency between the different speakers.

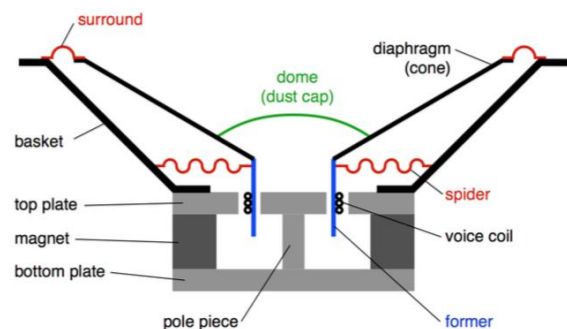


Figure 2.4: Different speaker names [3].

Figure 2.5 shows the inside of a common speaker. The general functioning mechanism of a speaker is the change of magnetic field when the voice coil is supplied with voltage or current. It will make the former, attached to the voice coil, to move with the diaphragm which will radiate sound waves. The surround acts as a suspension mechanism. The spider and the pole piece allow the former to move only in one degree of freedom. The materials used for diaphragms are usually stiff and well dampened to reduce structural resonance. But they also have to be light to have a quick transient response.



(a) Cross-section of a speaker [3].



(b) Diagram of the general parts in a speaker [3].

Figure 2.5: Common speaker configuration.

Thiele and Small parameters [4], [5] are used to describe and simplify the behavior of a loudspeaker if the wavelengths it generates are larger than its components. Then

it can be considered as a rigid piston having one transnational degree of freedom. Thus its response can be represented by a lumped electrodynamic circuit (Figure 2.6) that represents the electrical, mechanical and acoustical domains.

The Thiele and Small parameters of interest here are:

- R_c The DC resistance of the driver voice coil. [Ω]
- L_c The inductance of the driver voice coil. [H]
- B Magnetic flux density in driver air gap. [T]
- l Length of voice coil conductor in magnetic field. [m]
- M_{ms} moving mass of the driver including air load. [kg]
- C_{ms} compliance of the driver's suspension. [m/N]
- R_{ms} the mechanical resistance of the driver's suspension. [Ns/m]
- S_d surface area of the diaphragm. [m²]

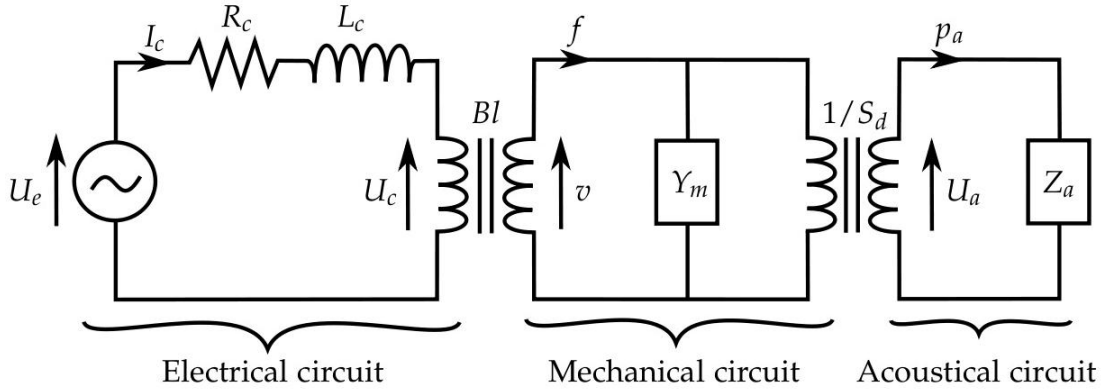


Figure 2.6: Electrodynamic model of a loudspeaker considering lumped elements [2].

U_e is the input voltage to the loudspeaker, I_c the electrical circuit current, U_c the voltage across the voice coil, v the velocity of the diaphragm, f the force applied on the diaphragm and surrounding air, Y_m is the mechanical admittance such as $Y_m = \frac{1}{R_{ms}} + \frac{1}{j\omega M_{ms}} + j\omega C_{ms}$, p_a is the generated acoustic pressure, U_a is the acoustic velocity.

The electrical and mechanical domains are linked by the relation:

$$f = BlI_c \quad (2.3)$$

The mechanical and acoustic domains are linked by the relation

$$p_a = \frac{f}{S_d} \quad (2.4)$$

Both relations are represented by a transformer in the circuit.

$Z_a = R_a + jX_a$ is the acoustic impedance composed of the radiation loss factor R_a which represents the radiated power into the environment and X_a is the energy stored in the near-field.

3 Methods

3.1 Measurement setup

The measurements were done in the anechoic chamber in the Applied Acoustics Division at Chalmers University of Technology.

Matlab was used as the data acquisition software. The data acquisition hardware was National Instruments' NI 9234 used with a sampling frequency of 51.2 kHz. The sound card was a M-AUDIO MobilePre with a sampling frequency of 44.1 kHz. The microphone was a B&K Free field 1/2" Type 4190 (Serial number 2455390). The Preampifier was a 1/2" B&K Type 2669-C (Serial number 3084953). The microphone amplifier is B&K Type 1708. The speaker amplifier was a NAD Stereo Integrated Amplifier 310.

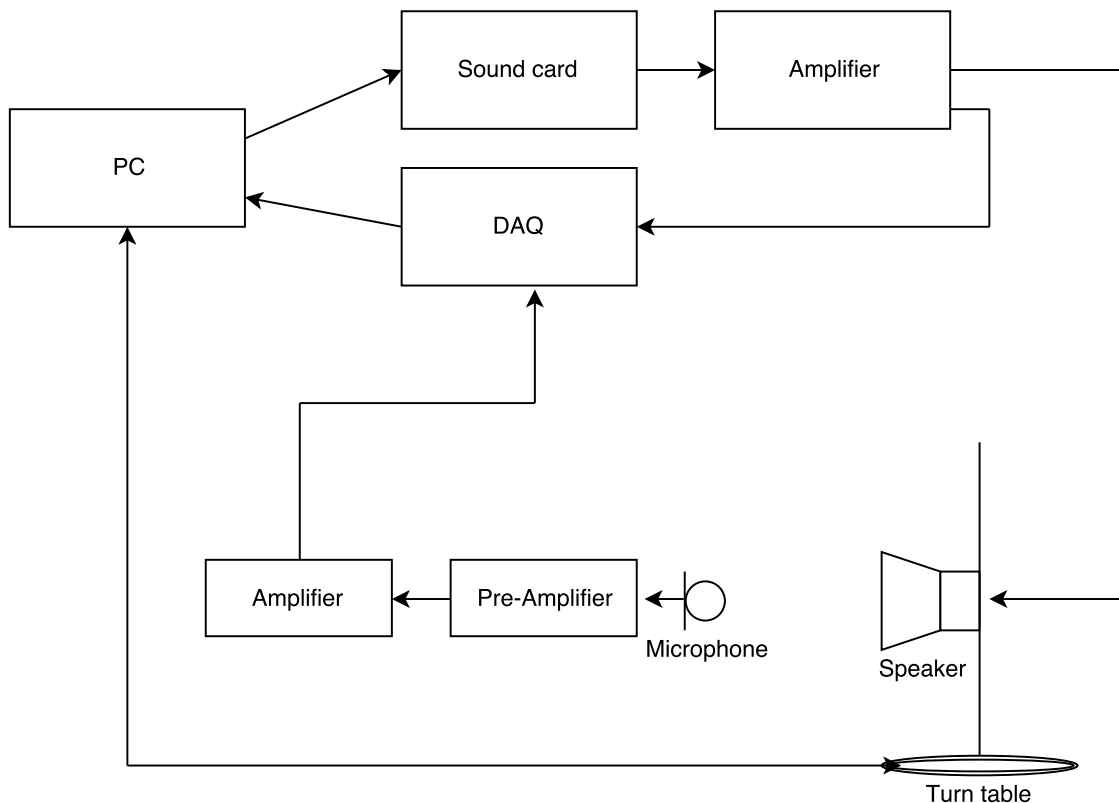


Figure 3.1: Sketch of the measurement setup.

3. Methods

The tweeter is a 25 mm Bowers&Wilkins speaker made for Volvo Cars (Figure 3.2). The frequency range of interest is from 2 kHz to 20 kHz. The unit is built in with a high pass capacitor to protect it from low frequencies. The capacitor was removed to reduce the error variables and to make the simulation simpler.



Figure 3.2: Picture of the Tweeter.

Four different 3D printed baffles were used. Each has a different interface with the tweeter (Figure 3.3). Baffle 1 is a straight mounting. Baffle 2 is a straight horn. Baffle 3 is an angled horn. Baffle 4 is an example of a bad mounting that might occur in the car industry. Both Baffle 3 and 4 are angled 25 degrees.

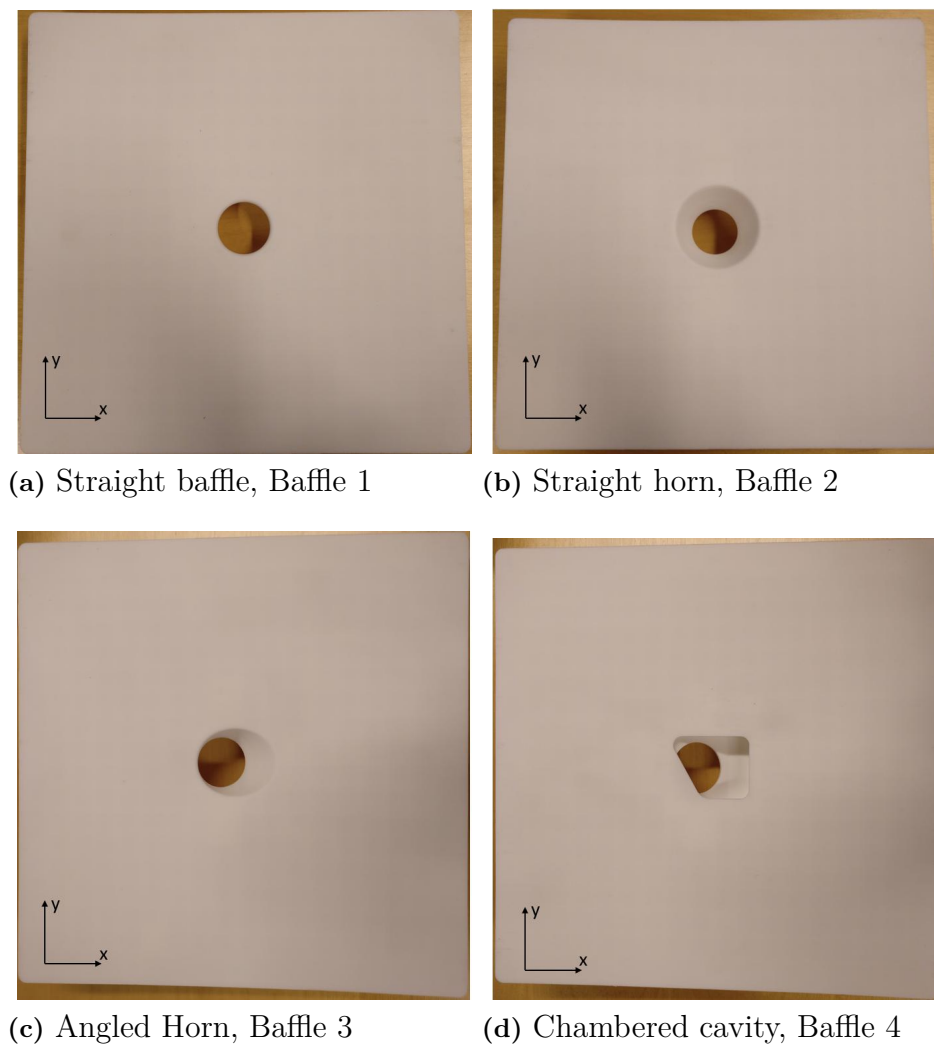


Figure 3.3: Pictures of the four different interfaces.

Baffle 4 has a chamber inside it that can be closed with different modules (Figure 3.4). This baffle was made this way because it represents a close to real life installation of tweeters in cars. The chamber is there to try to simulate a gap in the packaging.

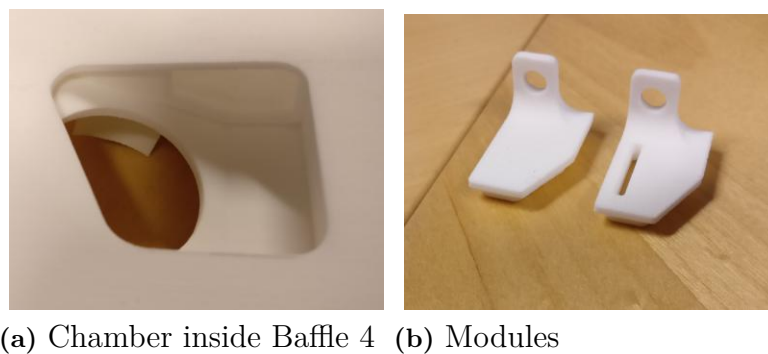


Figure 3.4: Baffle 4 detail.

3. Methods

Three different grilles with hexagonal holes were used. They were 3D printed as 3 millimeters plates with the grille in the middle. The grille plate was fixated with butyl tape to the 3D printed baffles.



Figure 3.5: Picture of the 3 mm thickness and 2 mm hole grille.

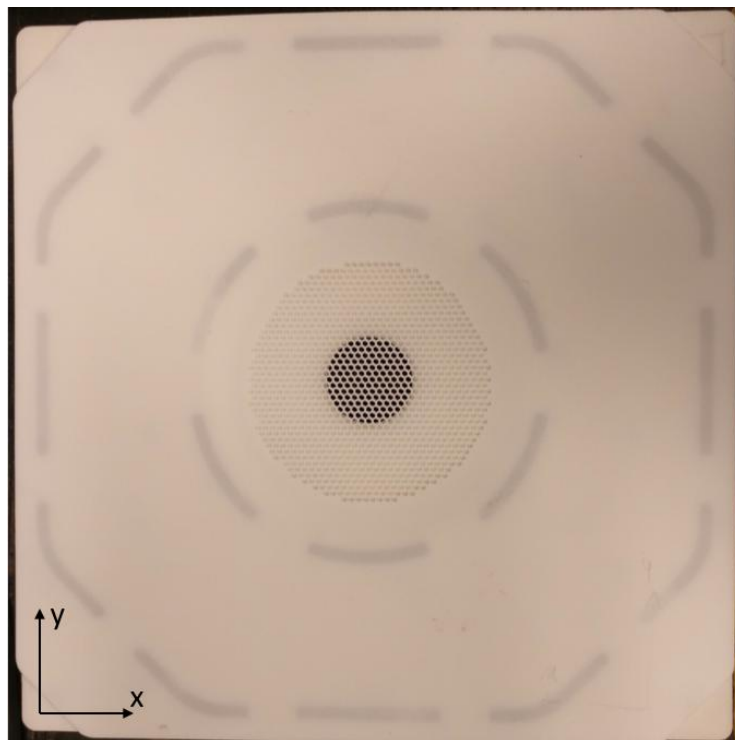


Figure 3.6: Picture of the 0.5 mm thickness and 2 mm hole grille.

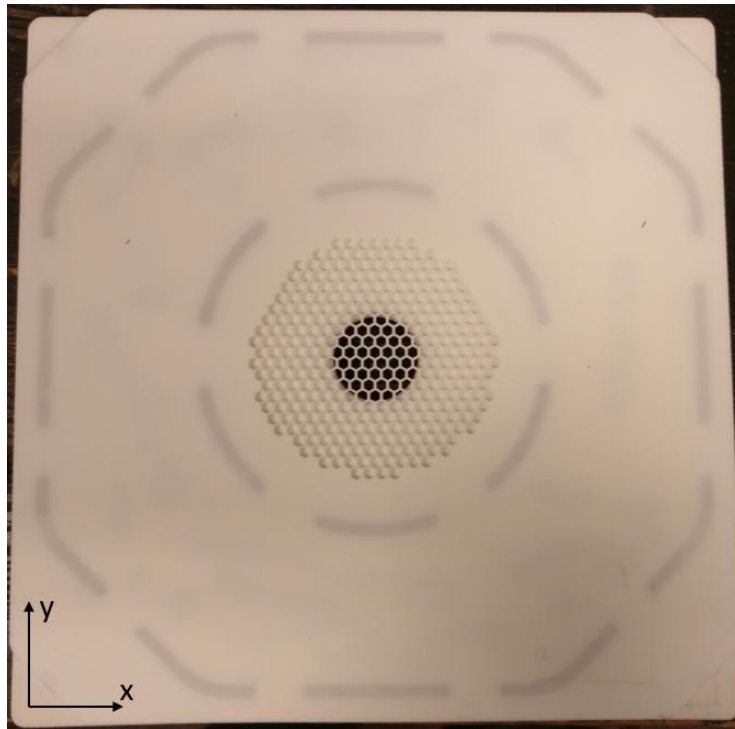


Figure 3.7: Picture of the 3 mm thickness and 4 mm hole grille.

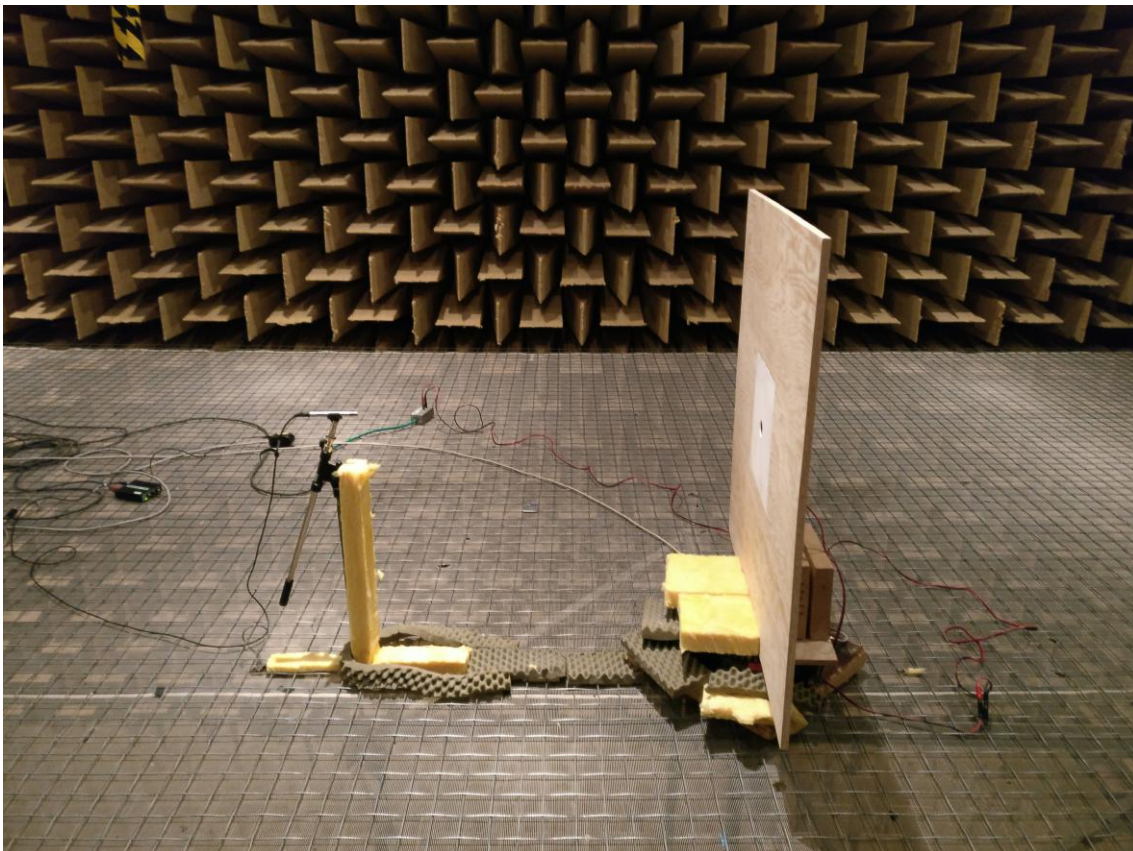


Figure 3.8: Picture of the measurement setup without edge absorption.

3. Methods

The 3D printed modules are mounted in the middle of a 1x1 meter 15 mm thickness plywood baffle. The microphone was placed 1 meter away from the baffle and facing the tweeter on axis. Some absorbers were added to reduced any unwanted reflections to the microphone. The first measurement was done without edge absorbers (Figure 3.8) and the response of the tweeter was not smooth.

Some absorbers were added to the edges of the baffle (Figure 3.9) to reduce the edge reflections. The comparison will be shown in the Preliminary Results Section.

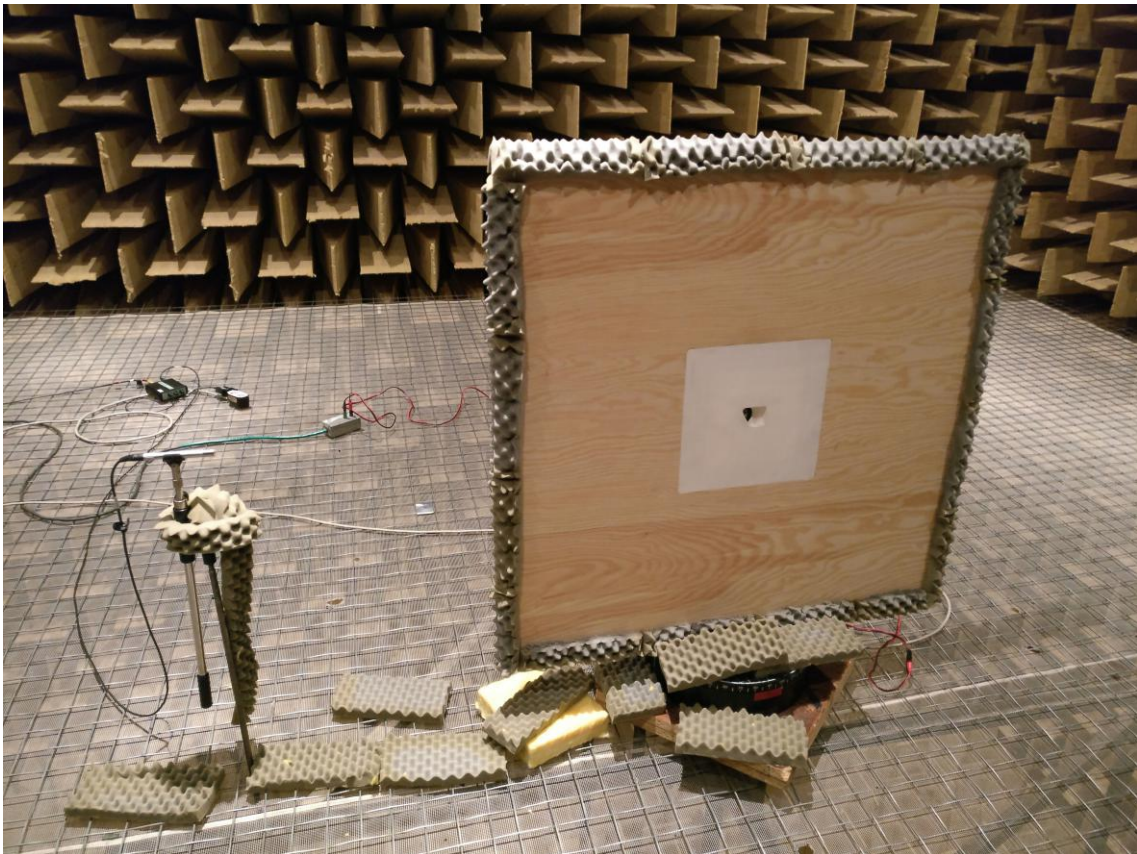


Figure 3.9: Picture of the measurement setup with edge absorption.

The background noise in the anechoic chamber was measured and can be found in the Appendix.

First the microphones were calibrated. Then two measurements were carried out. One on axis measurement with a logarithmic sin sweep of 4 seconds and one 180 degrees directivity measurement with an angle step of 5 degrees and a logarithmic sin sweep of 1 second.

All four baffles were measured. Then the three different grilles were measured each time on Baffle 1, Baffle 2 and Baffle 3.

3.2 Simulation

Actran provides two different ways to model a loudspeaker driver. The first one is to model the whole unit as a structural element knowing all the material properties of each different mechanical element of the driver. This method has a higher computational cost than the second method. It was not investigated because the supplier of the tweeter did not want to disclose the material properties. The second method is a Thiele and Small driver approximation. It takes as input the Thiele and Small parameters explained in the Theory Section and it assume the meshed surface area of the diaphragm as a rigid piston moving in one degree of freedom. More details are available in Actran's manual [2].

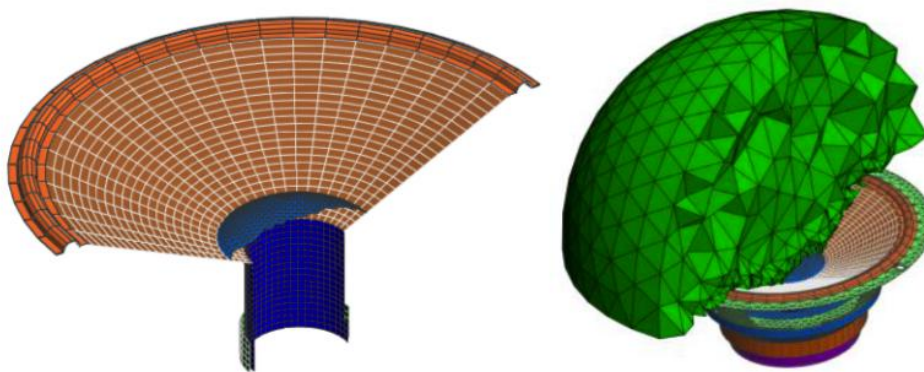


Figure 3.10: First method (on the right) and second method (on the left) to model a loudspeaker [7].

The second method will be less accurate at higher frequencies. But even though this study is at high frequencies, the driver is a 25 mm tweeter. So some inaccuracies might start to occur at around 12-13 kHz, when roughly half the wavelength will fit the diameter of the projected surface area.

The table below shows the supplier provided Thiele and Small parameters for the tweeter units. Note that these might slightly differ from the actual used tweeter as they might be from a different production batch.

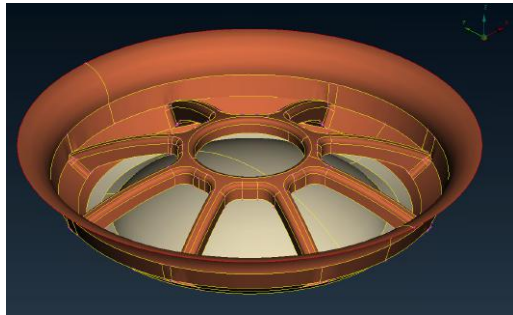
	Unit
R_c (Ω)	6.91
L_c (mH)	0.037
Bl (N/A)	2.143
M_{ms} (g)	0.238
C_{ms} (mm/N)	0.056
R_{ms} (kg/s)	2.735
S_d (mm ²)	772.5

Table 3.1: Thiele and Small parameters of tweeter

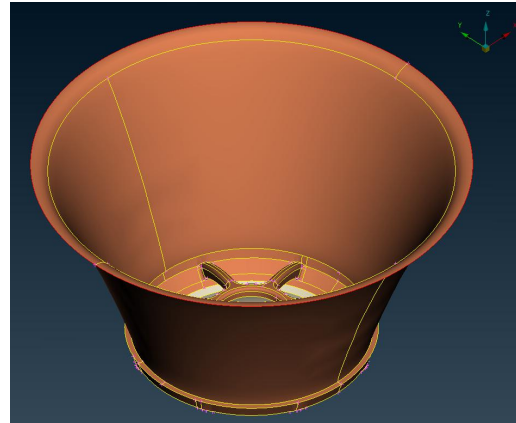
Note that all the simulations were done in mm/tonne, so some conversions were made to the SI units provided, according to the SI basic units [6]. Also M_{ms} is taken

3. Methods

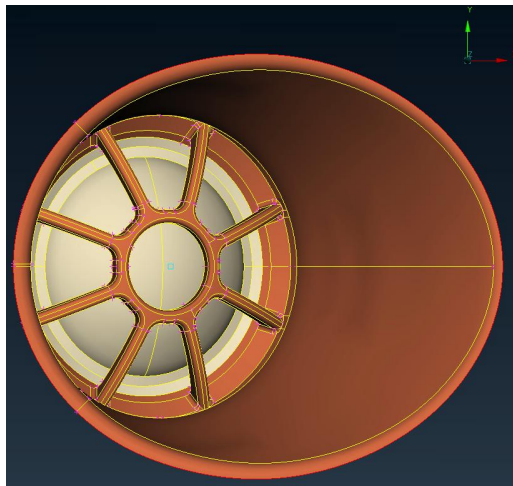
without the air-load as the mass of the air is taken into account when coupling the air mesh to the membrane.



(a) Baffle 1



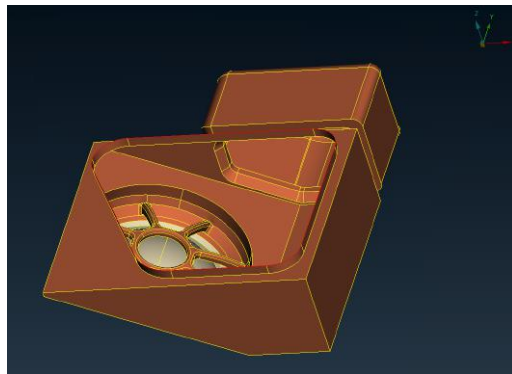
(b) Baffle 2



(c) Baffle 3



(d) Baffle 4 closed



(e) Baffle 4 open

Figure 3.11: Meshes of the different interfaces.

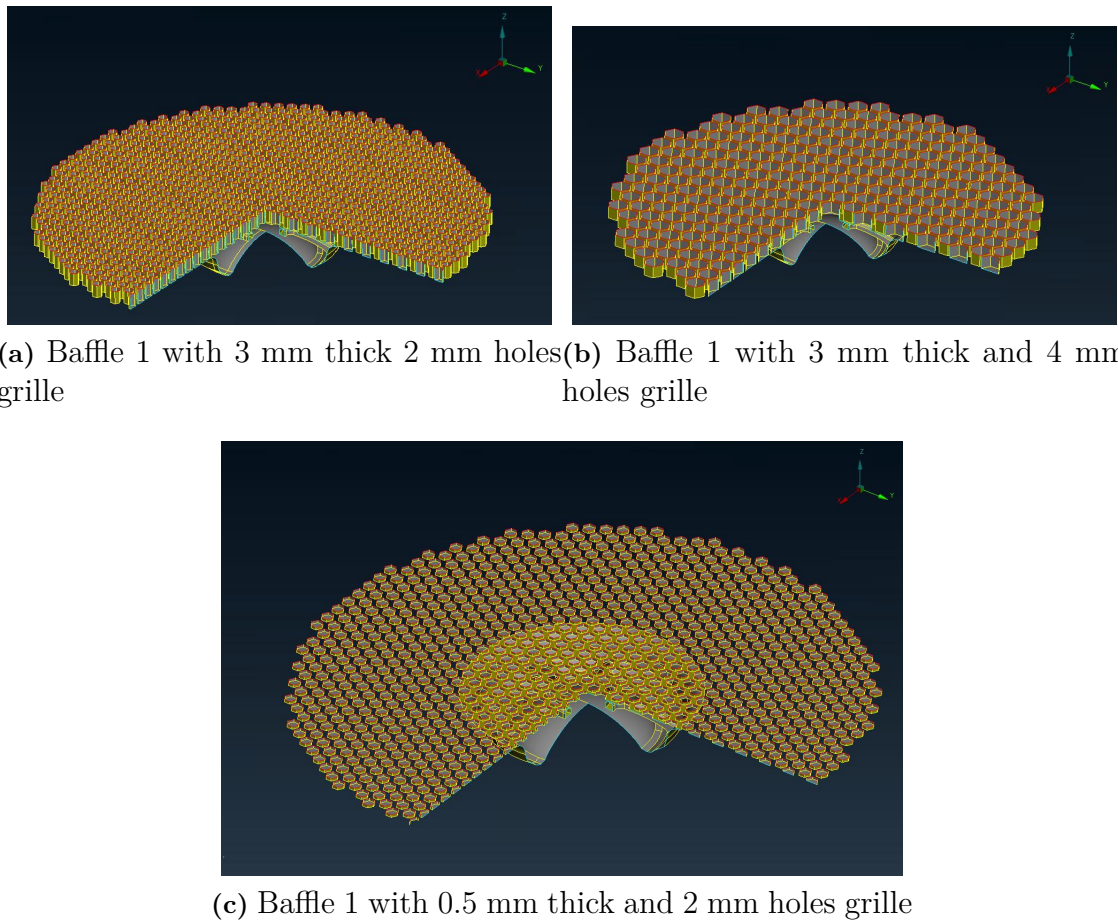


Figure 3.12: Meshes of the different grilles on baffle 1

The 3D models from the baffles, grilles and tweeter were provided by Volvo Cars. They were assembled, cleaned and meshed in Ansa (meshing software) before using them in Actran.

The tweeter membrane which is represented with the beige color in Figure 3.11 will be linked with the Model Driver function in Actran. While the brown color surfaces will bound the air fluid volume mesh (represented by the gray color, see Figure 3.14) that will be automatically generated by Actran with the Exterior Acoustic function. The mesh parameters of the tweeter membrane and boundary are

- 0.5 millimeters average distance between nodes
- 1st order element
- Triangular mesh type

The Exterior Acoustic function has multiple parameters. One of them is the adaptive exterior acoustic domain function. Basically Actran will create a mesh for each frequency band defined by the user to keep approximately the same number of nodes for each frequency band. So the running time and the error range will be approximately the same between a huge frequency range (Figure 3.13).

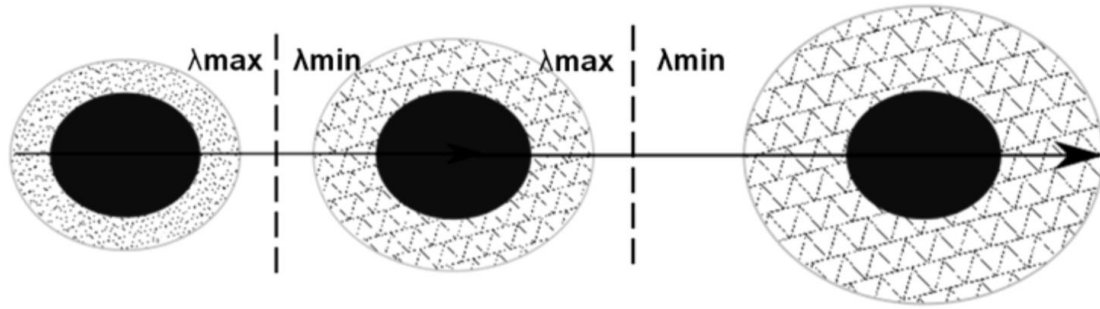


Figure 3.13: Adaptive mesh generation for different frequency bands [2].

After multiple trials these were the optimal parameters for a relatively fast and accurate computation.

- Infinite Element Domain
- 1.0 Thickness relative to wavelength
- 15 Elements per wavelength
- 10 Interpolation order
- Tetrahedron mesh type
- Adaptive mesh in Third Octave parts
- 1.2 Mesh Gradation

Some comparison will be discussed in the Preliminary Results part.

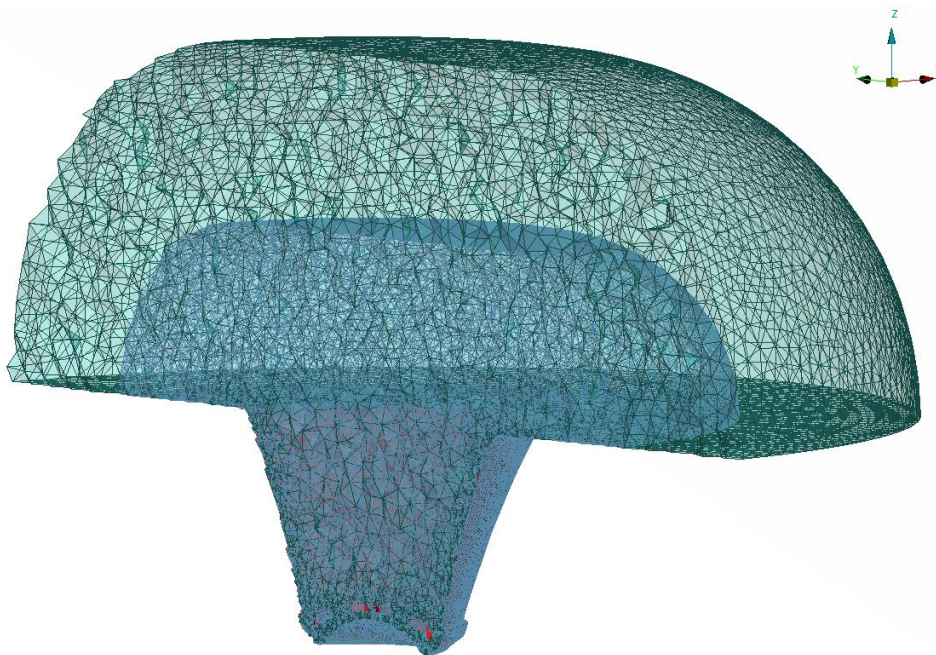


Figure 3.14: Automatic mesh generation by Actran for Baffle 2 at the frequency bands 5 kHz-6.3 kHz and 8 kHz-10 kHz.

The automatic mesh creation requires the user to align properly the structural mesh with the baffle. An infinite baffle will be placed at $Z=0$ to simulate the limited plywood baffle in measurement. No faces should be aligned with the infinite baffle.

Also the structural mesh has to have an enclosed volume or the mesh creation won't work. The grilles mesh were harder to make work as the back-plate had to be removed. After some tweaking to the CAD drawings it worked (Figure 3.15).

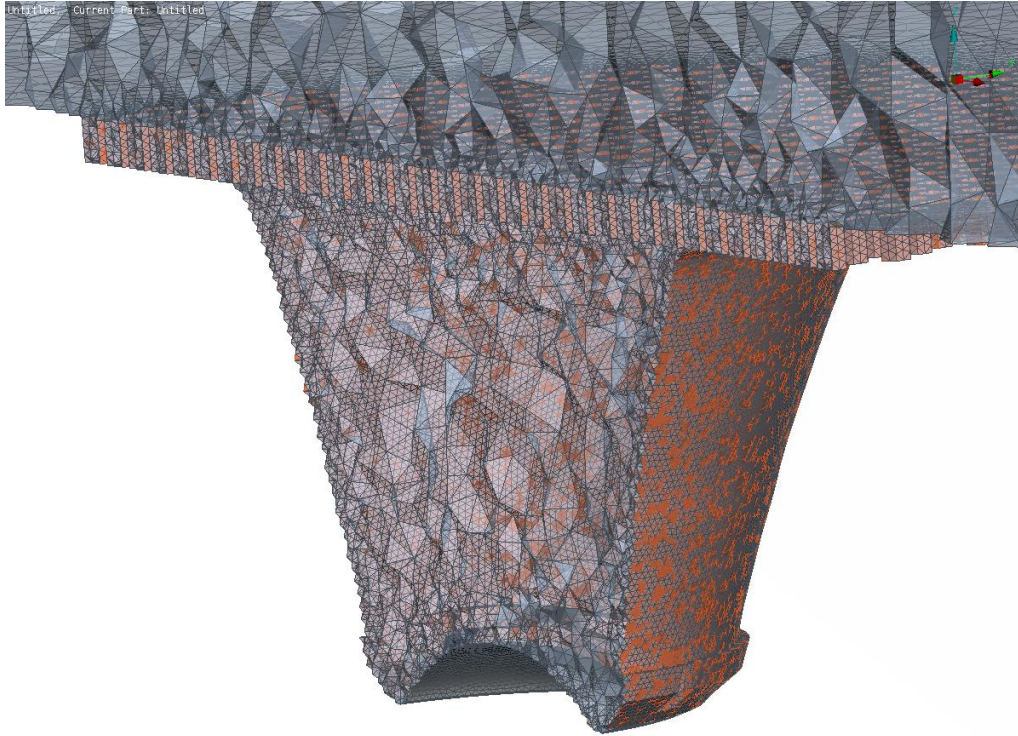


Figure 3.15: Automatic mesh generation by Actran for Baffle 2 with the 3 mm thickness 2 mm holes grille at the frequency band 5 kHz-6.3 kHz.

Two simulations were run from 2 kHz to 20 kHz, one with a step of 10 Hz for the directivity simulation at 1 meter, the other with a step of 100 Hz for the field points inside the cavity to visualize resonances as pressure maps .

Parallel frequency computing was used to accelerate run times. 32 threads were used on eight machines for each simulation. The 10 Hz step simulation ran for approximately an hour while the grille meshes ran for 2.5-3 hours. The 100 Hz step simulation ran for 7 minutes and 15 minutes for the grille meshes. The baffles without the grilles were less computationally heavy. It makes sense as the grille meshes have more nodes and the volume mesh is finer not only near the interface but also near the grilles (Figure 3.15). Note that the run times is an approximation as it differs from interface to interface due to the different numbers of nodes.

4 Results & Discussions

4.1 Preliminary testing

Theses preliminary results shows a fast summary of the thought process and early results to simple models/early measurements before going to the real interfaces and grilles.

After adding edge absorbers as mentioned in the Method Section, the response of the tweeter is a bit smoother with them (Figure 4.1), mainly from 2 kHz to 2.1 kHz the 5 dB jump was reduced to 2 dB. So the absorbers were left on the baffle for all the remaining measurements.

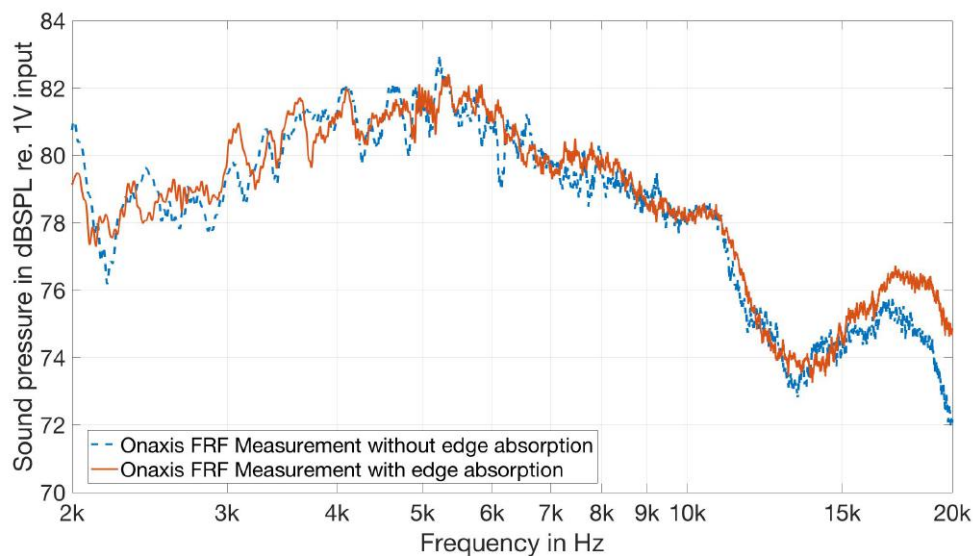


Figure 4.1: Sound pressure level comparison of the tweeter with and without edge absorbers.

After removing the built-in capacitor (Figure 4.2), its high pass effect is clearly shown. There is around a 7 dB difference at 2 kHz and 2 dB difference at 5 kHz. To reduce propagation of error and additional complexity in simulation, the capacitor was removed.

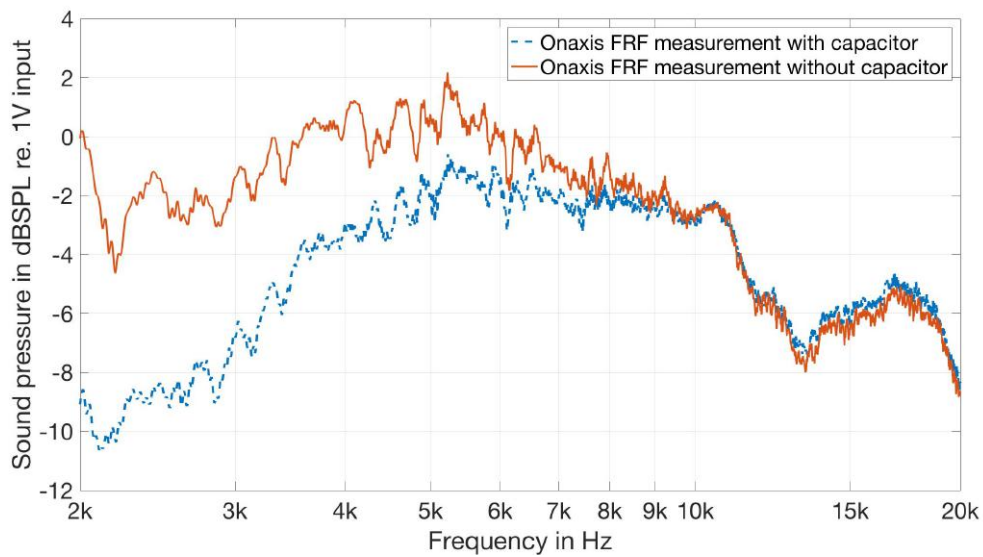


Figure 4.2: Sound pressure level comparison level of the tweeter with and without capacitor.

After running different simulations with different mesh parameters and boundary conditions (PML vs IFE) the parameters of the red curve (Figure 4.3) were chosen because it had the smoother response with respect to run time. It can be seen that the PML boundary condition is quite sinusoidal and when the thickness of the domain is higher for IFE the response is also sinusoidal. After some discussion with the FFT support (Company of Actran), the conclusion was that for larger sized domains PML gave better results while IFE was better for smaller sized domains. The frequency of the sinusoidal part of the response is inversely proportional to the radius of the domain.

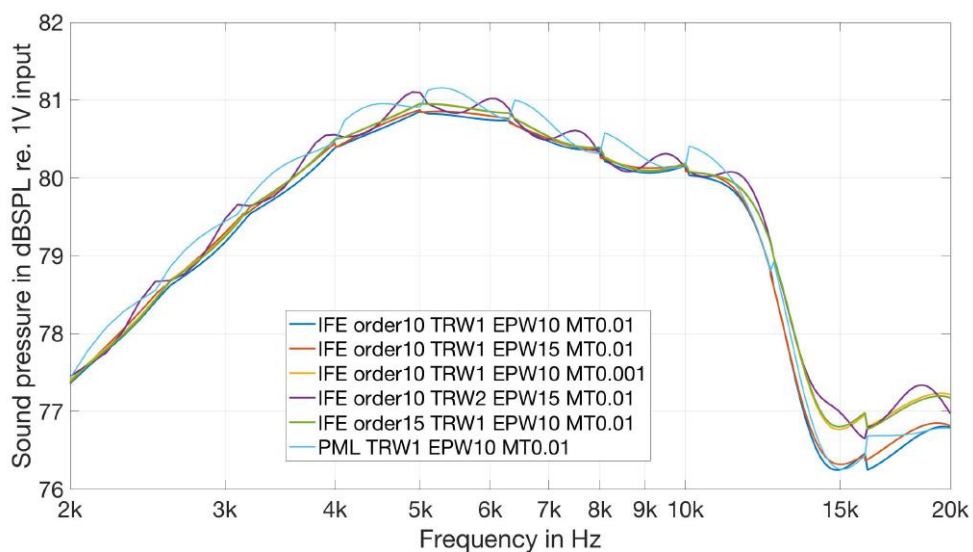


Figure 4.3: On-axis sound pressure level comparison between different mesh parameters.

During the initial simulation runs, we wondered how will the shape of the moving membrane affect the response at 1 meter. So three different membrane meshes were created (Figure 4.4) to see how the sound pressure level will change.

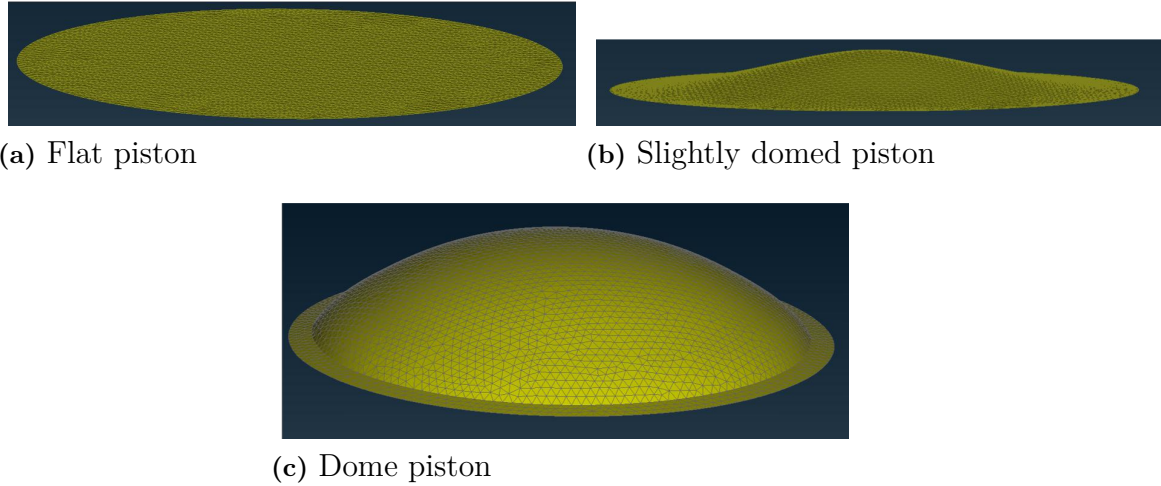


Figure 4.4: Meshes of the different "test" diaphragm shapes.

It can be seen from Figure 4.5 that at lower frequencies the response is similar then the difference gets higher steadily with the frequency increase. This makes sense as the higher the frequency, the lower the wavelength will be, and the membrane will start acting as multiple sound sources. So taking the dome piston at higher frequencies, there are less normal points aiming directly at the on-axis microphone point compared to the flat piston. Note that the small discontinuities represents the change of meshes due to the adaptive exterior acoustic mesh function discussed in the Method Section.

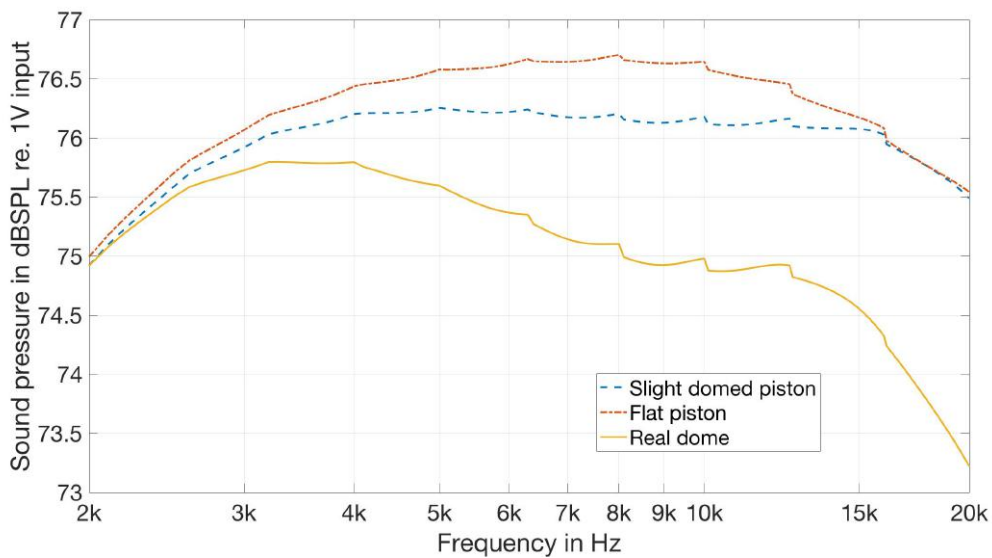


Figure 4.5: On-axis sound pressure level comparison between the three different simplified membrane shapes.

Another aspect that is crucial is the directivity of a speaker. The polar plot for the flat and dome membrane is shown in Figure 4.6. The tweeter is omnidirectional at lower frequencies and becomes more directional at higher frequencies. The flat piston follow well the theoretical radiation patterns while the dome membrane is more omnidirectional at higher frequencies than the flat piston. The problem with polar plots is to represent the overall frequency directivity response. So color plots will be used to show the sound pressure directivity over angle and frequency.

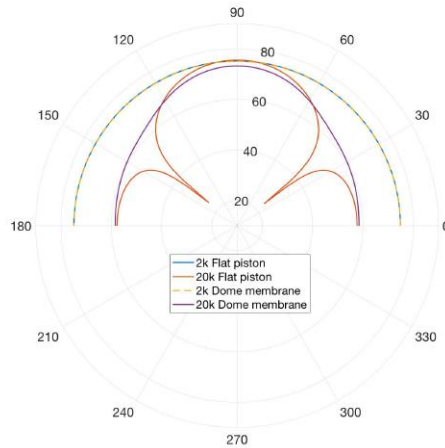


Figure 4.6: Directivity comparison between 2 kHz and 20 kHz of the dome and flat piston.

Each vertical line in the color plot represents a polar plot. From Figure 4.7, the flat piston is more directional on-axis then the dome piston. The dome piston is diffusing better the sound. This is usually why tweeter membranes have a dome membrane to make them more omnidirectional at higher frequencies.

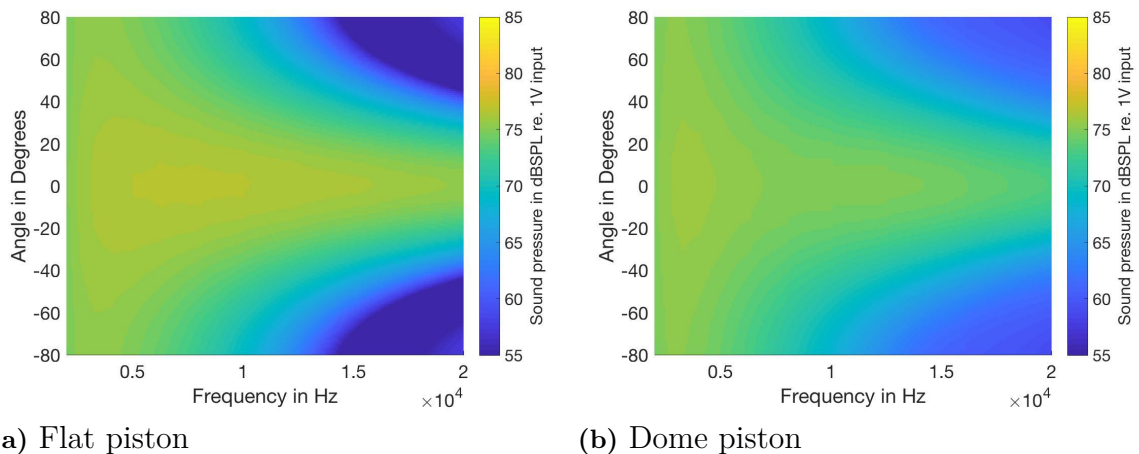


Figure 4.7: Directivity comparison between a flat and dome piston.

After placing the membrane in the interface of baffle 1 and running the simulation, the on-axis response wasn't quite flat (Blue curve Figure 4.8), there is a small sound

pressure level bump at around 5 kHz . The usual response of a loudspeaker in its operating frequency range starts with a low sound pressure level at low frequencies (here from 2 kHz to 4 kHz) then becomes flat till an upper frequency limit where resonance in the membrane or interface starts. So the height of the connection between the tweeter's packaging and the baffle was increase by 1 and 2 millimeters. The sound pressure level increased from 2 kHz to 5 kHz. The increase is higher at 4 kHz-5 kHz, 1 dB increase at 4.5 kHz when lowered by 2 millimeters. The diameter of the membrane at the lower level is 30 millimeters while at the end of the small horn it is 42 millimeters (Figure 3.11a). Half the wavelength of these diameters corresponds to approximately 5.5 kHz and 4 kHz. So the interface seems to acts like a small horn at frequencies where half the wavelength fits the diameters of the interface and is it more effective when the height between the driver and the radiation plane is larger. This also shows how sensitive the simulation is.

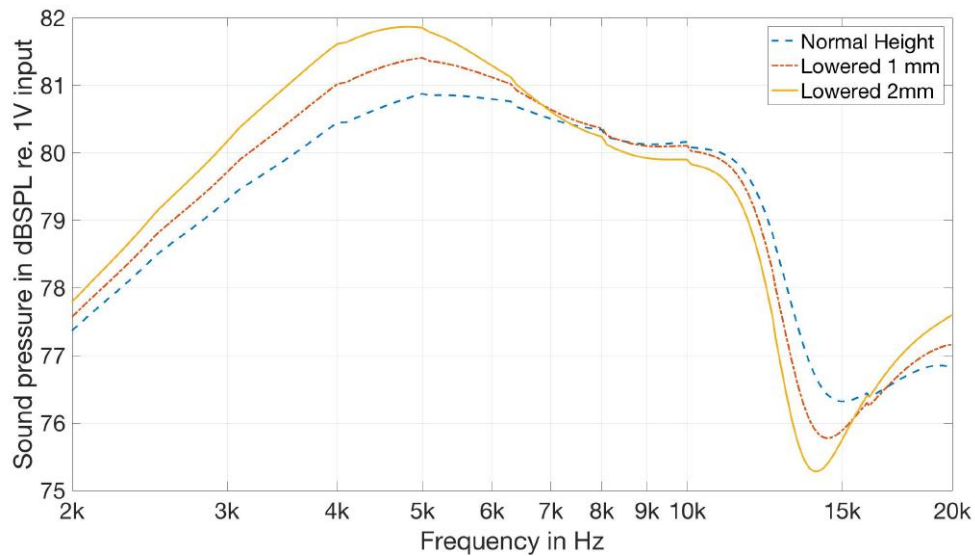


Figure 4.8: On-axis sound pressure level comparison between different heights of the baffle.

4.2 Interfaces

This part will focus on the simulation and measurements results for the different interfaces shown in Figure 3.3 and 3.11.

No filtering or averaging was applied to both simulation and measurement. Simulation and measurement have respectively a 10 Hz and 0.5882 Hz frequency step. The sound pressure level axis doesn't have fixed steps to show a more detailed representation of the results as the amplitudes differ drastically from case to case.

The on-axis frequency response of baffle 1 is shown in Figure 4.9 which is supposed to be the reference case as it is the closest to a flush baffle. The low frequency simulation response is quite accurate even though the measurement fluctuates a bit. The results start to deviate from 9 kHz to 20 kHz from measurement by 2 dB. One hypothesis for the reduction in amplitude can be due to the interface/packaging material which isn't reflecting all the incoming waves and that it has some absorption coefficient that isn't considered. So this can change the intensity of the cavity inner resonances at higher frequencies. There is also a small frequency shift in resonances, the frequency dip ends at 15 kHz for simulation while it ends at 14 kHz for measurement. Another hypothesis for the shift in frequency is that we are modeling the tweeter with Thiele and Smalls parameters assuming lumped elements. So at higher frequencies the membrane of the tweeter cannot be considered stiff anymore and will have structural resonances. This was predicted around 12-13 kHz in the Method Section (when half the wavelength will fit the diameter of the projected surface area of the membrane). The shift in frequency and the magnitude will differ also with slightly different Thiele and Smalls parameters. As mentioned in the Method Section, the measured Thiele and Smalls parameters and the measured tweeter are from a different production batch so they might slightly differ.

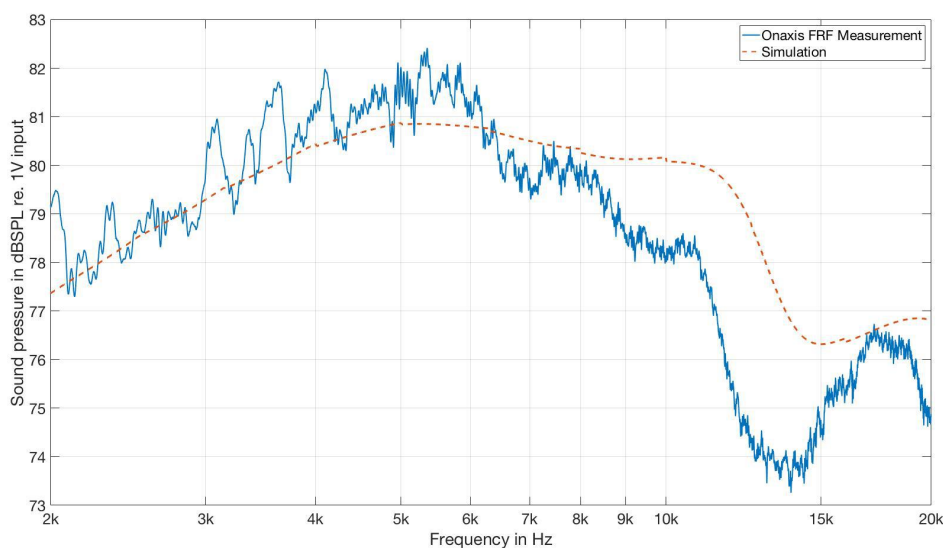


Figure 4.9: On-axis sound pressure level comparison between simulation and measurement of baffle 1.

4. Results & Discussions

The same trend can be seen for baffle 2 in Figure 4.10 which is the straight horn interface. Accurate low frequency response till we reach around 9 kHz where the results deviate by around 2 dB.

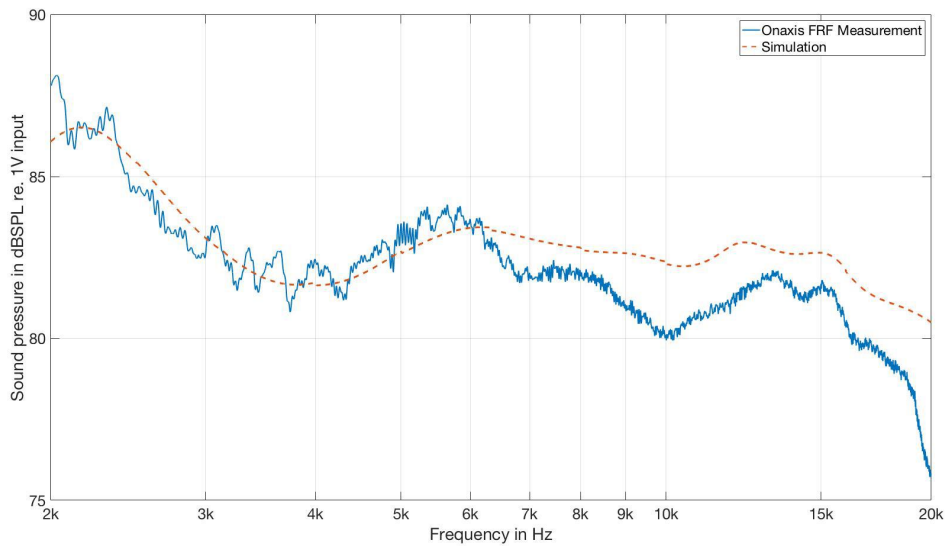


Figure 4.10: On-axis sound pressure level comparison between simulation and measurement of baffle 2.

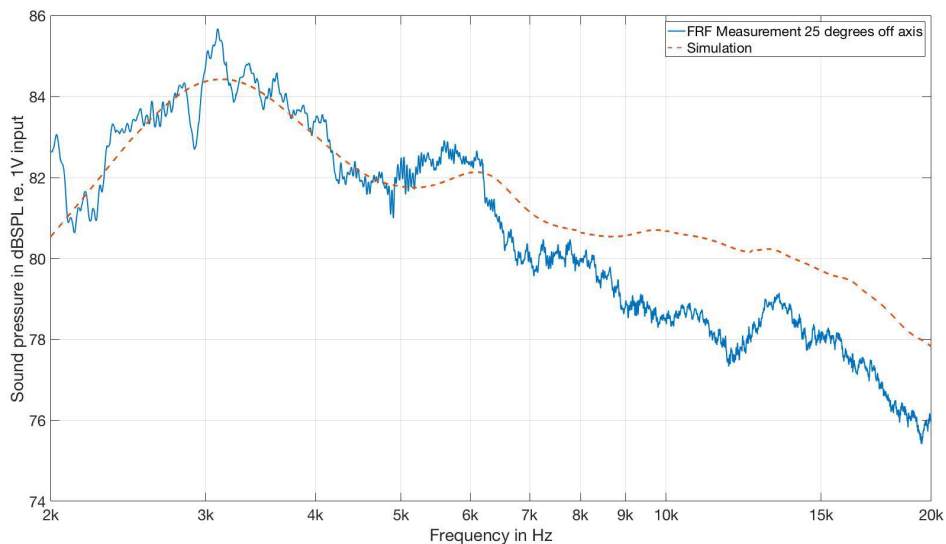


Figure 4.11: 25 degrees off axis sound pressure level comparison between simulation and measurement of baffle 3.

Note that for baffle 3 and 4 their 25 degrees off axis frequency response is taken into consideration as it is where the tweeter membrane is radiating on-axis. Also this is how usually it is oriented to the consumers' ears in cars.

Again same trend for baffle 3, the angled horn in Figure 4.11. Accurate low frequency simulation without consideration for the measurement fluctuation. Then the simulation starts to deviate at around 9 kHz by 2 dB.

Baffle 4 has three configurations, open, closed and closed with a small opening see Figure 3.4. In Figure 4.12, the closed and closed with small opening configuration are practically the same (it is also the case in simulation see Figure A.2 in the Appendix). So the closed with small opening configuration for baffle 4 will not be considered further on.

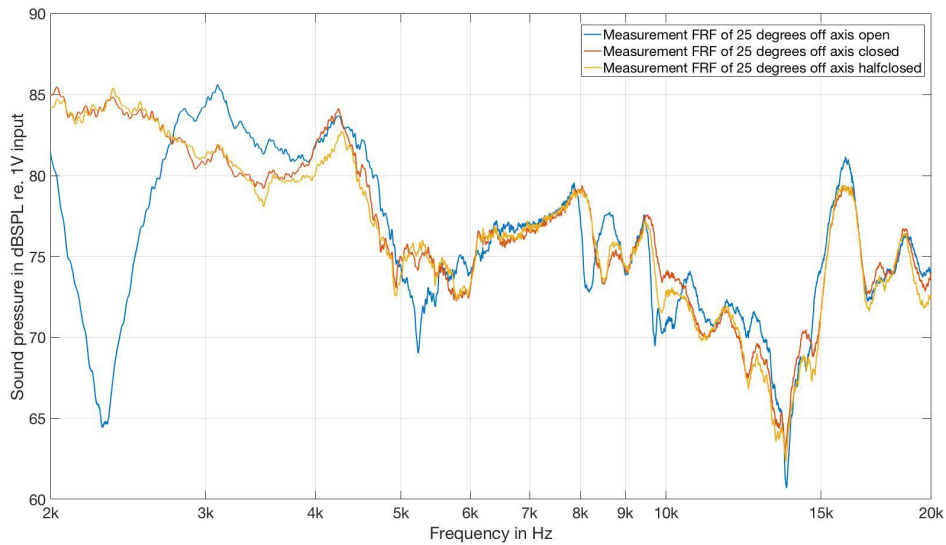


Figure 4.12: 25 degrees off axis sound pressure level comparison between the measurement of baffle 4's three different configurations.

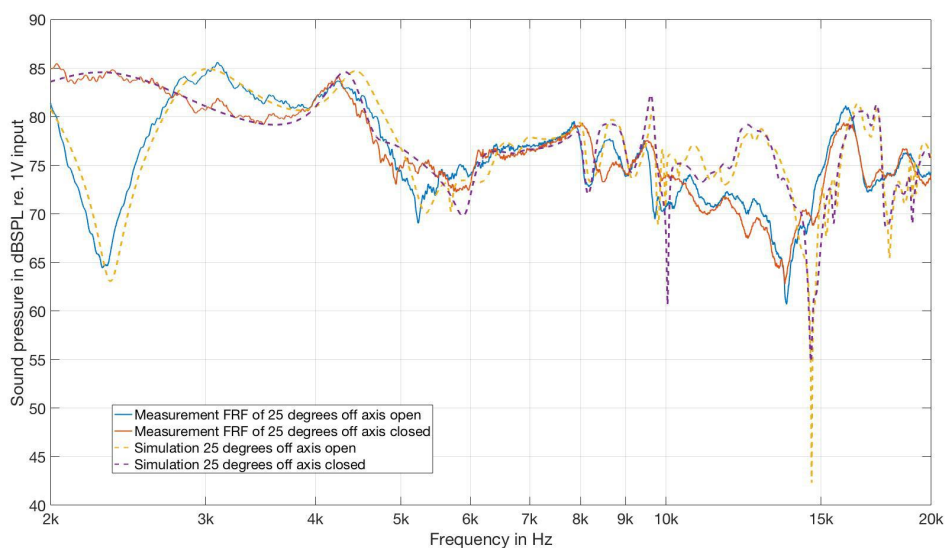


Figure 4.13: 25 degrees off axis sound pressure level comparison between simulation and measurement of baffle 4's open and closed configuration.

It is interesting to see how the presence of the small chamber affects the response of the tweeter. In Figure 4.13 there is a clear anti-resonance at 2.3 kHz for the open configuration, 20 dB difference between both configuration. Then at 3 kHz the open configuration is around 4 dB higher than the closed one. There are also minor differences at higher frequencies between both configurations. As for the simulations the low frequencies is accurate as usual. There are some resonances and anti-resonances that are exaggerated in simulation at 10 kHz, 14 kHz and 14.9 kHz. This is probably due to the first hypothesis mentioned before.

Comparing all measurements of the four interfaces in Figure 4.14 it is obvious that there is a difference in sound pressure level at the listener's ears. Baffle 4's response is far from flat while the three more simple interfaces have acceptable frequency responses. Baffle 2 and 3 with their horns allow a better radiation from 2 kHz to 4 kHz and from 6 kHz to 20 kHz. Baffle 2 has a stronger effect than baffle 3 because of its longer size.

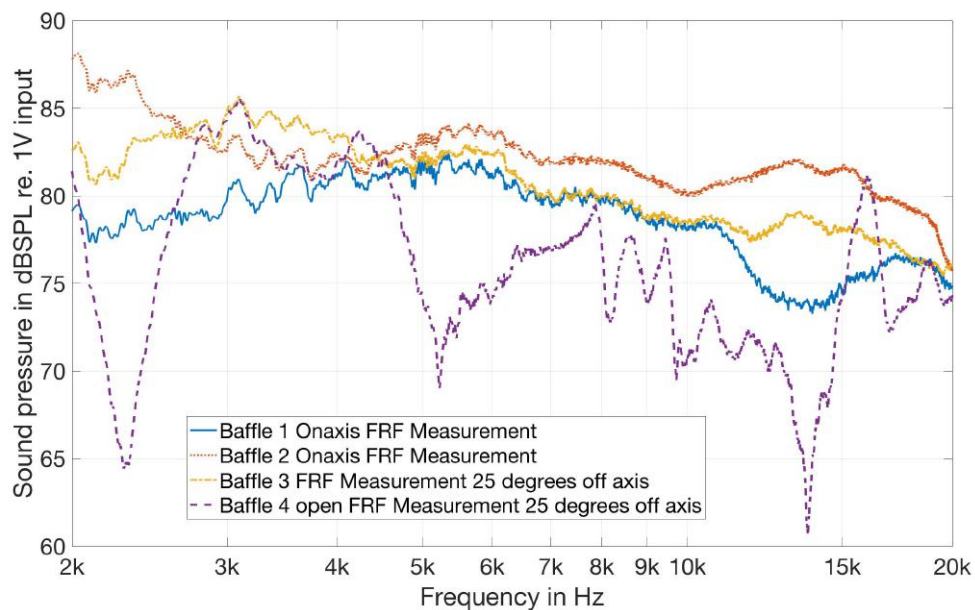


Figure 4.14: Sound pressure level comparison between the measurement of all the baffles.

Doing the simulation comparison for the all the interfaces in Figure 4.15 the same overall behavior can be seen. The simulations are reliable so far for the on-axis frequency response function cases.

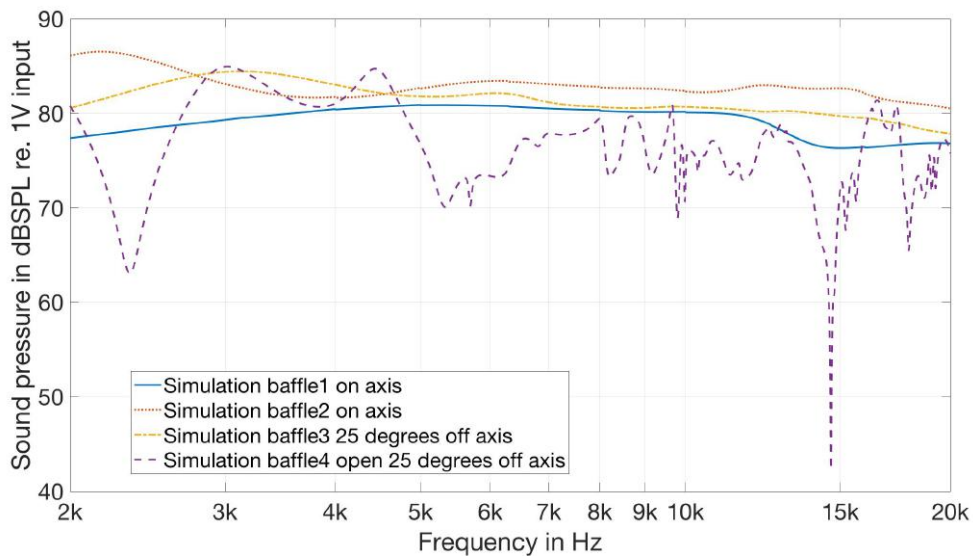


Figure 4.15: Sound pressure level comparison between the simulation of all the baffles.

In Figure 4.16 the directivity of baffle 1 is shown. The measurement plot looks more pixelated due to the 5 degrees step limitation in measurement. The simulation predicts well the response of this configuration. Note that the plots are limited to -80 to 80 degrees as the first and last measurement points of the directivity procedures are not so accurate as the baffle alignment with the microphone is tricky.

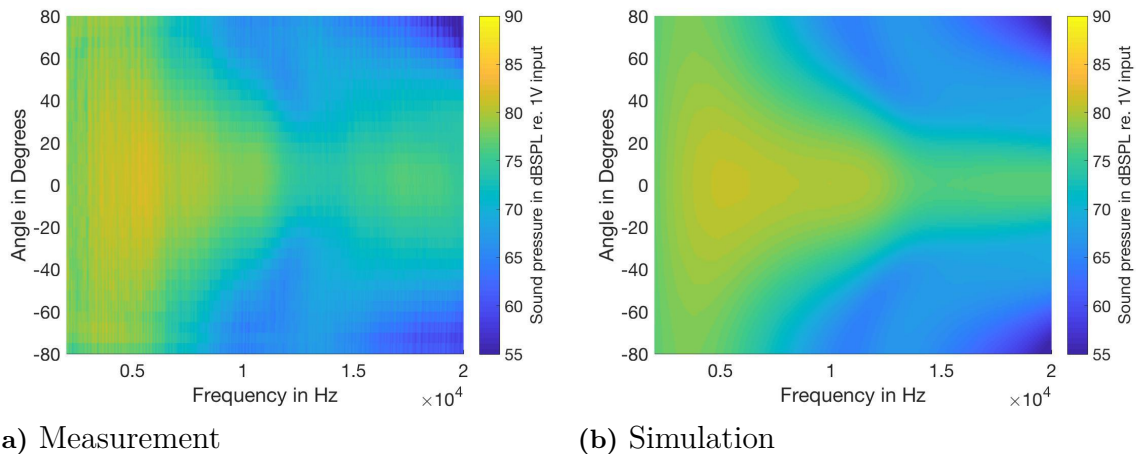


Figure 4.16: Directivity comparison of baffle 1 between measurement and simulation.

In Figure 4.17 the directivity of baffle 2 is also well predicted. The effectiveness of the horn interface is quite clear. The response is much more directional than baffle 1. In this case the horn makes the response more directional while usually horns are used to spread the higher frequencies in all directions. This is due to the horn not having an extreme shape.

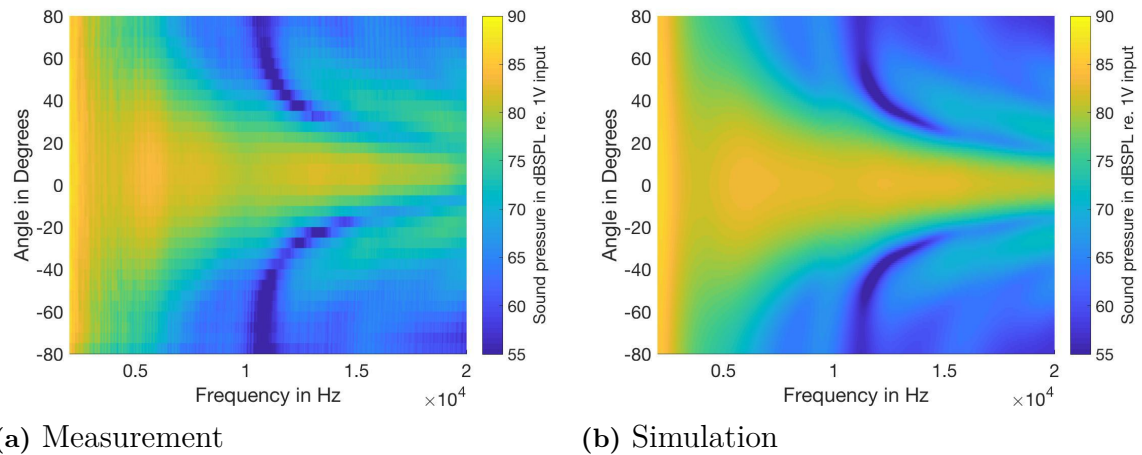


Figure 4.17: Directivity comparison of baffle 2 between measurement and simulation.

In Figure 4.18 the difference between the response of the horn and straight baffles shows how the interface will affect directivity of the tweeter compared to a straight baffle configuration which is usually how it is measured and reported in the data sheet of the supplier. There is a large increase in sound pressure level from 2 kHz to 3 kHz. This is due to the horn shape which will allow a smoother impedance change between the driver which has high impedance and the surrounding air which has low impedance. This transition increases the efficient of the driver allowing it to be a better radiator. The second increase is from 11 kHz to 20 kHz which is probably due to the horn redirecting the high frequency waves on axis.

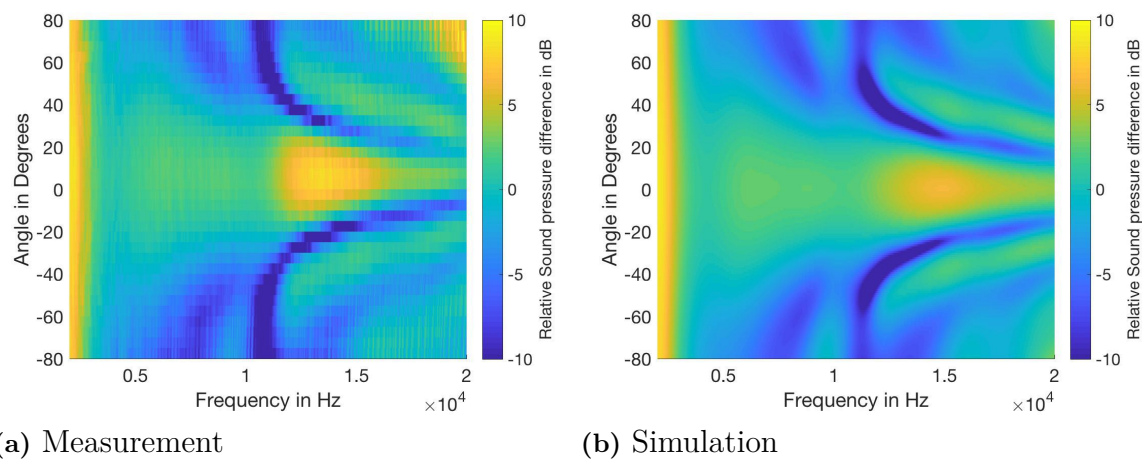


Figure 4.18: dB difference between baffle 2 and baffle 1.

To explain why the pressure is changing before any cavity resonances occurs, some electro-acoustic analogies can be qualitatively drawn. To simplify the representation the electrical part will be neglected. In Figure 4.19 both a piston with and without cavities are represented with similar Thiele and Small parameters. The air in the cavity has mass and stiffness properties before radiating into the outside environment. The electroacoustic mechanical impedance circuit can be drawn (Figure 4.20)

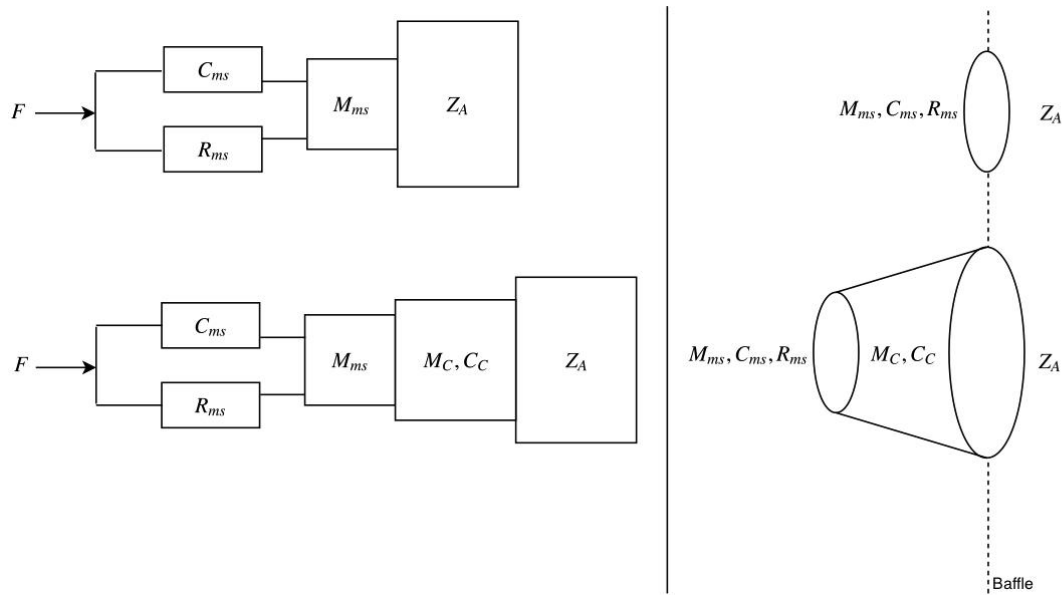


Figure 4.19: Mechanical representation of a piston with and without cavity.

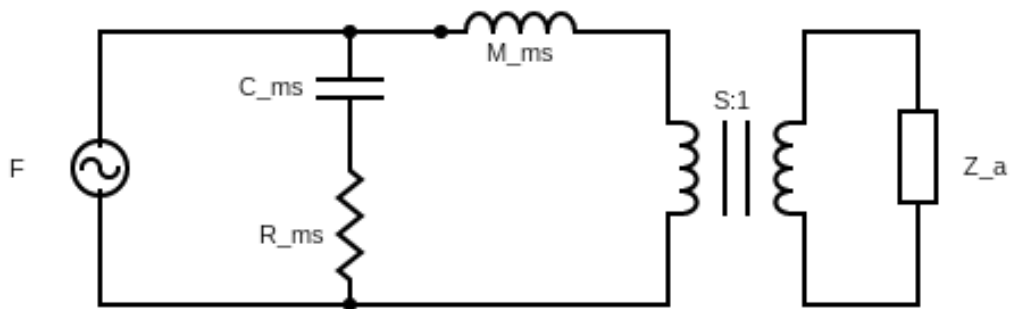


Figure 4.20: Electroacoustic representation of a piston without cavity in mechanical impedance circuit.

After some conversions, the acoustical impedance circuit can be drawn for both cases (Figure 4.21).

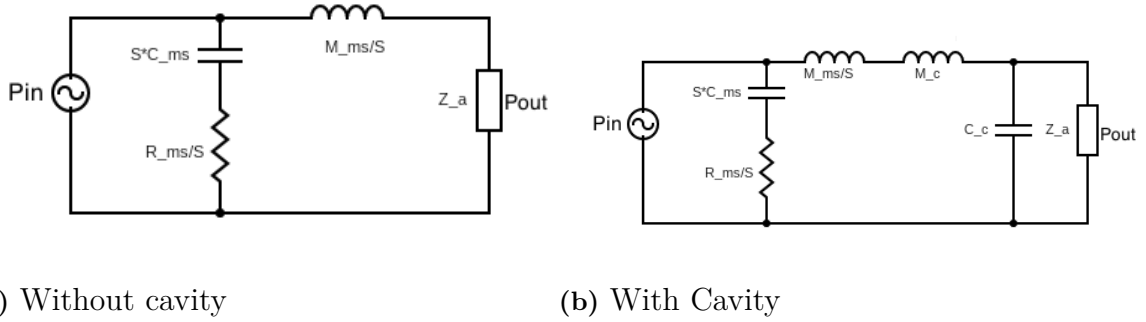


Figure 4.21: Electroacoustic representation of a piston with and without cavity in acoustical impedance circuit.

Note that Z_A is assumed to not change. The transfer functions from input pressure to radiated pressure are obtained:

-Without cavity:

$$\frac{P_{out}}{P_{in}} = \frac{Z_A}{Z_A + j\omega M_{as}} \quad (4.1)$$

-With cavity:

$$\frac{P_{out}}{P_{in}} = \frac{Z_A}{Z_A - \omega^2 C_c (M_{as} + M_c) - j\omega^3 C_c^2} \quad (4.2)$$

with $M_{as} = \frac{M_{ms}}{S}$.

The dynamics of the system do change quite a lot due to the presence of the cavity. The cavity will make the output pressure higher for the same input. Note that this analogy is only valid for lumped elements, at higher frequencies the air cavity will have resonances which are not accounted for in this equation. Another issue with this analogy is how to get the mass and compliance inside the cavity as we have an open end, where to draw the line between cavity and outside air is a problem.

In Figure 4.22 the directivity of the angled horn shows how an angled horn can focus the sound pressure towards the listeners and potentially reduce unwanted reflections from the surrounding of the car if it is placed on the door.

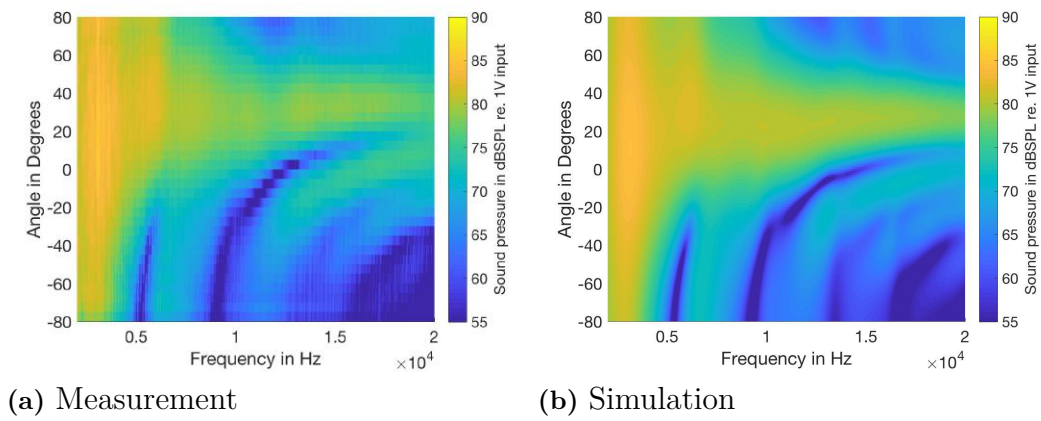


Figure 4.22: Directivity comparison of baffle 3 between measurement and simulation.

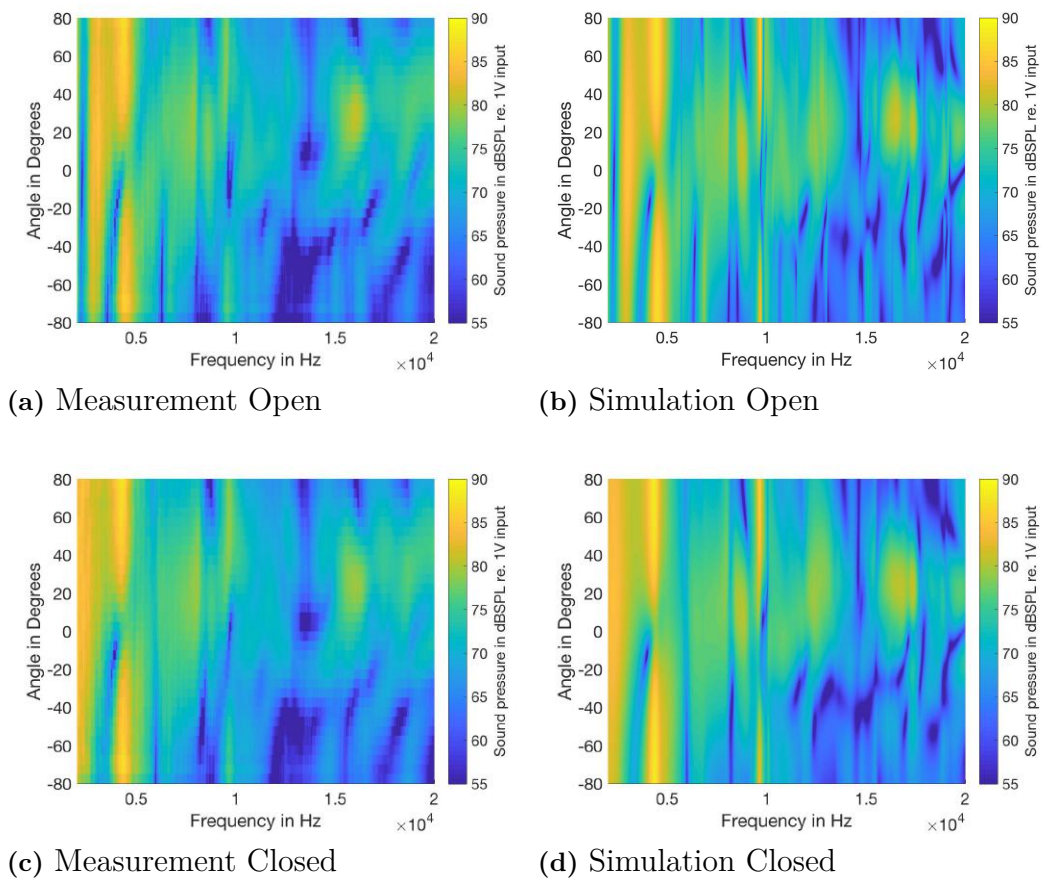
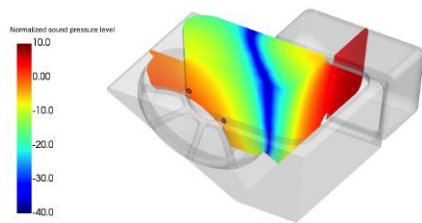


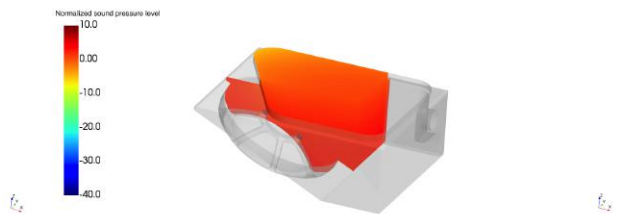
Figure 4.23: Directivity comparison of open/closed baffle 4 between measurement and simulation.

In Figure 4.23 the directivity of both configurations of baffle 4 clearly shows that it is not an ideal interface. The angle of the driver is barely evident.

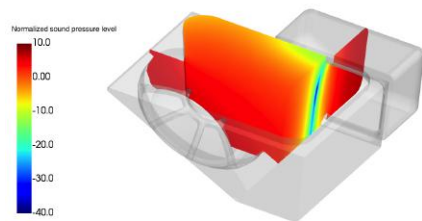
The reason why baffle 4 is such a bad interface is due to the resonances happening inside the interface (Figure 4.24). When half the wavelength becomes in the order of the size of the interface resonances start to emerge. The first one occurs at 2.3 kHz for the open configuration and it happens with the diagonal length of the interface. The length of the diagonal is around 82 millimeters which corresponds to half the wavelength of 2.1 kHz. This is a complex interface so getting exact dimensions fitting the wavelength will not be straight forward. When the configuration is closed, there is no resonance occurring at 2.3 kHz as the interface is smaller than half the wavelength of this frequency. These resonances affect the radiation of sound outside the cavity. The resonance at 2.3 kHz is clearly affecting the directivity and on-axis sound pressure level for the open configuration (Figure 4.13 and 4.23). The resonance at 3 kHz is also clearly affecting the directivity at 1 meter (Figure 4.23) the open configuration is radiating better than the closed one.



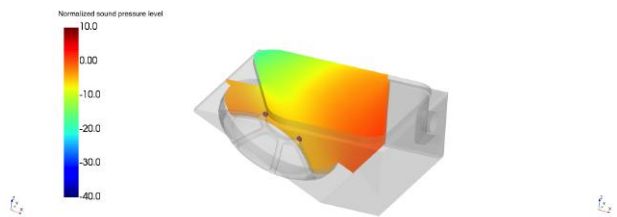
(a) Open 2.3 kHz



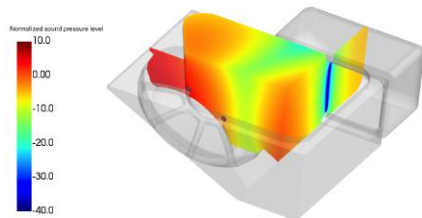
(b) Closed 2.3 kHz



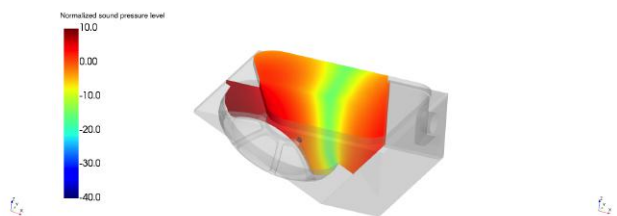
(c) Open 3 kHz



(d) Closed 3 kHz



(e) Open 4 kHz



(f) Closed 4 kHz

Figure 4.24: Comparison of the standing waves patterns between the open and closed configurations of baffle 4.

Because the frequency step was different between measurement and simulation, the frequency response functions were averaged over third octave bands to get an error estimate. The RMS error was computed and averaged over all the frequency response functions from -80 to 80 degrees. The third octave band error is shown for each interface in the table 4.1 as well as the total average RMS error. As seen in the previous comparative graphs the simulations are more accurate at the lower frequencies. The RMS difference is most often below 1 dB from 2 kHz to 6 kHz while at higher frequencies the difference is around 2-3 dB and sometimes reaching 5 dB. The overall error is acceptable for checking designs before building any physical prototyping to see how a cavity will affect the tweeter radiation.

Interface\Frequency	2500	3150	4000	5000	6300	8000	10000	12500	16000	Total
Baffle 1	0.44	0.49	0.71	0.78	0.32	0.54	1.47	2.27	1.71	1.16
Baffle 2	0.70	0.39	0.50	0.70	0.65	0.95	2.52	3.23	2.99	1.77
Baffle 3	0.45	0.42	0.44	0.56	0.62	1.47	2.29	2.36	2.43	1.50
Baffle 4 open	1.07	0.88	0.57	1.38	1.17	1.28	2.94	5.12	1.65	2.23
Baffle 4 closed	0.51	0.47	0.74	0.97	0.61	1.41	3.20	5.59	1.71	2.33

Table 4.1: RMS error for the different interfaces in dB.

4.3 Grilles

In this section the addition of grilles will be discussed.

The grilles are shown in Figures 3.5, 3.7, 3.6 and their meshes in Figure 3.12. They were only measured for the baffle 1,2 and 3 . Baffle 4 was excluded as its response is quite messy. The on-axis comparison between measurement and simulation of the 3mm thickness and 2mm hole will only be discussed in this section, as it is the grille that affects most the response. The graphs for the others grilles are presented in the Appendix section.

In Figure 4.25 the simulation is predicting the overall on-axis behavior of baffle 1 attached with the 3 mm thick and 2 mm hole grille. However it is a bit less accurate than the case without the grille (Figure 4.9). There is a small inaccuracy of 2.5 dB at 2.7 kHz. The other inaccuracy is the anti-resonance occurring at 11.5 kHz in measurement but at 13 kHz in simulation. This inaccuracy is also seen in the case without the grille, but at different frequencies, this will be discussed later.

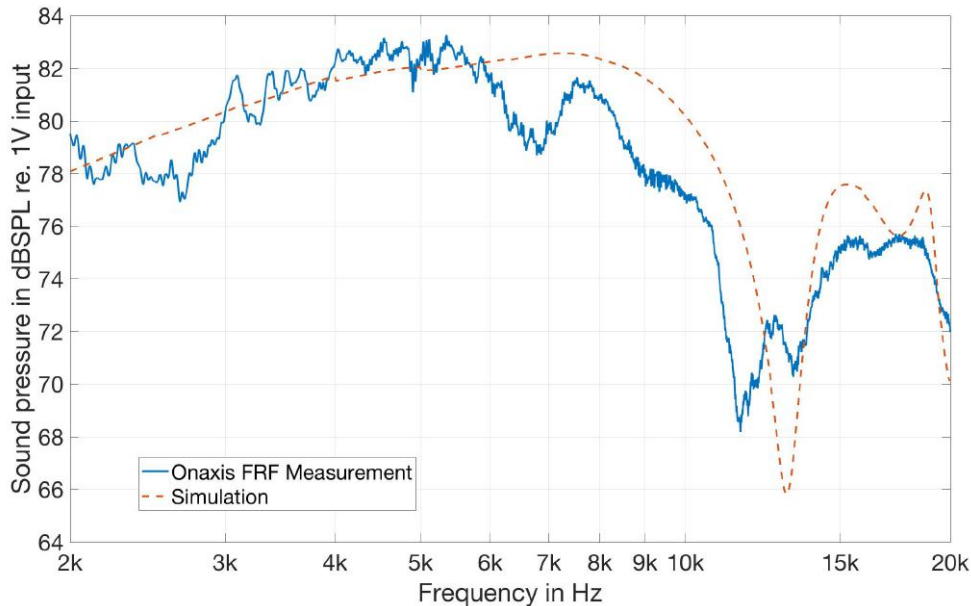


Figure 4.25: On-axis sound pressure level comparison between simulation and measurement of baffle 1 with 3 mm thick 2 mm hole grille.

The RMS error is within the same range as the different interfaces. The more restrictive grille has a slightly larger error than the other configurations (Table 4.2). The other RMS error table of the other grille/interface configurations will be available in the Appendix.

Interface\Frequency	2500	3150	4000	5000	6300	8000	10000	12500	16000	Total
3mm thick 2mm hole	0.85	0.68	0.72	0.95	1.94	2.86	3.26	2.69	3.19	2.18
3mm thick 4mm hole	0.98	0.65	0.56	0.69	1.15	1.71	2.68	2.72	2.51	1.74
0.5mm thick 2mm hole	0.72	0.75	0.87	0.80	0.97	1.56	2.50	2.50	1.90	1.56

Table 4.2: RMS error for the different grilles on baffle 1 in dB.

Comparing all measurements of the different baffles in Figure 4.26, the grilles do color the frequency response a bit. At 4.5 kHz there is a 2 dB increase for the 3 mm thick 2 mm hole grille. At 8 kHz there is an increase of 1.5 dB for all grilles. Then at 11-13 kHz there is the anti-resonance that has a higher quality factor with the more restricted grilles.

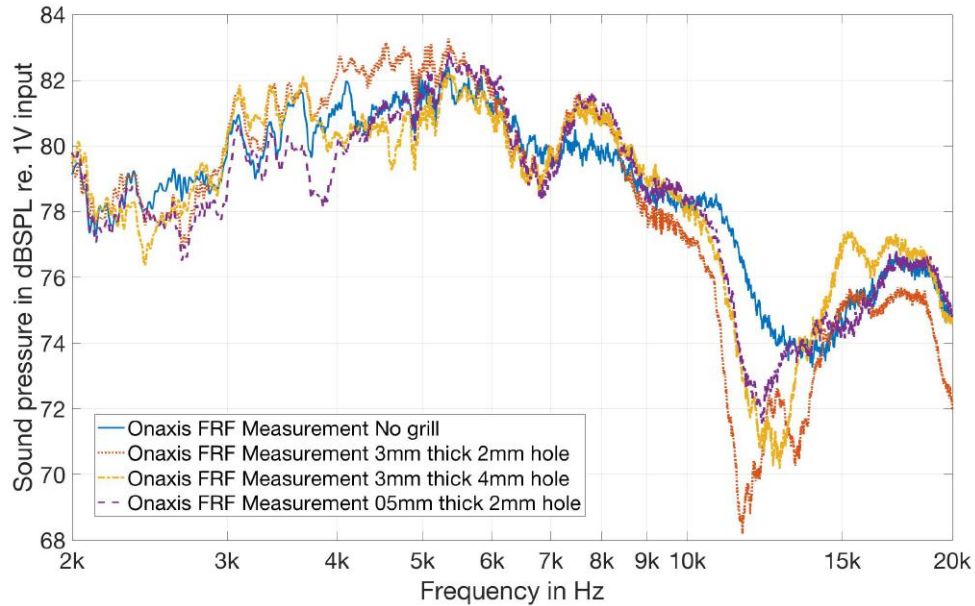


Figure 4.26: On-axis sound pressure level comparison between the measurement of baffle 1 with the different grilles.

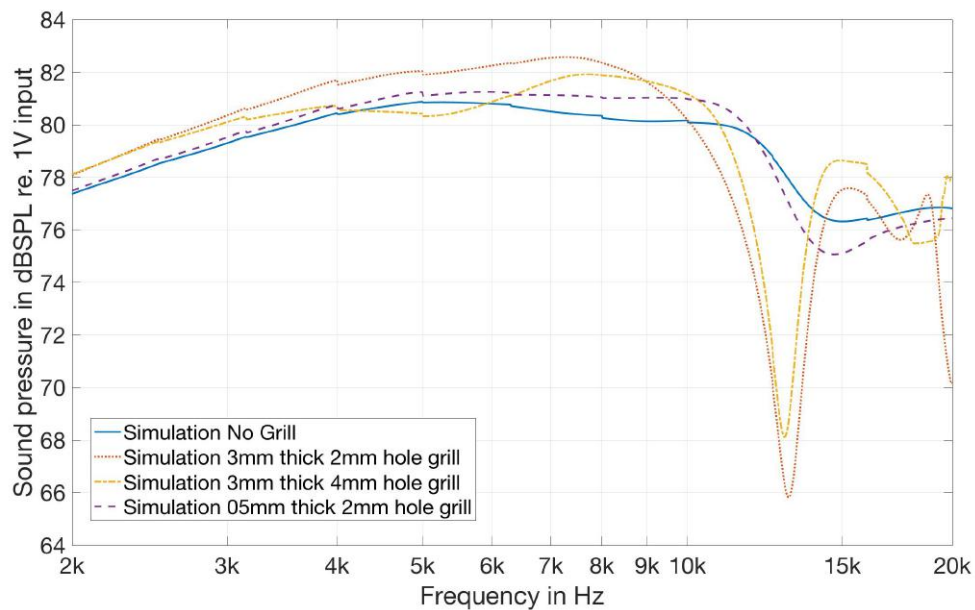


Figure 4.27: On-axis sound pressure level comparison between the simulation of baffle 1 with the different grilles.

4. Results & Discussions

The simulation trends are similar even though the 0.5 millimeters grille has a stronger effect in measurement (Figure 4.27).

Figure 4.28 and 4.29 shows that the 3 mm 2 mm hole grille is mostly transparent at lower frequencies. At around 10 kHz and on-wards the grille starts to mess with the directivity.

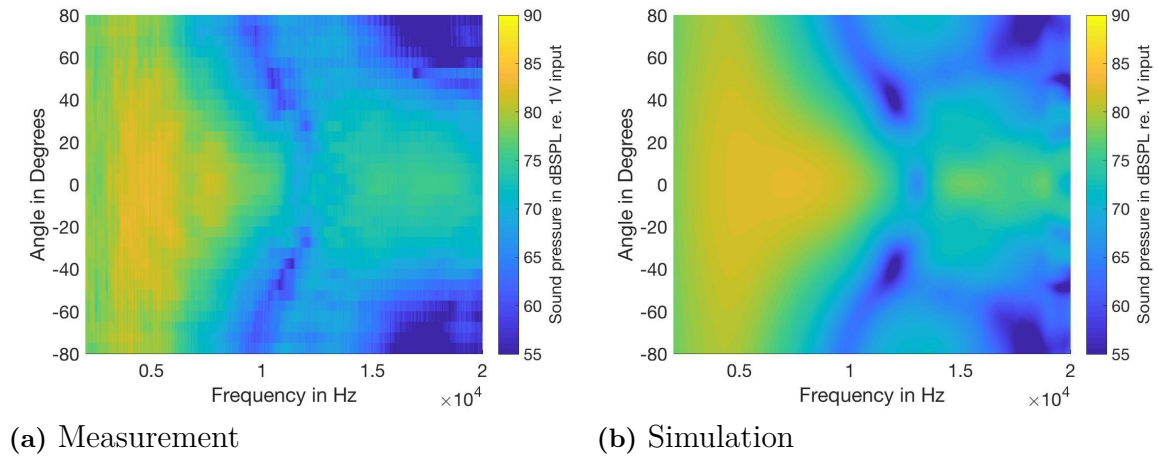


Figure 4.28: Directivity comparison between measurement and simulation of baffle 1 with 3 mm thick and 2 mm hole grille.

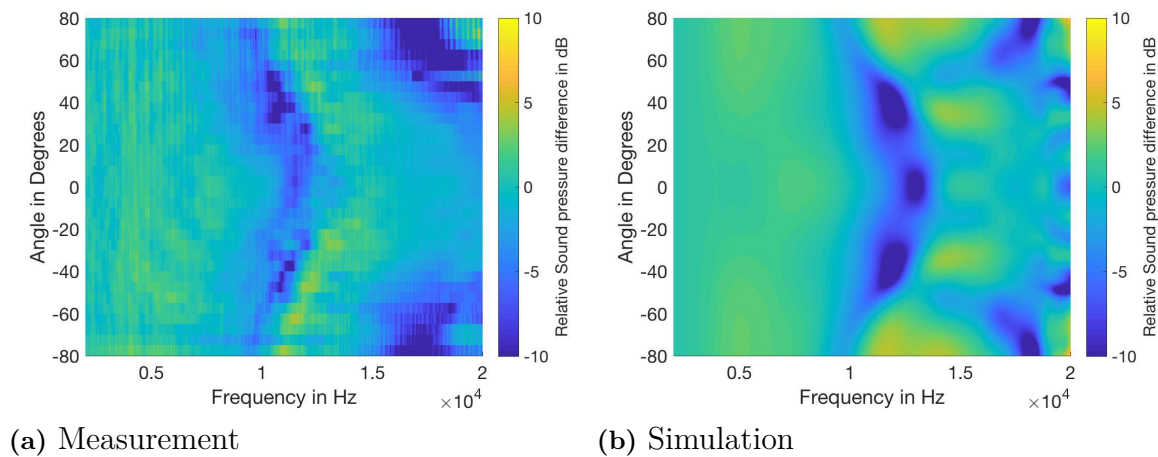


Figure 4.29: dB difference between baffle 1 with 3 mm thick and 2 mm hole grille and baffle 1 without grille.

Figure 4.30 and 4.31 show almost the same behavior with the 3 mm thick and 4 mm hole grille. It is slightly more transparent than the 3 mm thick 2 mm hole grille.

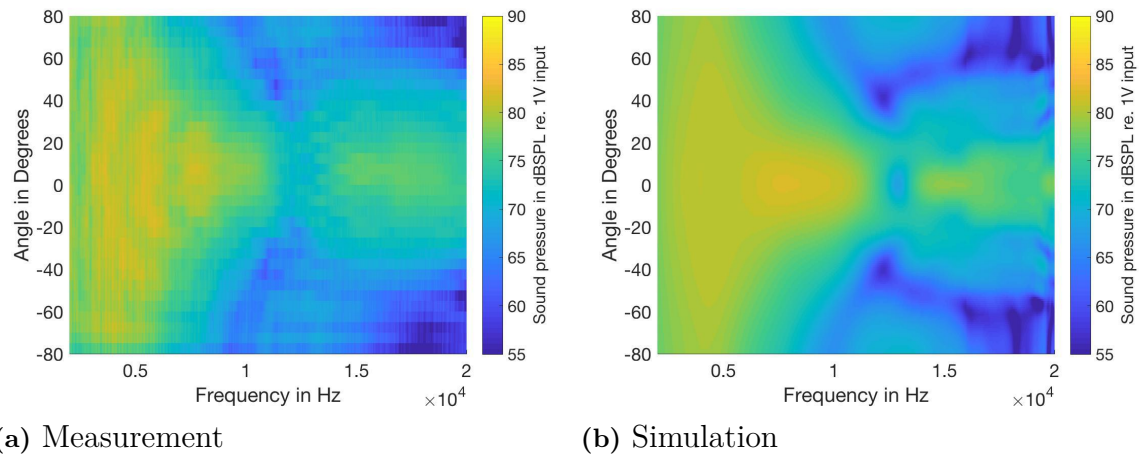


Figure 4.30: Directivity comparison between measurement and simulation of baffle 1 with 3 mm thick and 4 mm hole grille.

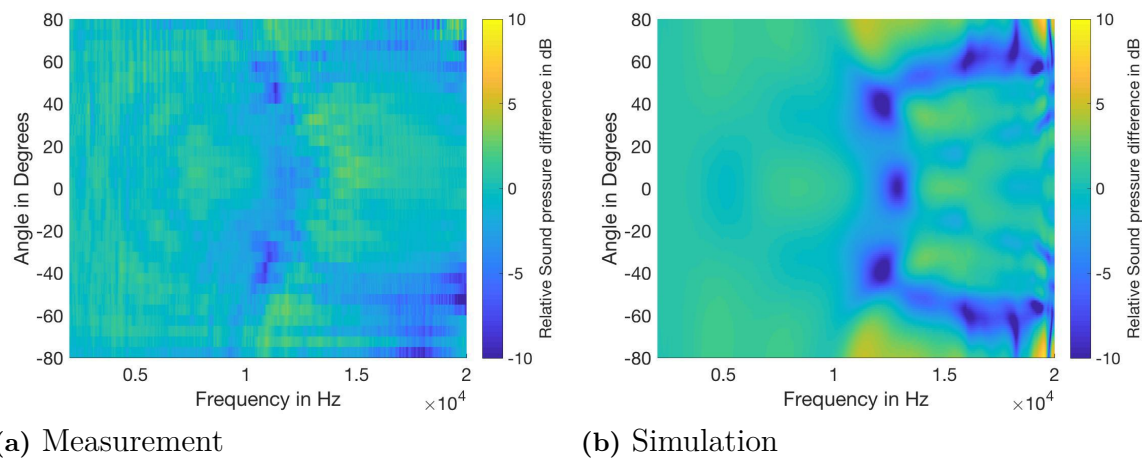


Figure 4.31: dB difference between baffle 1 with 3 mm thick and 4 mm hole grille and baffle 1 without grille.

The 0.5 mm thick and 2 mm hole grille is almost transparent from Figure 4.32 and 4.33. It seems that the more the grille is restricting air flow the more it has an effect on its frequency response. Reducing air flow happens with the increase of the thickness and/or the reduction in hole size considering of course the same hole pattern.

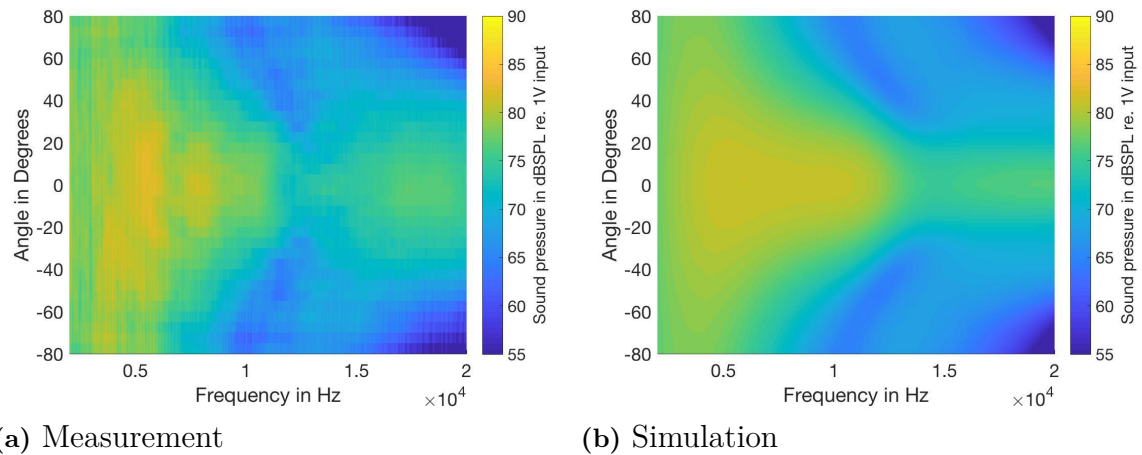


Figure 4.32: Directivity comparison between measurement and simulation of baffle 1 with 0.5 mm thick and 2 mm hole grille.

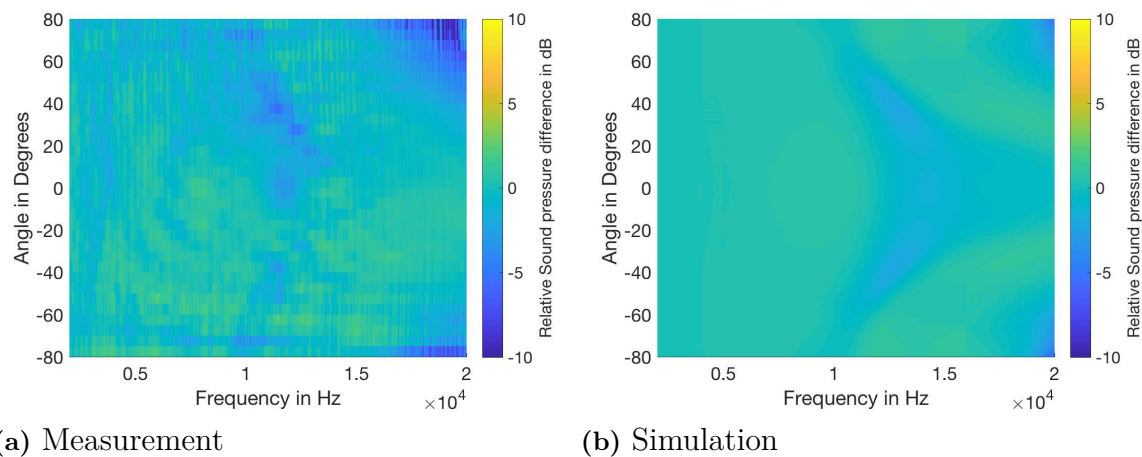


Figure 4.33: dB difference between baffle 1 with 0.5 mm thick and 2 mm hole grille and baffle 1 without grille.

One hypothesis is that the grilles with the cavity will act as a Helmholtz resonator. The Helmholtz absorption equation simplifies the reality into a mass-spring system, the air inside the cavity acts as a spring and the mass of the air inside the openings (in this case inside the grilles) as mass. No relations were found. The analogy is not accurate as the membrane behind the cavity is moving and generating sound pressure, while the Helmholtz absorption equation is considering an incoming wave from the outside. The previously mentioned electro-acoustic analogy is still valid in this case before any cavity resonances. And the major changes in sound pressure level between all configurations are due to the cavity resonances which is explained below.

Figure 4.34 shows the pressure distribution happening at 9.5 kHz inside the interface. 9.5 kHz is when the frequency starts to roll to the on-axis anti-resonance for the 3 mm thick 2 mm grille configuration. It is clear that at 9.5 kHz the resonance has already started for this grille (Figure 4.34b). While for the no grille and 0.5 mm thick grille the resonance is not happening. The most restrictive grille changes drastically the impedance at the cavity opening. When half the wavelength of the operating frequency starts fitting the cavity dimensions, stronger resonances will appear because the rigid part of the grille will act as a rigid boundary and will reflect better the waves inside the cavity.

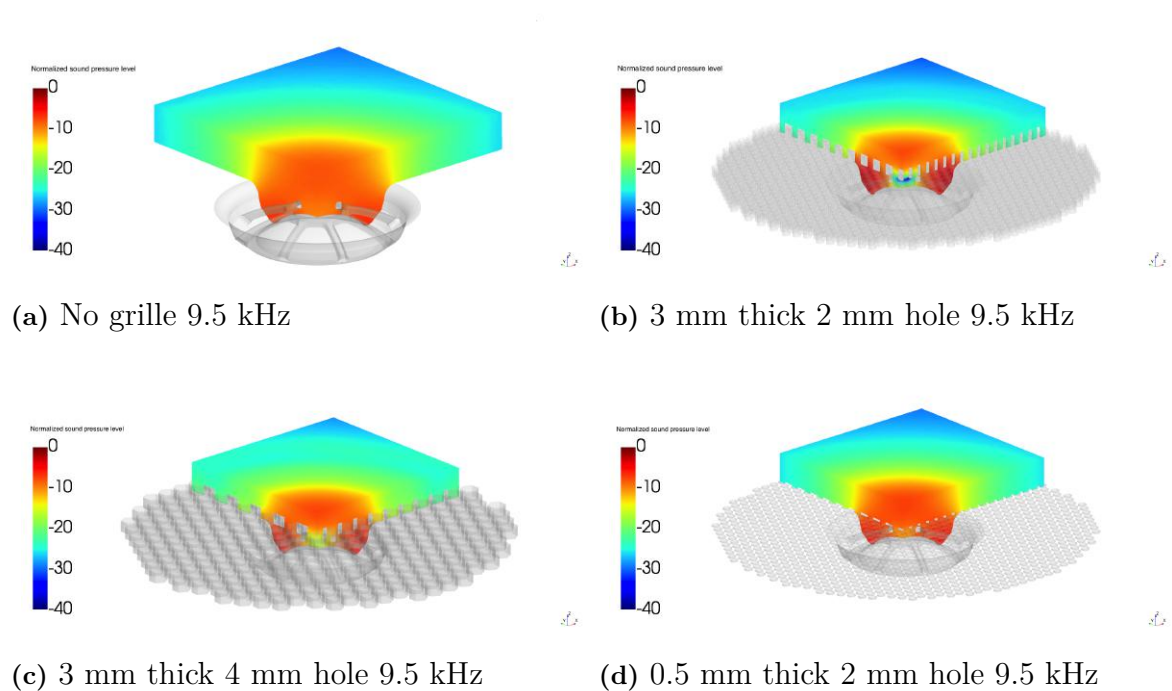


Figure 4.34: Comparison of the resonances occurring inside the interface between all the grille configuration for baffle 1 at 9.5 kHz.

11.5kHz is when the on-axis sound pressure level response is getting lower for the 3 mm thick 2 mm hole grille than without it. Figure 4.35 shows the different pressure variances for the different grille configurations at this frequency. The resonance is affecting the radiation.

4. Results & Discussions

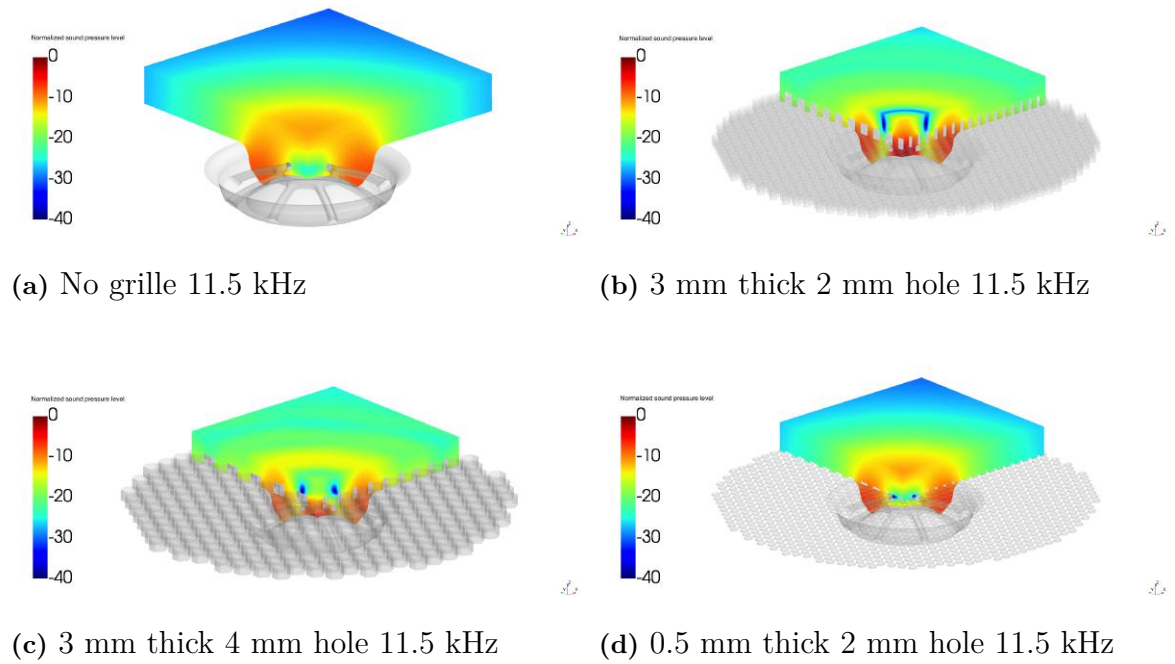


Figure 4.35: Comparison of the resonances occurring inside the interface between all the grille configuration for baffle 1 at 11.5 kHz.

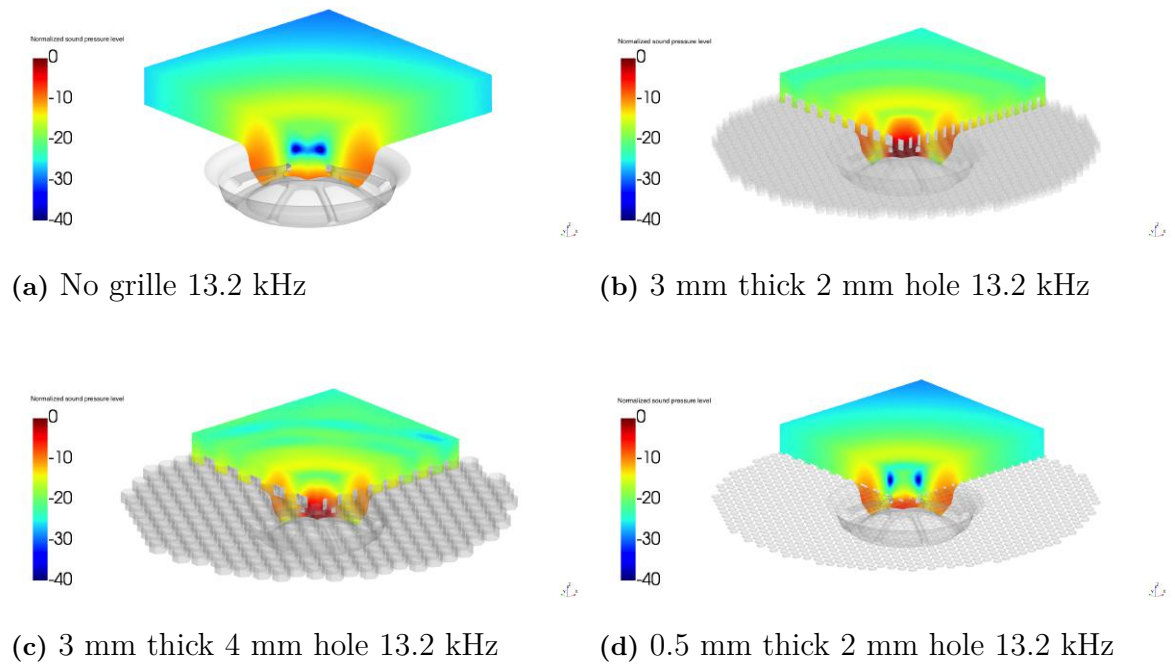


Figure 4.36: Comparison of the resonances occurring inside the interface between all the grille configuration for baffle 1 at 13.2 kHz.

13.2 kHz is the on-axis anti-resonance of the 3 mm thick 2 mm hole grille configuration. However the sound pressure level of the 3 mm thick 2 mm hole grille (Figure 4.36b) is higher inside the cavity than the configuration without the grille (Figure 4.36a).

So an extended pressure map was computed to see what is happening outside the cavity (Figure 4.37). It seems that a comb filter effect is happening at around 30 mm away from the tweeter. The center of the tweeter and the rim of the baffle act as two different sources to create this effect due to their distance difference. Note that the white data points in Figure 4.37b are used as distance reference to calculate the theoretical frequency where this comb filter is occurring if we assume these two sources. The first theoretical frequency where minimum sound pressure level happens is at 13.9 kHz which is close to the frequency where this effect occurs.

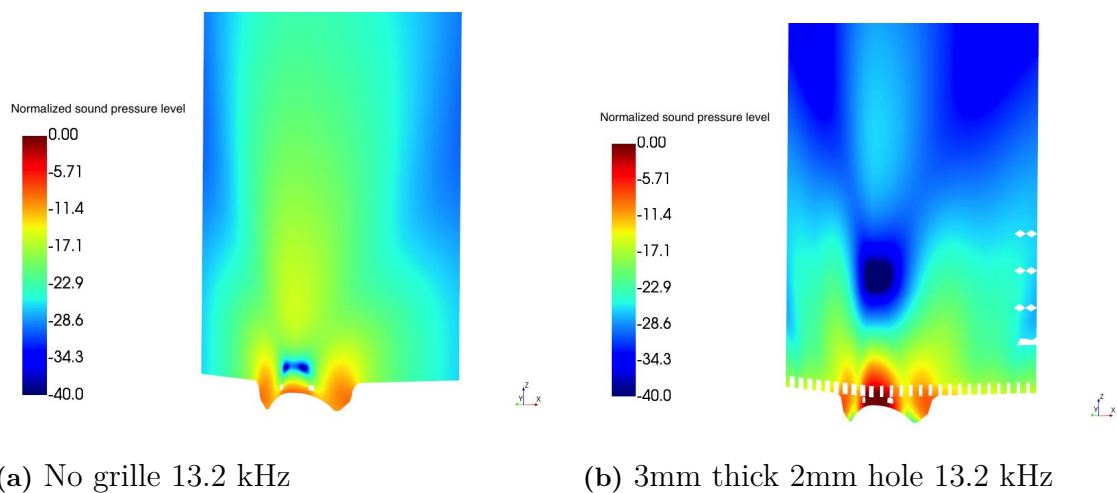


Figure 4.37: Comparison of the extended pressure maps between the 3 mm thick 2 mm hole grille and without grille for baffle 1 at 13.2 kHz.

In Figure 4.38 simulation is again mostly accurate at low frequencies however the frequency shift starts at 6 kHz this time. It was less apparent before adding the grille in Figure 4.10. The measurement response at 18.5 kHz seems to be a measurement error. The two other grilles comparisons are presented in the Appendix.

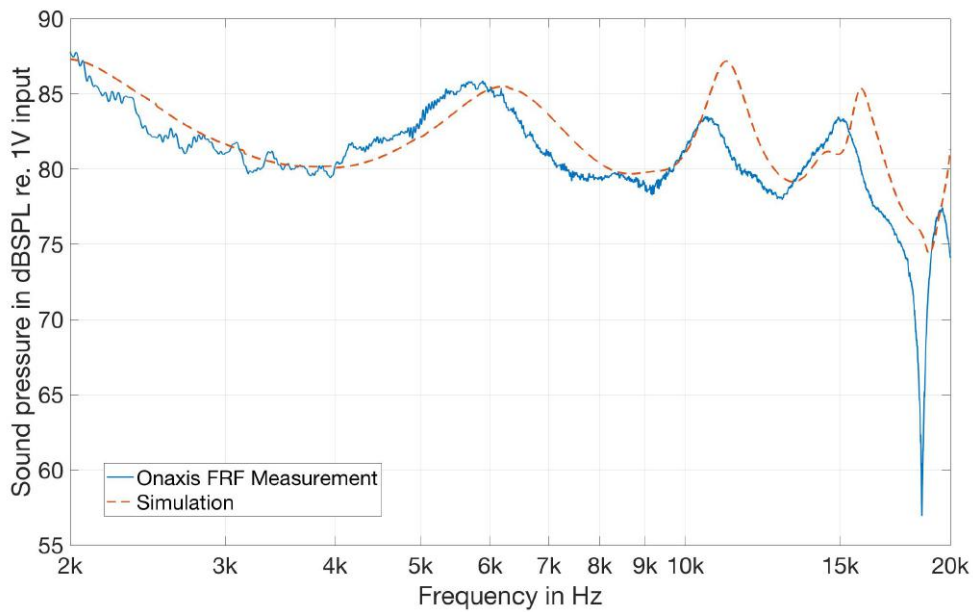


Figure 4.38: On-axis sound pressure level comparison between simulation and measurement of baffle 2 with 3mm thick 2mm hole grille.

Adding the grilles to baffle 2 also colors the frequency response shown in Figure 4.39. As seen in baffle 1 the stronger coloration occurs for the 3mm thick 2 mm hole grille. Note that the range of the sound pressure level axis was modified to the same range as the simulation in Figure 4.40 due to the extreme response in measurement.

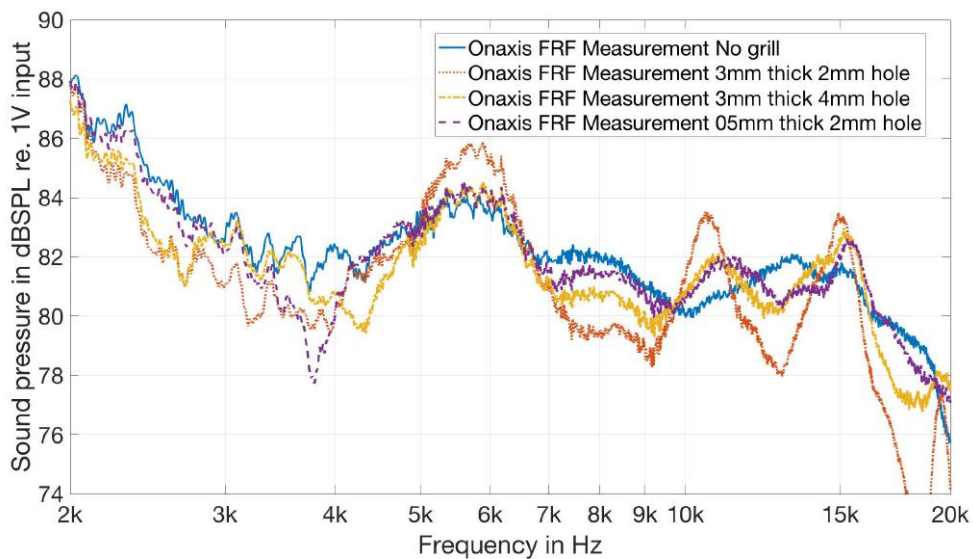


Figure 4.39: On-axis sound pressure level comparison between the measurement of baffle 2 with the different grilles.

The simulations again follow the same trends as measurement.

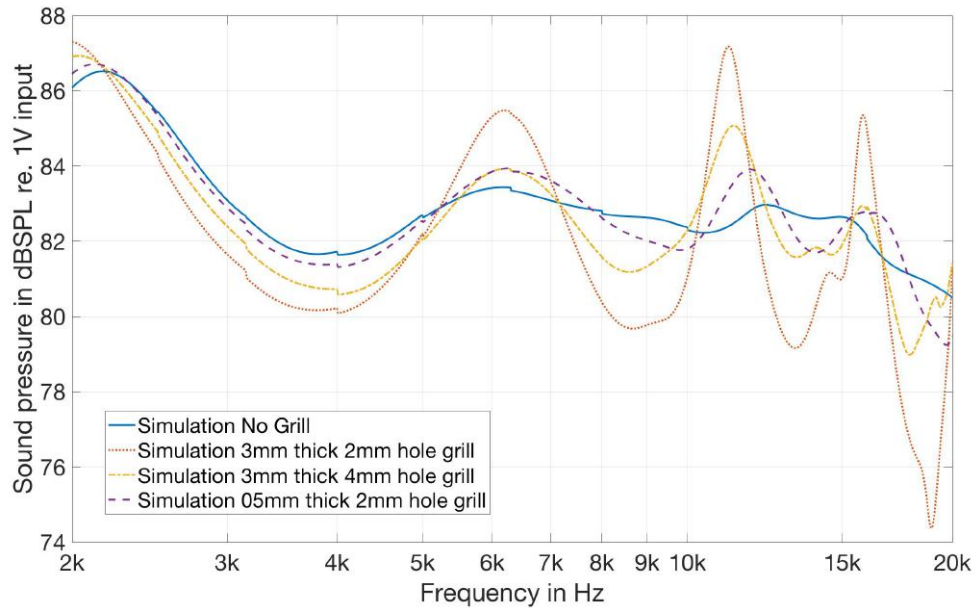


Figure 4.40: On-axis sound pressure level comparison between the simulation of baffle 2 with the different grilles.

The effect of the grilles on the baffle 2 happens at 6 kHz now compared to 9 kHz on baffle 1. There is a stronger change in frequency response compared to baffle 1 as seen in Figure 4.41 and 4.42.

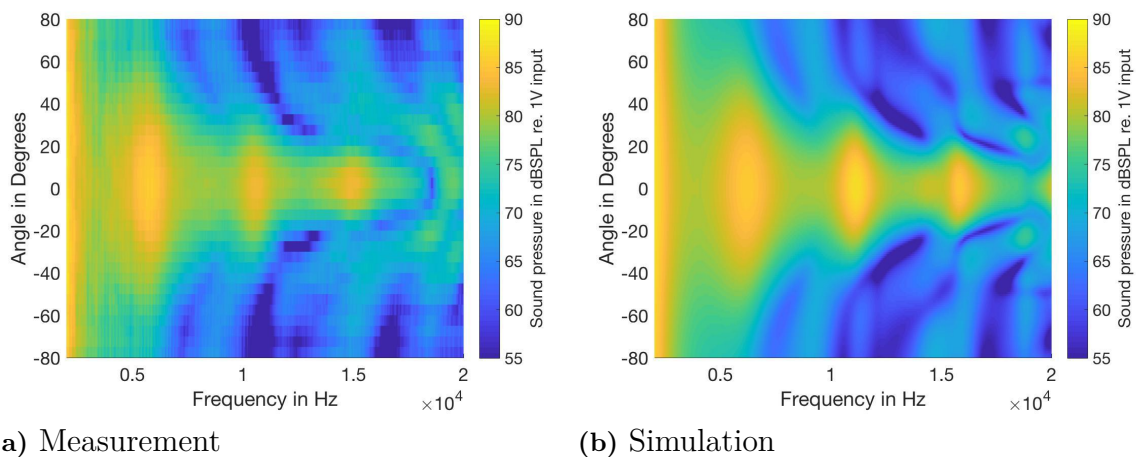


Figure 4.41: Directivity comparison between measurement and simulation of baffle 2 with 3 mm thick and 2 mm hole grille.

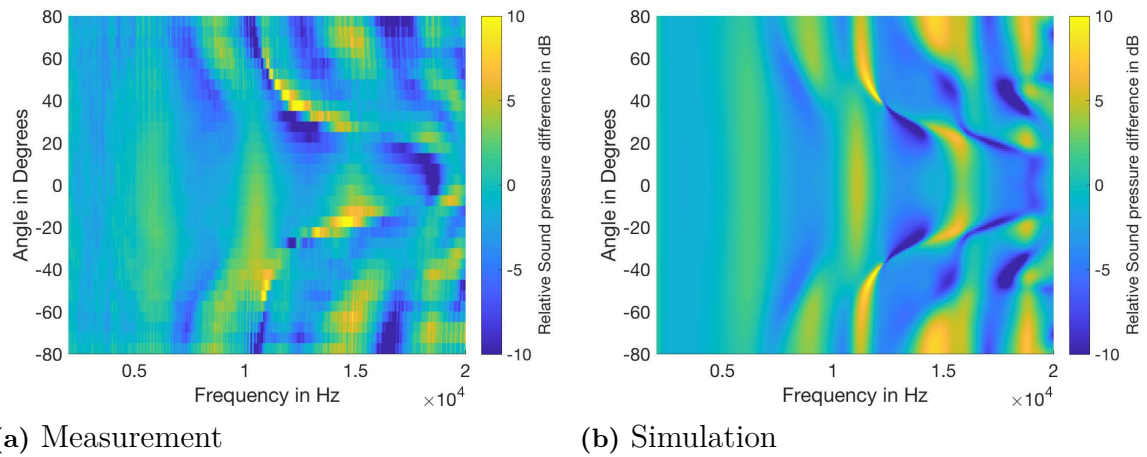


Figure 4.42: dB difference between baffle 2 with 3 mm thick and 2 mm hole grille and baffle 2 without grille.

The effect of the grille 3 mm thick 4 mm hole (Figure 4.42 and 4.43) is again not as extreme as the 3 mm thick 2 mm hole grille. The resonances happens mostly at the same frequencies, the change is in the quality factor of these resonances.

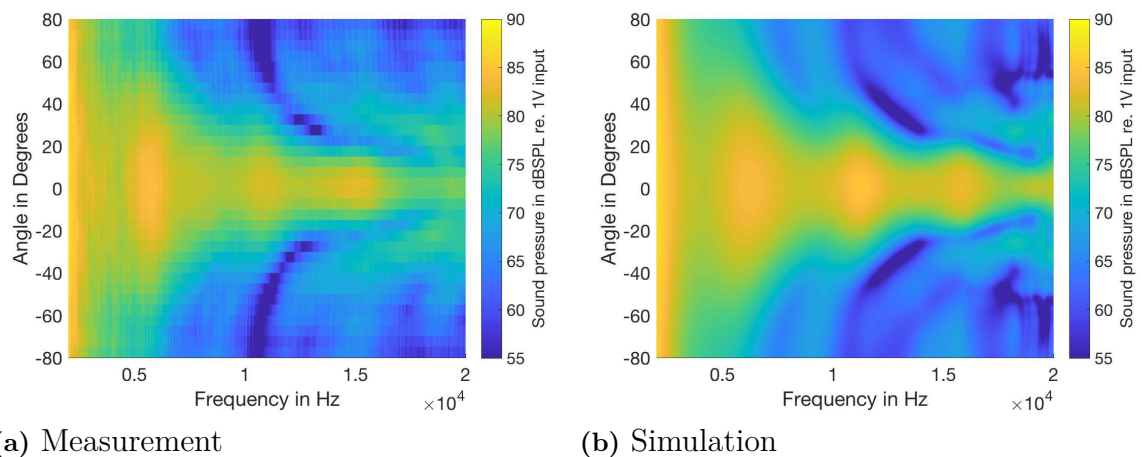


Figure 4.43: Directivity comparison between measurement and simulation of baffle 2 with 3 mm thick and 4 mm hole grille.

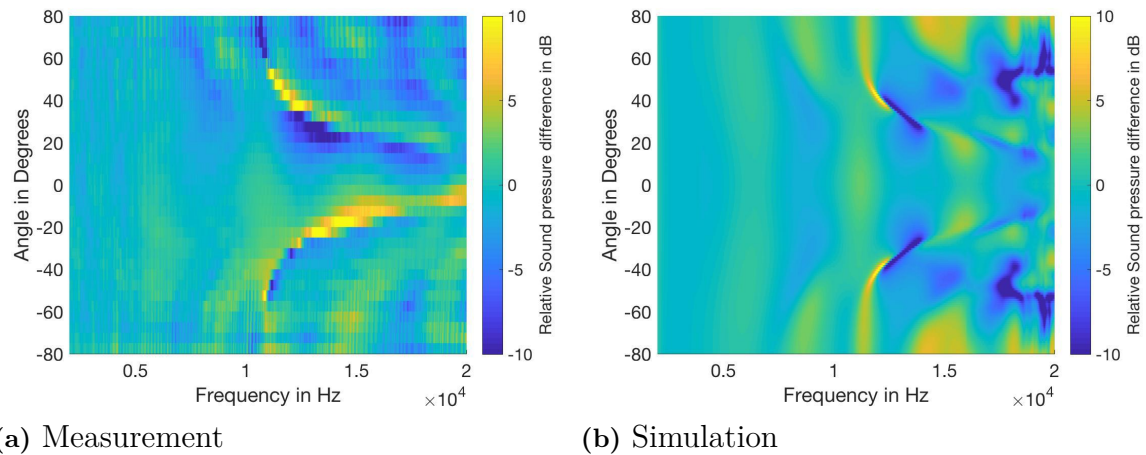


Figure 4.44: dB difference between baffle 2 with 3 mm thick and 4 mm hole grille and baffle 2 without grille.

The effect of the 0.5 mm thick 2 mm hole grille is again mostly transparent. However in the difference graph (Figure 4.46) there is a zone where the measurement seems a bit shifted on the angle axis. This is also present in the two other grilles measurements (Figure 4.42a and 4.44a). This is probably due to an error in the measurement procedure while setting up the wood baffle on the rotating table for the baffle 2 measurement. It is possible that it was not perfectly aligned to the microphone leading to a small angle shift when subtracting to the grille measurement.

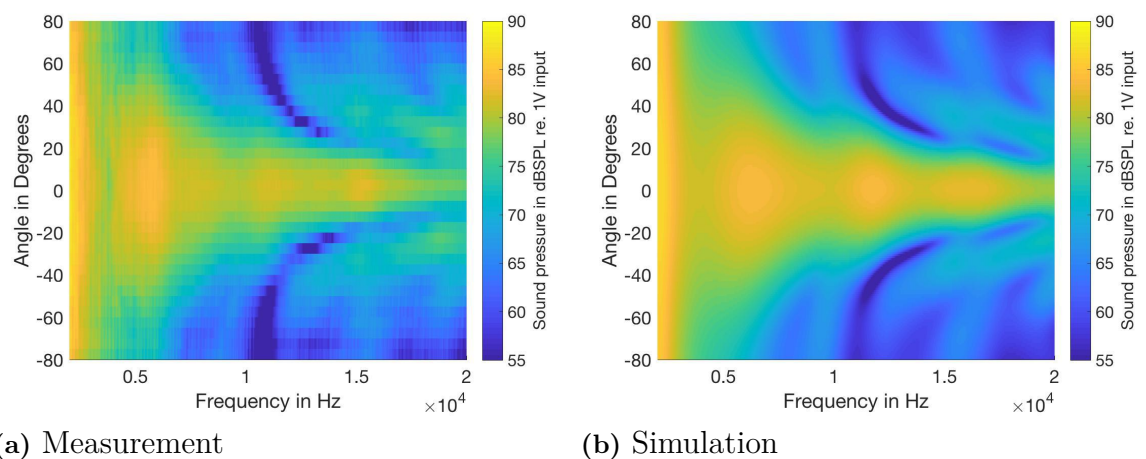


Figure 4.45: Directivity comparison between measurement and simulation of baffle 2 with 0.5 mm thick and 2 mm hole grille.

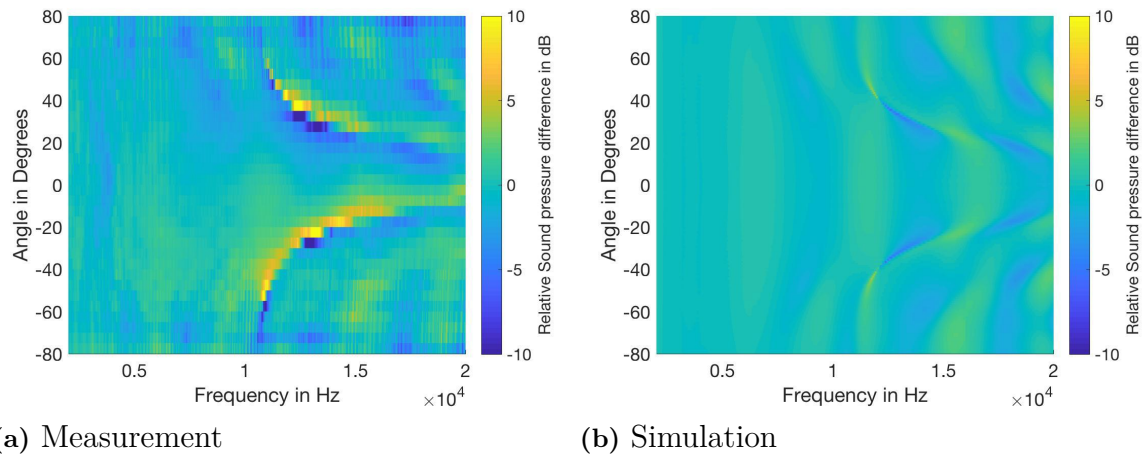


Figure 4.46: dB difference between baffle 2 with 0.5 mm thick and 2 mm hole grille and baffle 2 without grille.

The pressure distribution inside the interface of baffle 2 under the different grille configuration is seen on Figure 4.47. The resonance at 6.1 kHz is much stronger for the 3 mm thick 2 mm hole grille. This resonance allows for a better radiation of this specific frequency. Again these results are coherent with the observations made for baffle 1. The resonances are starting earlier than baffle 1 due to the size of the interface which is bigger.

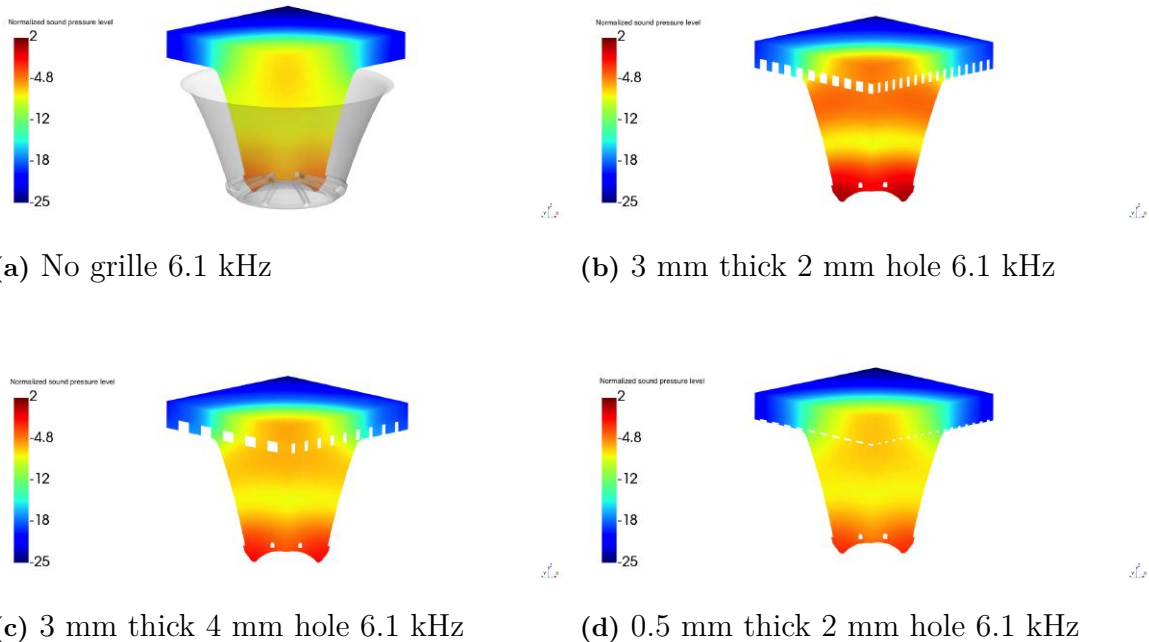


Figure 4.47: Comparison of the resonances occurring inside the interface between all the grille configuration for baffle 2 at 6.1 kHz.

At 9 kHz there is an anti-resonance at the end of the horn which affects the on axis

radiation (Figure 4.48b).

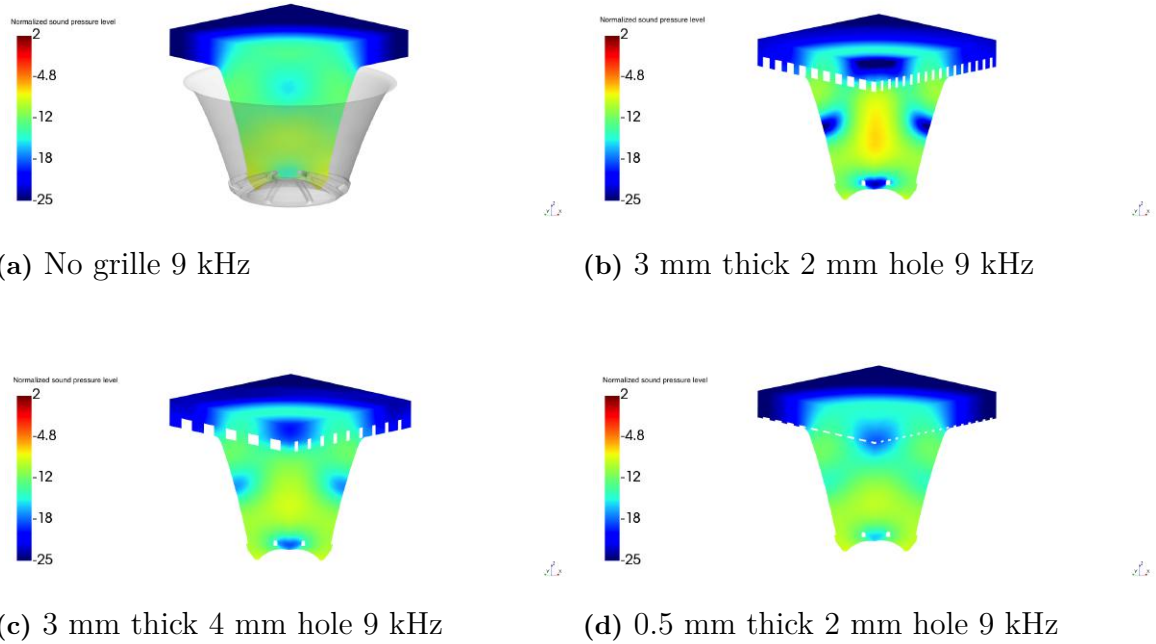


Figure 4.48: Comparison of the resonances occurring inside the interface between all the grille configuration for baffle 2 at 9 kHz.

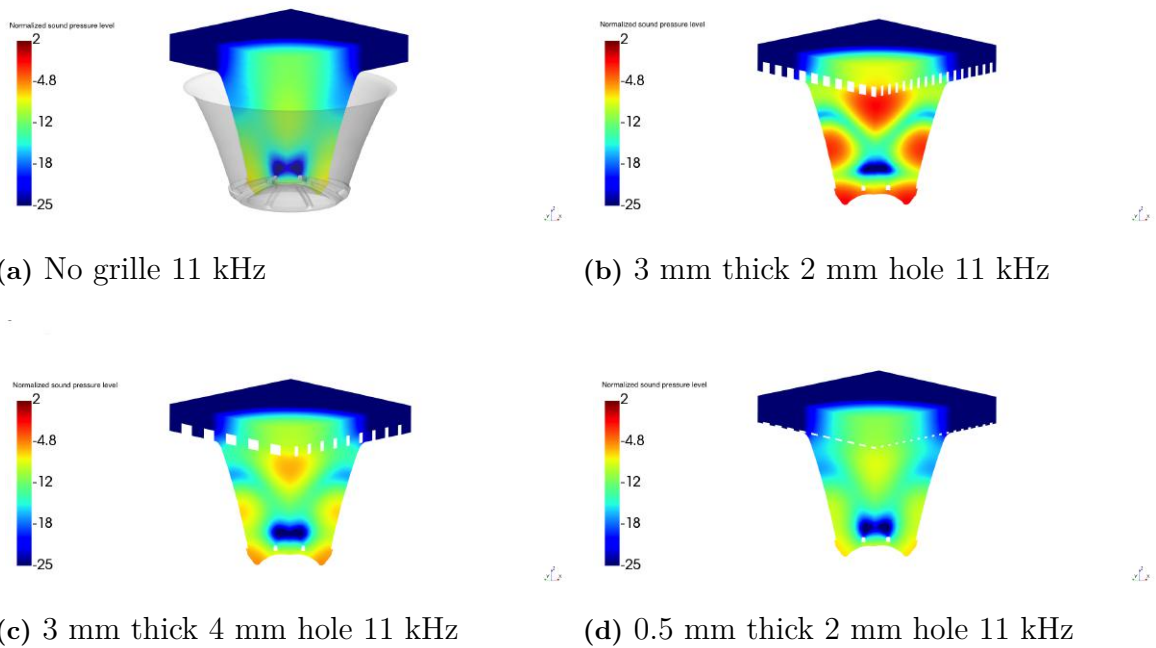


Figure 4.49: Comparison of the resonances occurring inside the interface between all the grille configuration for baffle 2 at 11 kHz.

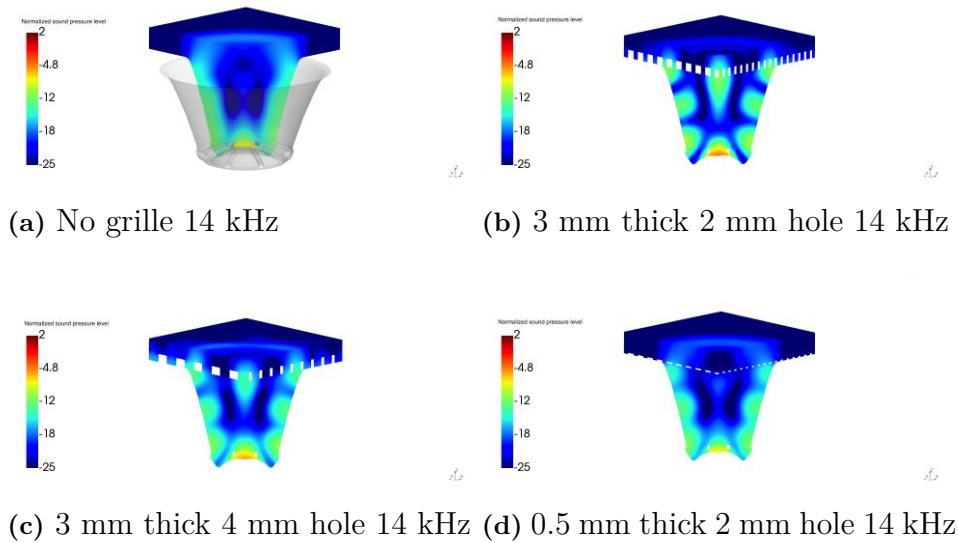


Figure 4.50: Comparison of the resonances occurring inside the interface between all the grille configuration for baffle 2 at 14 kHz.

Again at 11 kHz (Figure 4.49) there is a resonance and at 14 kHz (Figure 4.50) there is an anti-resonance at the opening. The resonance in the length direction is always stronger with the most restrictive grille and is weaker gradually with less restrictive grilles. All the frequencies shown in these plots have local minimums and maximums in the on-axis frequency response functions.

Comparing simulation and measurement for the angled baffle in Figure 4.51, the same trends as the other cases are seen.

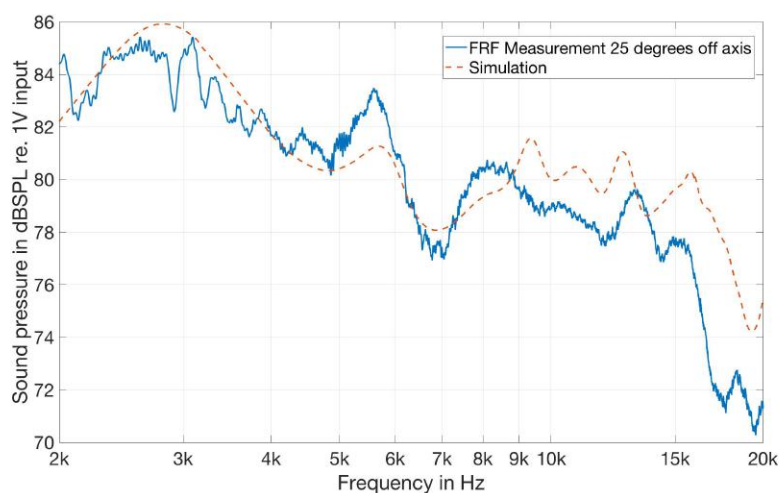


Figure 4.51: 25 degrees off axis sound pressure level comparison between simulation and measurement of baffle 3 with 3 mm thick 2 mm hole grille.

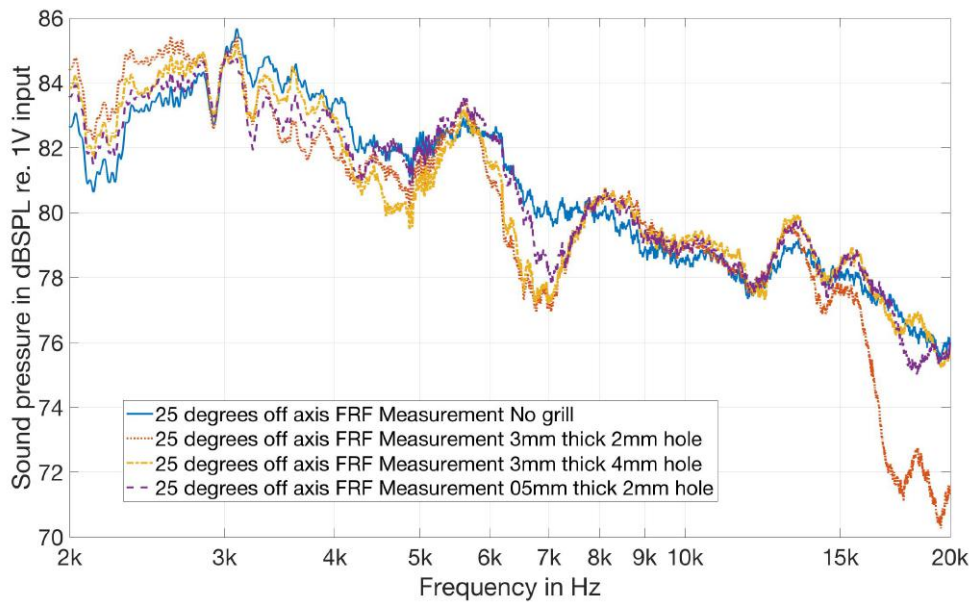


Figure 4.52: 25 degrees off axis sound pressure level comparison between the measurement of baffle 3 with the different grilles.

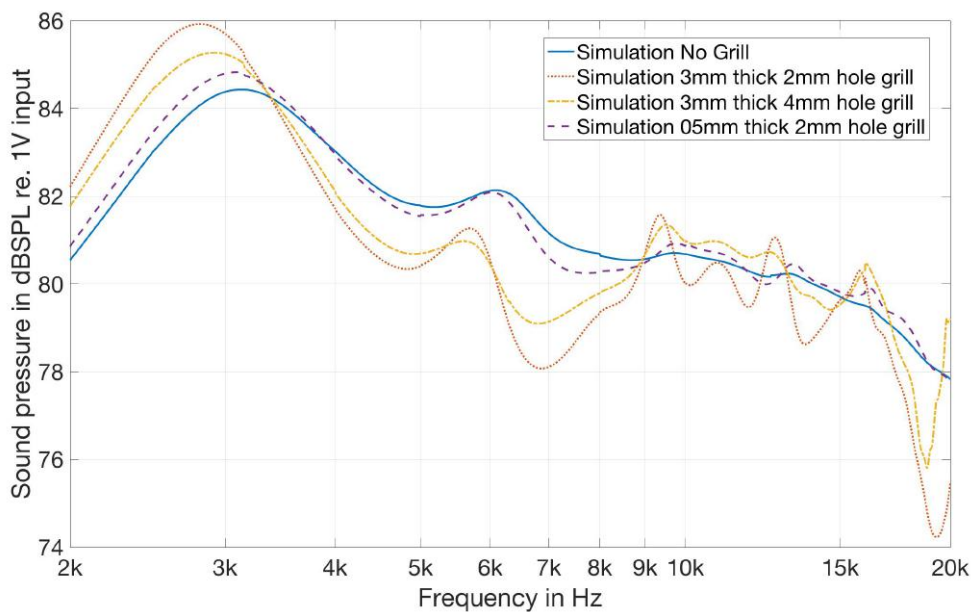


Figure 4.53: 25 degrees off axis sound pressure level comparison between the simulation of baffle 3 with the different grilles.

For the angled baffle the grilles had a lower effect than the straight horn but that is expected as it is a smaller interface, however they also have a lower effect than the flush baffle. There is a clear difference at 6.6 kHz in measurement (Figure 4.52) and a slight difference at 2.5 kHz. The differences are captured in simulation (Figure 4.53) however they are more accentuated.

4. Results & Discussions

As for the directivity plots, the 25 degrees off axis difference is small as seen in the frequency response plots above, however there is more sound pressure leakage off the 25 degrees axis.

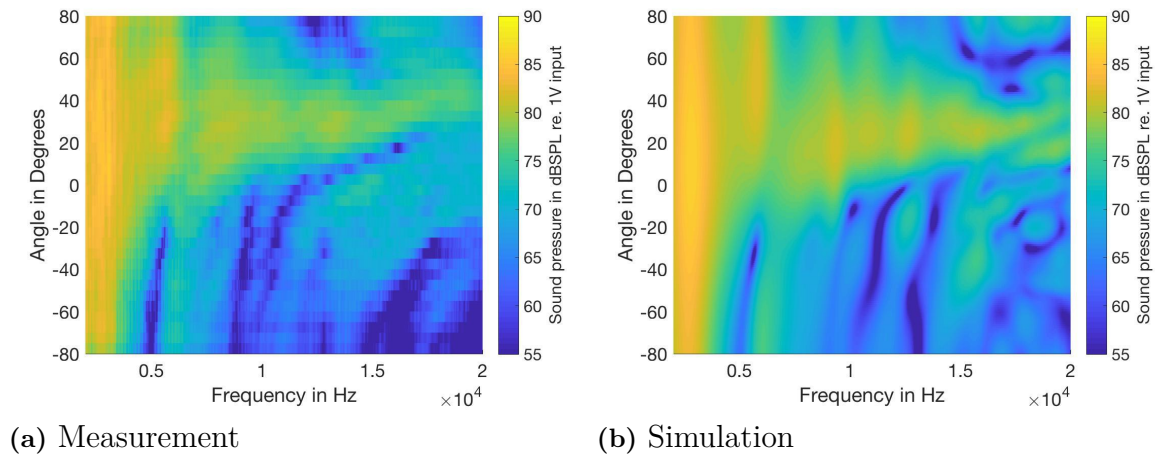


Figure 4.54: Directivity comparison between measurement and simulation of baffle 3 with 3 mm thick and 2 mm hole grille.

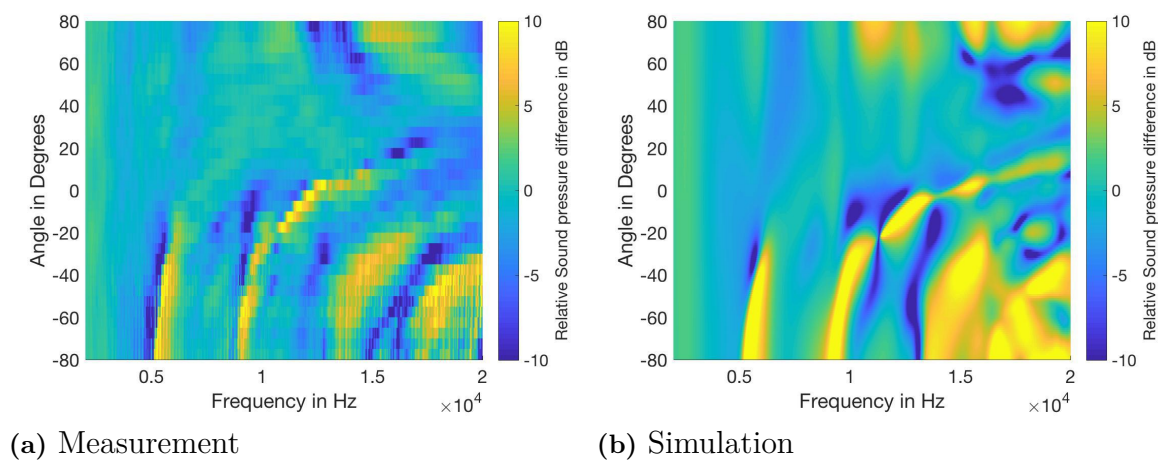


Figure 4.55: dB difference between baffle 3 with 3 mm thick and 2 mm hole grille and baffle 3 without grille.

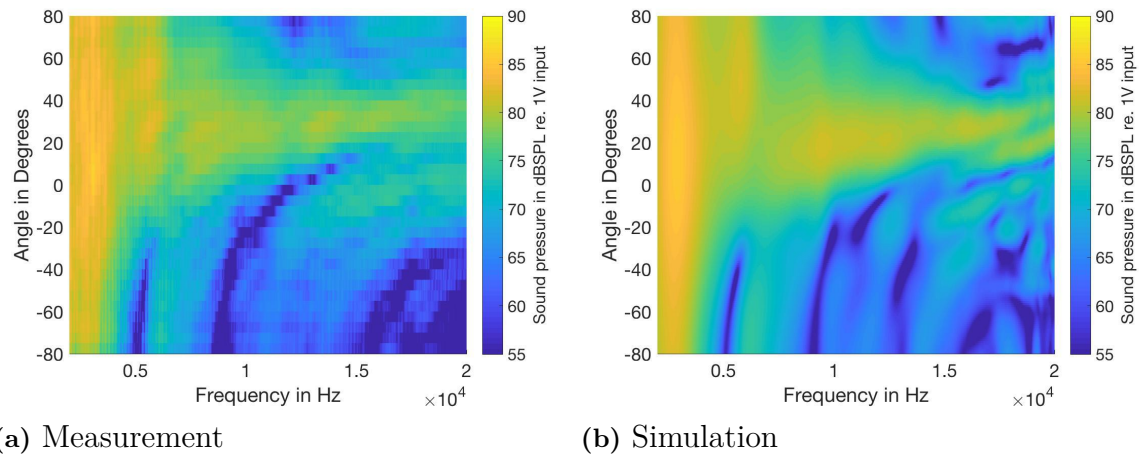


Figure 4.56: Directivity comparison between measurement and simulation of baffle 3 with 3 mm thick and 4 mm hole grille.

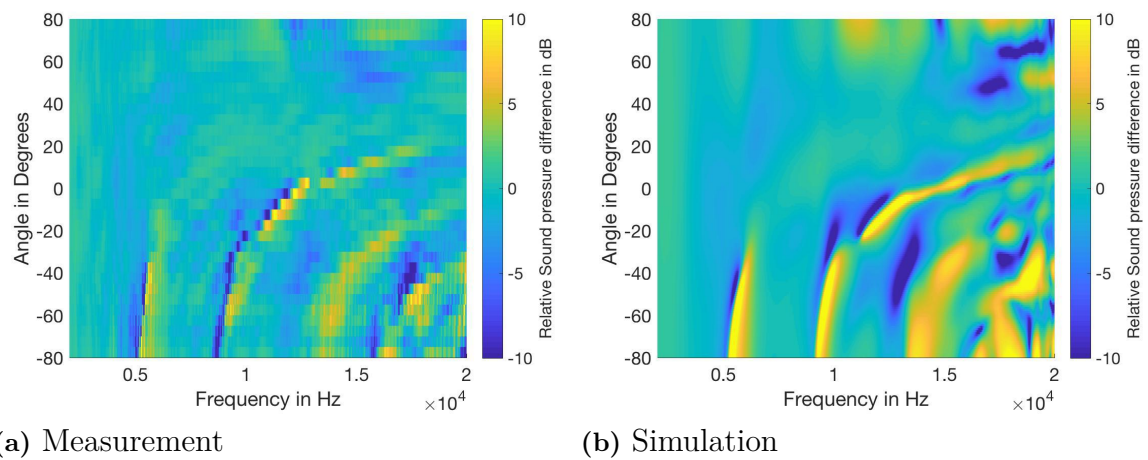


Figure 4.57: dB difference between baffle 3 with 3 mm thick and 4 mm hole grille and baffle 3 without grille.

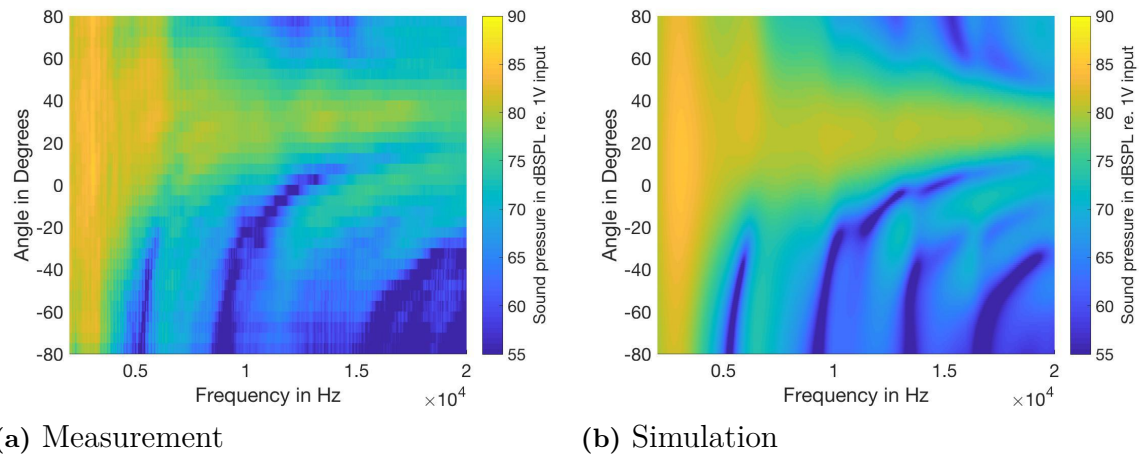


Figure 4.58: Directivity comparison between measurement and simulation of baffle 3 with 0.5 mm thick and 2 mm hole grille.

The sound pressure off axis is higher for the most airflow restrictive grille (Figure 4.55) than the least restrictive ones (Figure 4.59).

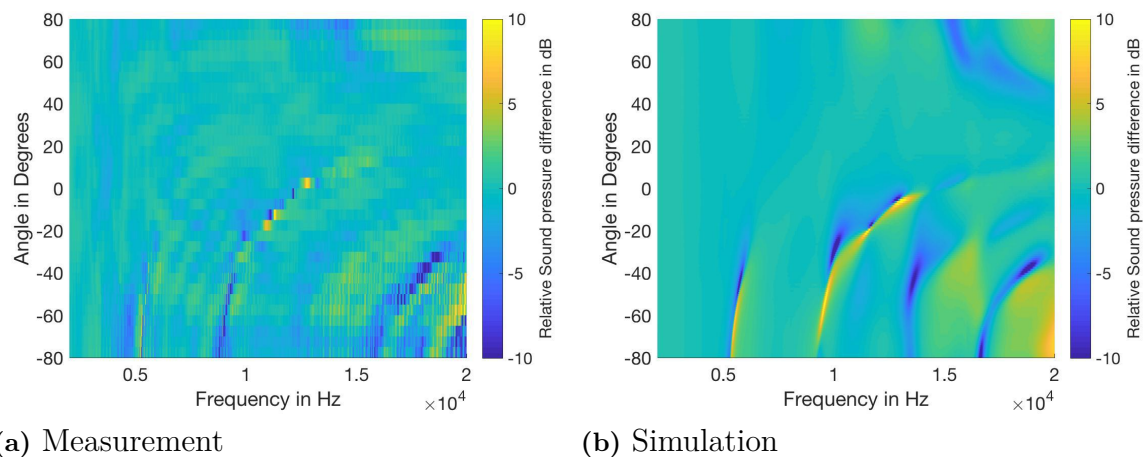


Figure 4.59: dB difference between baffle 3 with 0.5 mm thick and 2 mm hole grille and baffle 3 without grille.

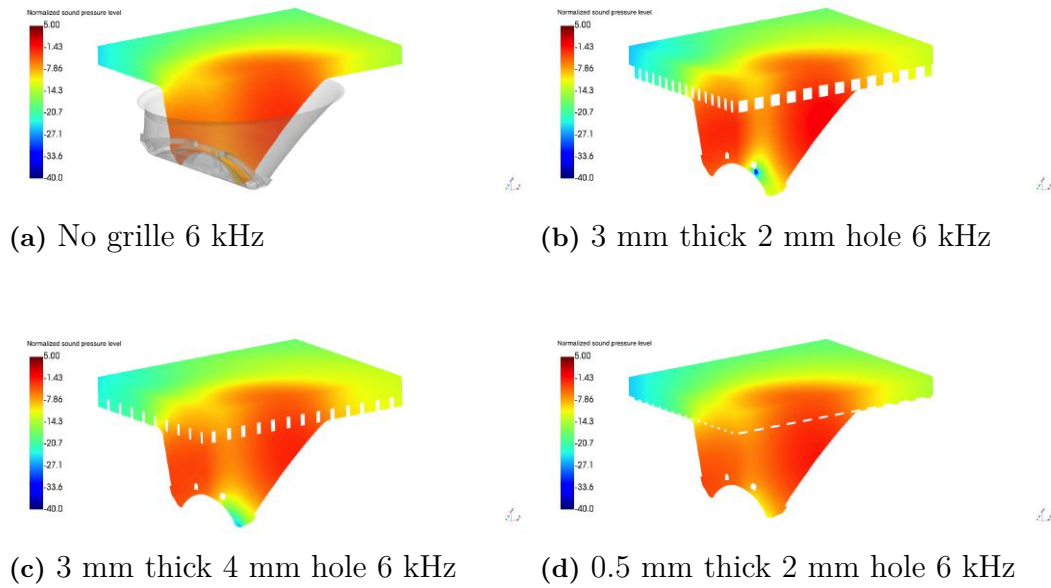


Figure 4.60: Comparison of the resonances occurring inside the interface between all the grilles configuration for baffle 3 at 6 kHz.

This leak can also be traced back to cavity resonances. They are again stronger when the grille is more restrictive see Figure 4.60 and 4.61.

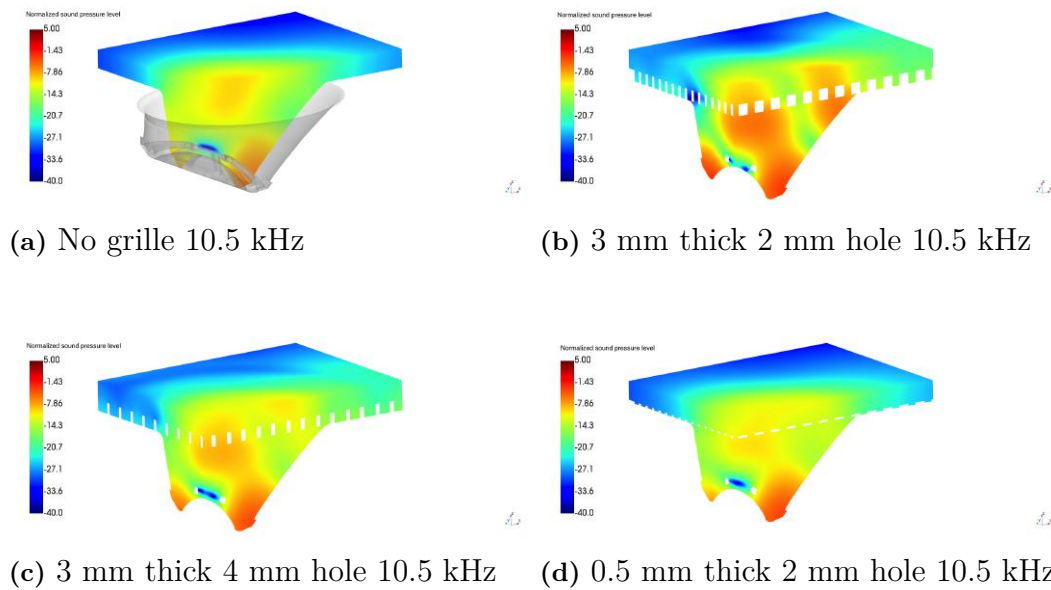


Figure 4.61: Comparison of the resonances occurring inside the interface between all the grilles configuration for baffle 3 at 10.5 kHz.

4.4 Frequency Equalization

One possible solution to make the frequency response of the tweeter flat is to measure the on-axis response and then apply digital filtering. But the directivity of the tweeter will also be affected by the equalization filter. So the difference applied to the on-axis response to reach the target flat frequency response (here the on-axis maximum sound pressure level was chosen as the target) was added to all the responses from -80 to 80 degrees. The figures below shows how the directivity will be theoretically, if equalization is applied.

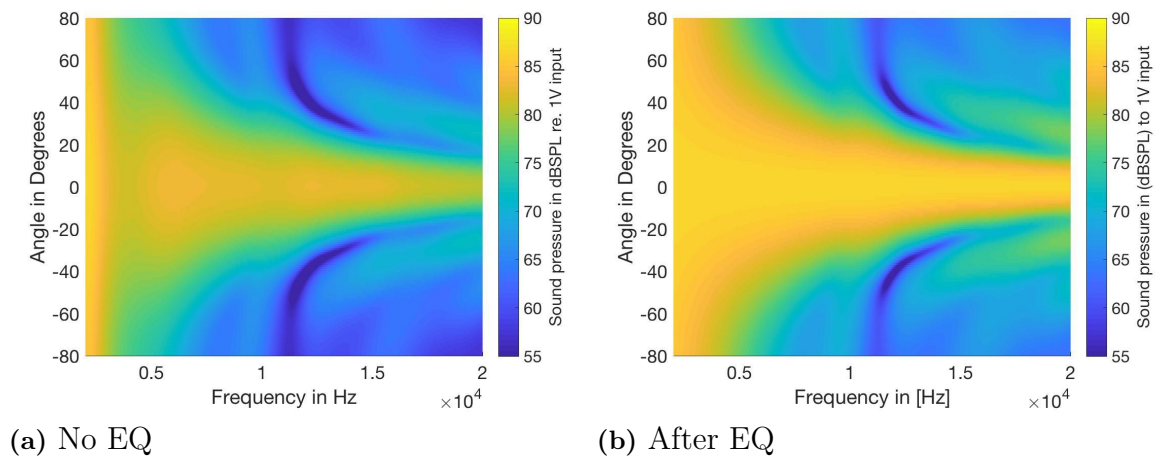


Figure 4.62: Directivity comparison before and after on-axis frequency equalization for baffle 2.

Equalizing the straight horn baffle with the grille (Figure 4.63) is somewhat similar to the configuration without the grille (Figure 4.62). The resonances of the grille (at 6kHz, 11 kHz and 16 kHz) are relatively attenuated.

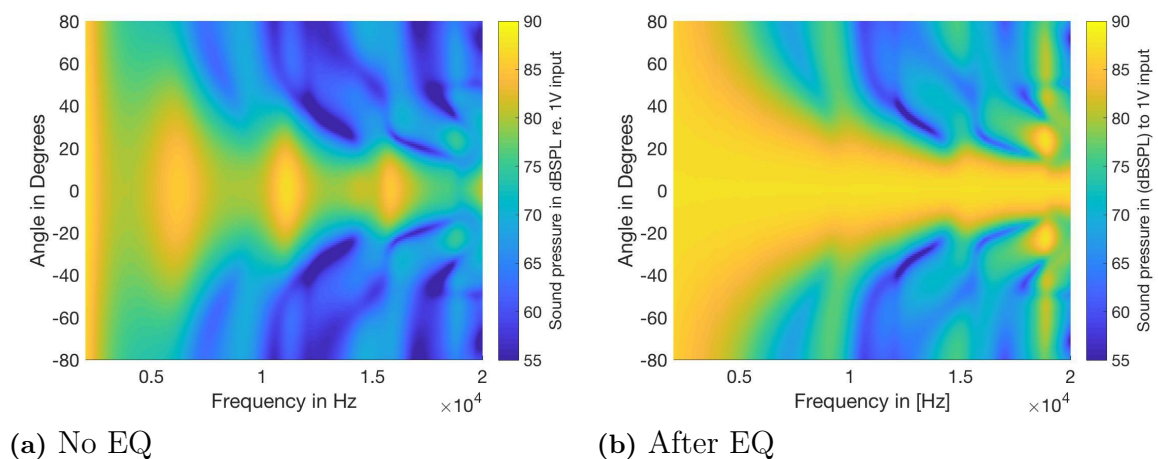


Figure 4.63: Directivity comparison before and after on-axis frequency equalization for baffle 2 with 3 mm thick 2 mm hole grille.

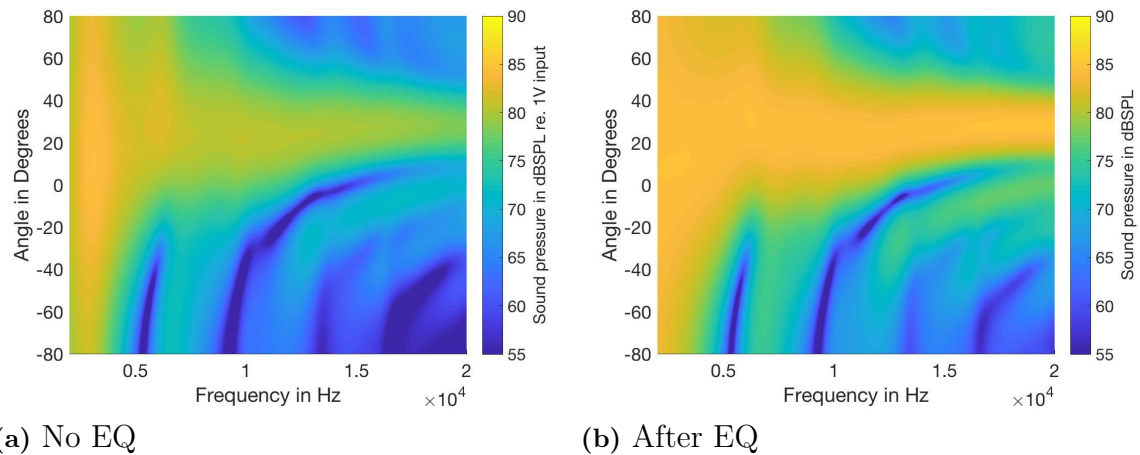


Figure 4.64: Directivity comparison before and after 25 degrees off axis frequency equalization for baffle 3.

Equalizing the angled horn baffle with the grille didn't have the same effect as the straight horn baffle (Figure 4.65). The resonances of the grille are attenuated at 25 degrees however for the other extreme angles the responses is worse for example 6 kHz is much more amplified from 0 to -80 degrees. Inside the car this might amplify unwanted reflections inside the cabin.

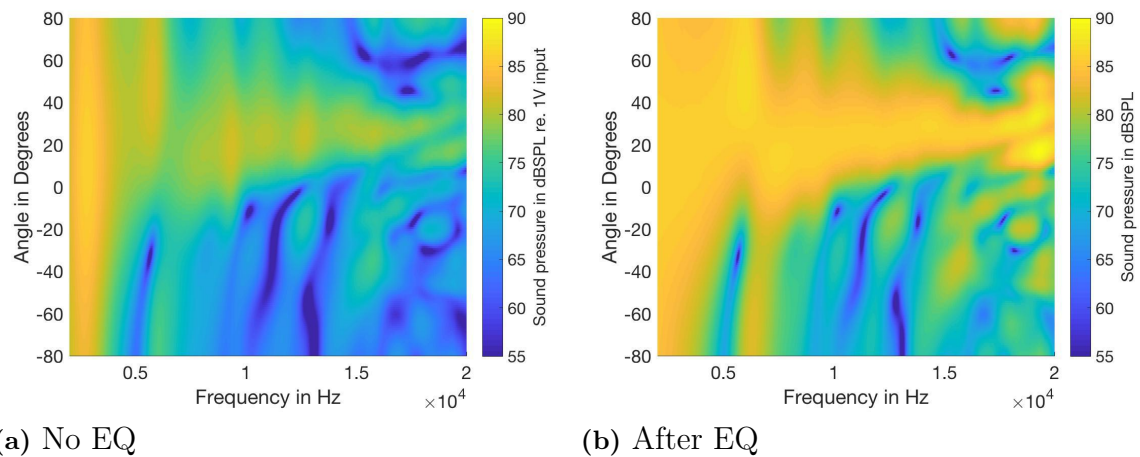


Figure 4.65: Directivity comparison before and after 25 degrees off axis frequency equalization for baffle 2 with 3 mm thick 2 mm hole grille.

The response of baffle 4 is still problematic even after equalization (Figure 4.66). It is better at and around 25 degrees (where the equalization was applied) but this was expected. However resonances are extremely amplified outside the sweet spot and will lead to unwanted reflections inside the car cabin.

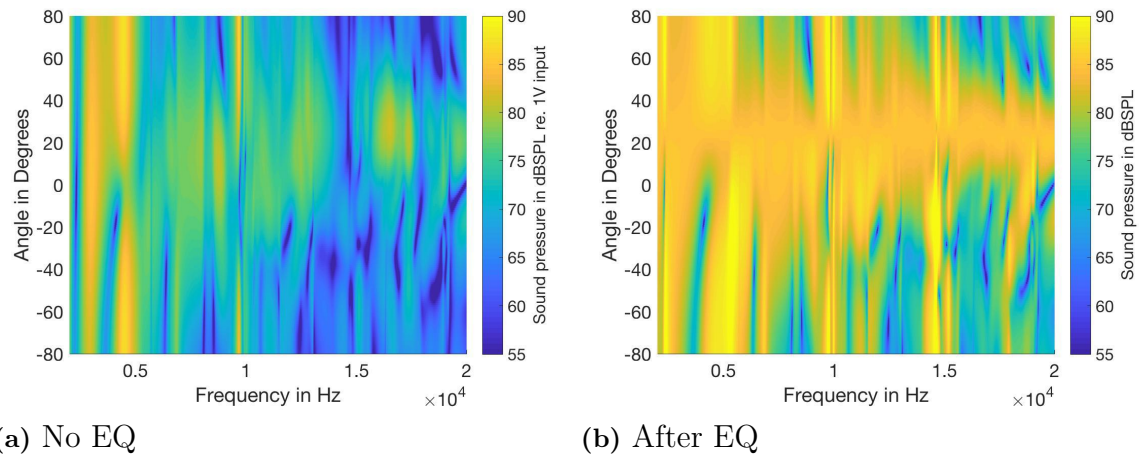


Figure 4.66: Directivity comparison before and after 25 degrees off axis frequency equalization for baffle 4 open.

5 Conclusion

The FEM simulations managed to run till 20kHz. FEM is usually not considered at these frequencies. The effect of grilles and interfaces was overall well predicted by the FEM simulation software even at high frequencies. Computation time was also reasonable with the hardware used by Volvo Cars. This will allow engineers to detect and quantitatively present, before any physical prototyping, how the installation details will affect the radiation of tweeters.

The installation details of tweeters does affect its radiation performance. Interfaces if not properly designed can create resonances that will affect the radiation drastically like Baffle 4 in this thesis. Horn shaped interfaces can help focus the sound in a specific region and increase the sound pressure level at certain frequencies. Grilles will change the impedance at the opening, and cause stronger reflections inside the cavity. Grilles that have a lower airflow resistivity will be more transparent. Thicker and smaller diameter grilles will have a higher airflow resistivity. One way to reduce the resonance effect added with the grilles is to bring the grille closer to the tweeter membrane.

For future work, the simulation can be expanded to a car cavity. The simulation will be much more computationally heavy and material properties inside the cabin will be important to have correct boundary condition. The computation frequency will also probably be reduced, and new computation algorithms like DGM can be used to compute larger number of nodes. Another area that can be studied is the time domain response of the speaker with different installation details. This will probably require a full mechanical simulation of the speaker and not a Thiele and Small approximation.

References

- [1] Earl G. Williams. Fourier Acoustics: Sound Radiation and Nearfield Acoustical Holography, Academic Press, 1999.
- [2] Free Field Technologies: "Actran 18.0 User's guide Vol. 1: Installation, Operations, Theory and Utilities".
- [3] Jens Ahrens. ElectroAcoustics Lecture, Division of Applied Acoustics, Chalmers University of Technology.
- [4] Richard H. Small. Vented-Box Loudspeaker Systems Part 1: Small-Signal Analysis. JAES Volume 21 Issue 5 pp. 363-372.
- [5] A. N. Thiele. Loudspeaker in Vented Boxes: Part 1. JAES Volume 19 Issue 5 pp. 382-392.
- [6] SI units. <https://www.theaemt.com/technical-info/general-engineering/si-units> .
- [7] Markus Brandstetter; Ze Zhou; Gregory Lielens. Numerical Methods for Loudspeaker Installation Effects Prediction: Detailed Evaluation on a Car Door Model. 2017.

A Appendix

A.1 Background noise

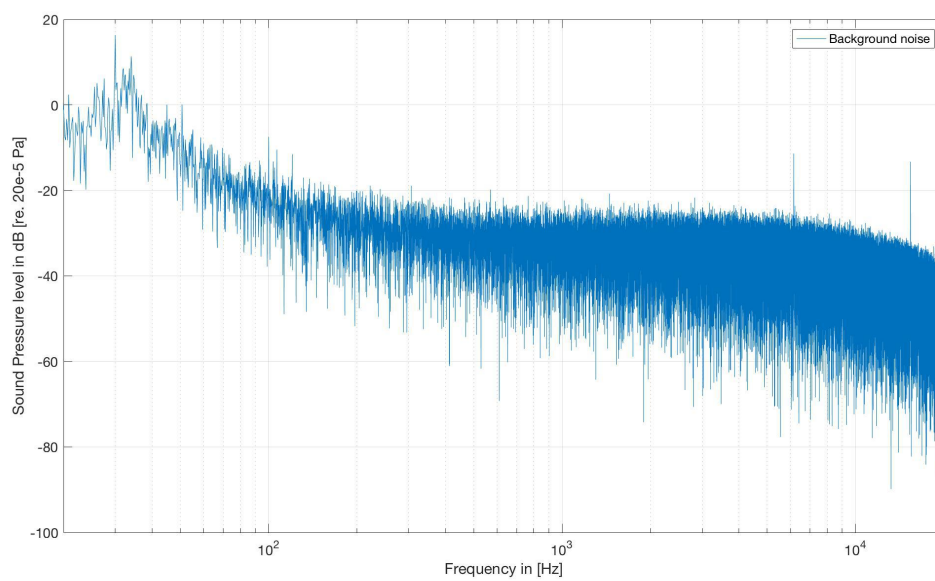


Figure A.1: Measurement of the background noise in the anechoic chamber.

A.2 More results

A.2.1 Interfaces

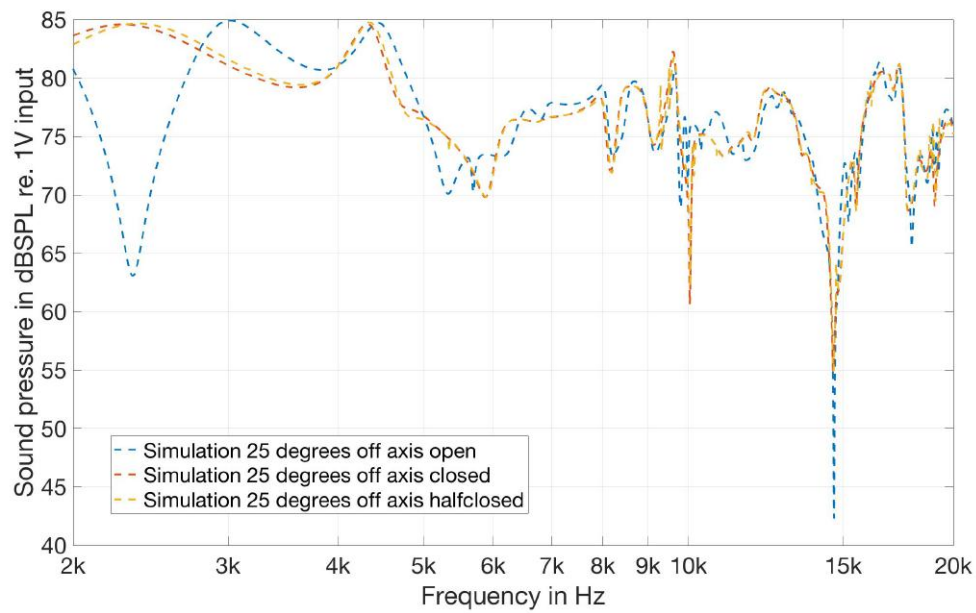


Figure A.2: 25 degrees off axis sound pressure level comparison between the simulation of baffle 4's three different configurations.

A.2.2 Grilles

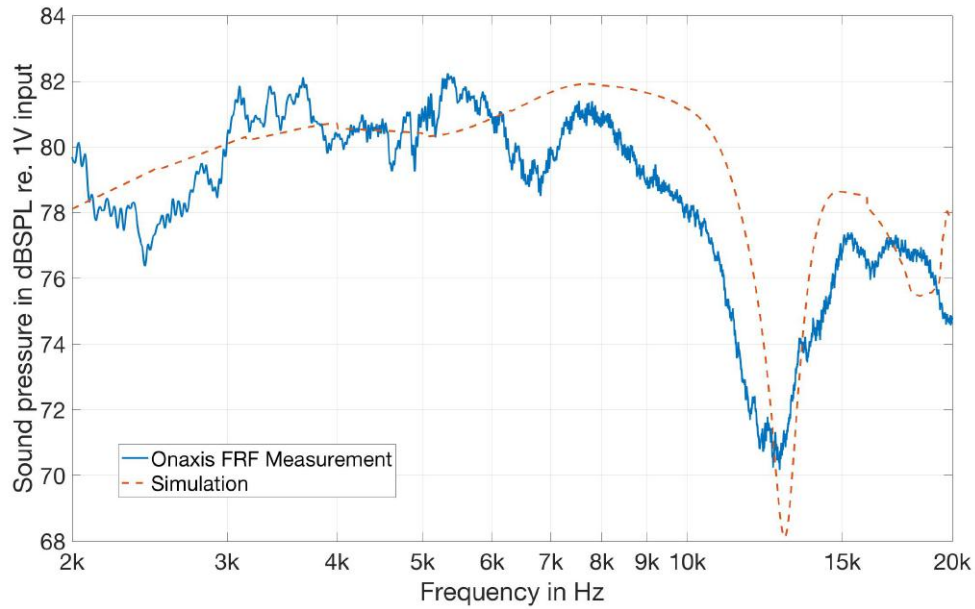


Figure A.3: Directivity comparison between measurement and simulation of baffle 1 with 3 mm thick and 4 mm hole.

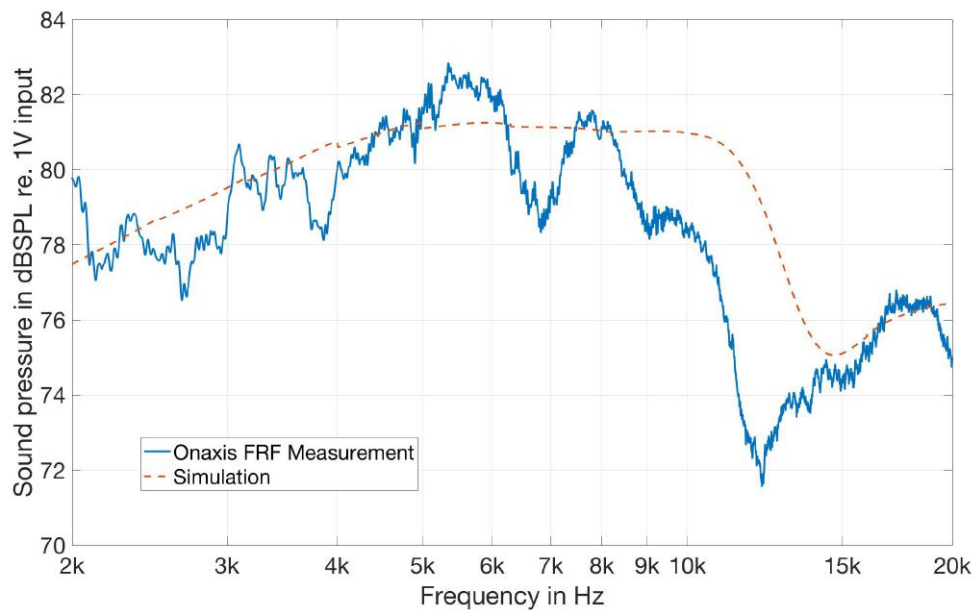


Figure A.4: Directivity comparison between measurement and simulation of baffle 1 with 0.5 mm thick and 2 mm hole.

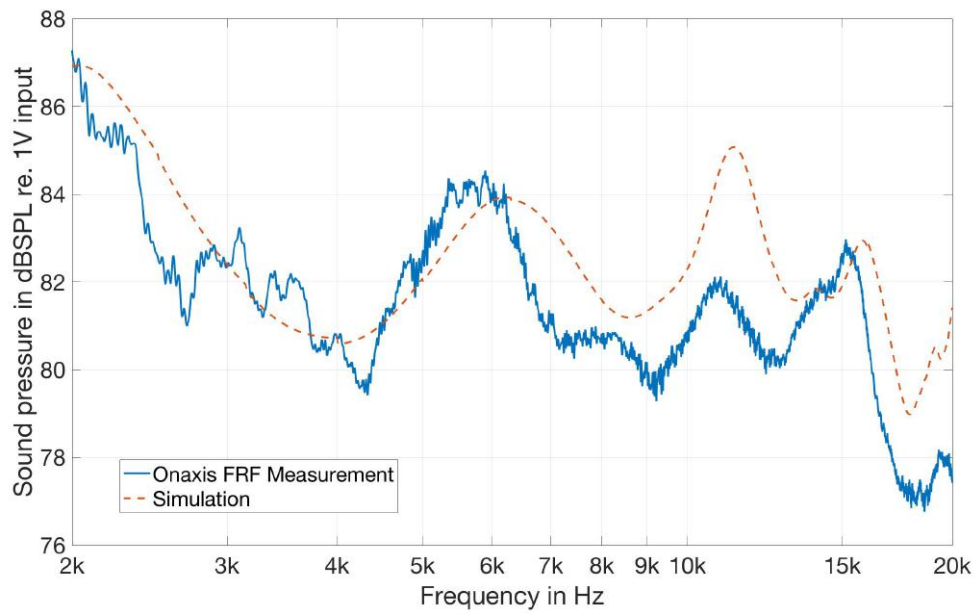


Figure A.5: Directivity comparison between measurement and simulation of baffle 2 with 3 mm thick and 4 mm hole.

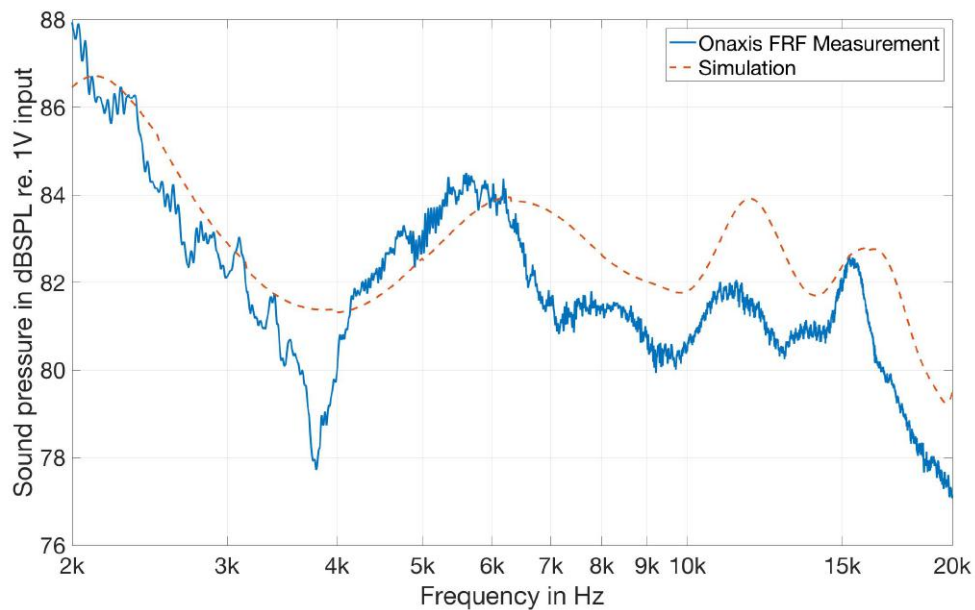


Figure A.6: Directivity comparison between measurement and simulation of baffle 2 with 0.5 mm thick and 2 mm hole.

Interface\Frequency	2500	3150	4000	5000	6300	8000	10000	12500	16000	Total
3mm thick 2mm hole	1.01	0.71	0.51	0.77	1.49	1.33	2.90	3.25	3.28	2.00
3mm thick 4mm hole	1.14	0.49	0.34	0.49	1.13	1.71	3.18	3.19	3.32	2.04
0.5mm thick 2mm hole	0.74	0.79	0.53	0.67	0.53	1.43	2.39	2.95	2.38	1.64

Table A.1: RMS error for the different grilles on baffle 2 in dB.

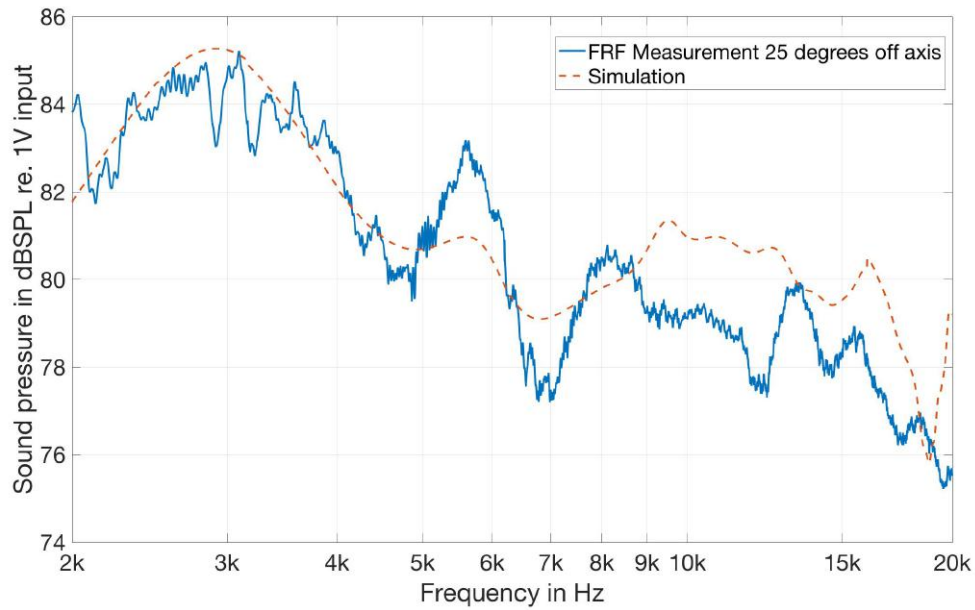


Figure A.7: 25 degrees off axis sound pressure level comparison between simulation and measurement of baffle 3 with 3 mm thick 4 mm hole grille.

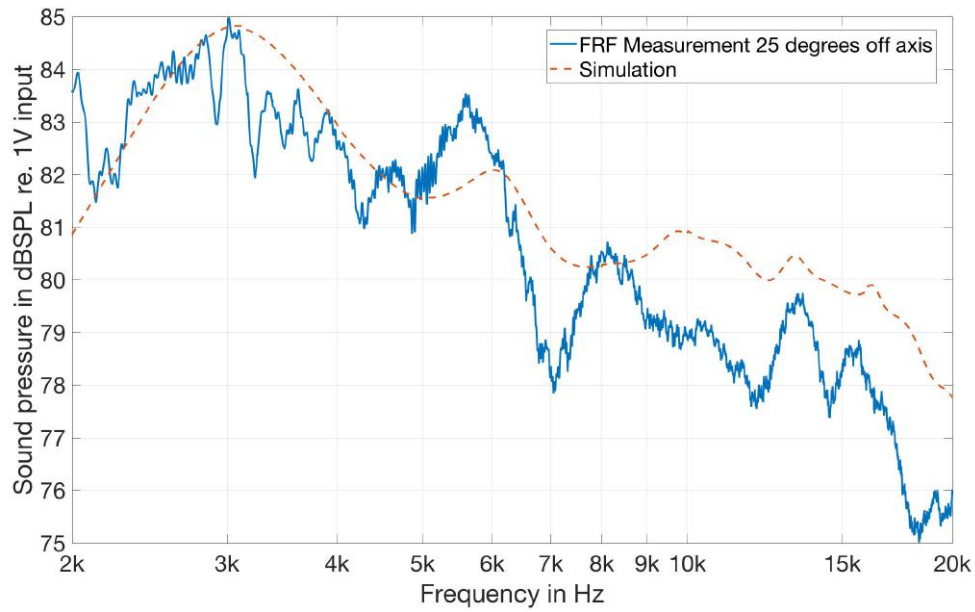
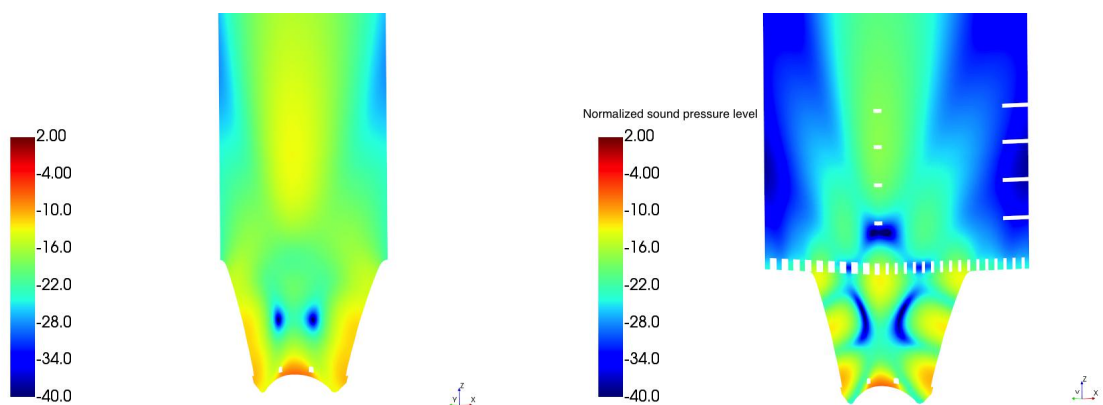


Figure A.8: 25 degrees off axis sound pressure level comparison between simulation and measurement of baffle 3 with 0.5 mm thick 2 mm hole grille.

Interface\Frequency	2500	3150	4000	5000	6300	8000	10000	12500	16000	Total
3mm thick 2mm hole	1.15	1.19	1.06	1.81	1.58	2.19	3.52	3.60	4.80	2.64
3mm thick 4mm hole	0.94	0.70	0.46	0.94	1.05	1.74	2.31	3.00	2.90	1.81
0.5mm thick 2mm hole	0.71	0.74	1.16	1.21	1.12	1.77	2.47	2.56	2.87	1.80

Table A.2: RMS error for the different grilles on baffle 3 in dB.



(a) No grille 13.5 kHz

(b) 3 mm thick 2 mm hole 13.5 kHz

Figure A.9: Comparison of the extended pressure maps between the 3 mm thick 2 mm hole grille and without grille for baffle 2 at 13.5 kHz.